Journal of the Geological Society, London, Vol. **168**, 2011, pp. 633–672. doi: 10.1144/0016-76492010-139.

Crustal–lithospheric structure and continental extrusion of Tibet

M. P. SEARLE[1]*, J. R. ELLIOTT[1], R. J. PHILLIPS[2] & S.-L. CHUNG[3]
[1]*Department of Earth Sciences, Oxford University, South Parks Road, Oxford OX1 3AN, UK*
[2]*Institute of Geophysics and Tectonics, School of Earth and Environment, University of Leeds, Leeds LS2 9JT, UK*
[3]*Department of Geosciences, National Taiwan University, Taipei 106, Taiwan*
**Corresponding author (e-mail: mike.searle@earth.ox.ac.uk)*

Abstract: Crustal shortening and thickening to *c*. 70–85 km in the Tibetan Plateau occurred both before and mainly after the *c*. 50 Ma India–Asia collision. Potassic–ultrapotassic shoshonitic and adakitic lavas erupted across the Qiangtang (*c*. 50–29 Ma) and Lhasa blocks (*c*. 30–10 Ma) indicate a hot mantle, thick crust and eclogitic root during that period. The progressive northward underthrusting of cold, Indian mantle lithosphere since collision shut off the source in the Lhasa block at *c*. 10 Ma. Late Miocene–Pleistocene shoshonitic volcanic rocks in northern Tibet require hot mantle. We review the major tectonic processes proposed for Tibet including 'rigid-block', continuum and crustal flow as well as the geological history of the major strike-slip faults. We examine controversies concerning the cumulative geological offsets and the discrepancies between geological, Quaternary and geodetic slip rates. Low present-day slip rates measured from global positioning system and InSAR along the Karakoram and Altyn Tagh Faults in addition to slow long-term geological rates can only account for limited eastward extrusion of Tibet since Mid-Miocene time. We conclude that despite being prominent geomorphological features sometimes with wide mylonite zones, the faults cut earlier formed metamorphic and igneous rocks and show limited offsets. Concentrated strain at the surface is dissipated deeper into wide ductile shear zones.

The Tibetan Plateau region, bordered by the Himalaya along the south, the Tien Shan along the NW, the Kun Lun and Altyn Tagh ranges along the north and the Long Men Shan range along the east, is the largest region of high elevation (average 5.023 km; Fielding *et al.* 1994) and thick crust (70–90 km thick; Wittlinger *et al.* 2004; Rai *et al.* 2006) in the world (Fig. 1). The Tibetan Plateau is made up of several terranes progressively accreted onto the stable North Asian Siberian–Mongolian craton since the Early Mesozoic (Dewey *et al.* 1988). From north to south the plateau is composed of the Kun Lun–Songpan Ganze, Qiangtang and Lhasa terranes. In western Tibet the Karakoram terrane is the western equivalent to the Qiangtang, and the Kohistan–Ladakh–Gangdese batholith makes up the southern part of the Lhasa terrane (Searle & Phillips 2007). The southernmost part of the geomorphological Tibetan Plateau is the Tethyan Himalaya, part of the Indian plate south of the Indus–Yarlung Tsangpo suture zone. The Neo-Tethyan Indus suture zone marks the zone of collision between the Indian plate to the south and the Asian amalgamated terranes to the north. The Indus–Yarlung Tsangpo suture zone runs from the Nanga Parbat Western Himalayan syntaxis region across Ladakh and southern Tibet to the Namche Barwa Eastern Himalayan syntaxis region and then swings south into Burma.

Models for the growth of the Tibetan Plateau range from early, pre-India–Asia collision thickening and uplift in the Lhasa and southern Qiangtang blocks and Karakoram terrane (England & Searle 1986; Murphy *et al.* 1997; Hildebrand *et al.* 2001; Kapp *et al.* 2005; Searle *et al.* 2010*a*) through gradual uplift following the India–Asia collision (50–0 Ma) to sudden uplift at *c*. 7–8 Ma (Molnar *et al.* 1993). The India–Asia collision itself must have been a continuing process since the Late Cretaceous–Early Palaeocene obduction of ophiolites onto the Indian passive continental margin and initial contact between Indian and Asian crust, through to final withdrawal of the Tethyan Ocean with ending of marine sedimentation in the Indus–Yarlung Tsangpo suture zone. The final marine sediments in the suture zone and along the northern margin of India have been precisely dated at 50.5 Ma (planktonic foraminifera zone P8 and shallow benthic zone SBZ10; Garzanti *et al.* 1987; Rowley 1998; Zhu *et al.* 2005; Green *et al.* 2008). In this paper we equate the Late Ypresian (Early Eocene) timing of final marine sedimentation along the suture zone as defining the India–Asia collision.

Unlike the Himalaya where deep crustal metamorphic and granitic rocks are exposed and exhumation and erosion rates are high, most of the Tibetan Plateau has low relief, exhumed deep crustal rocks are uncommon, and erosion rates and exhumation rates are extremely low. Therefore we are reliant on deep crustal seismic experiments (tomography, receiver functions and seismic anisotropy), notably the INDEPTH (Zhao *et al.* 1993; Nelson *et al.* 1996; Haines *et al.* 2003; Tilmann *et al.* 2003) and Hi-CLIMB (Chen & Tseng 2007; Heténi *et al.* 2007; Nábelek *et al.* 2009) profiles, to interpret the structure of the lower crust. The composition of the lower crust and upper mantle can directly be known only from xenoliths entrained in ultrapotassic or potassic (shoshonitic) volcanic rocks that have sampled the lower crust on their way up to the surface (e.g. Hacker *et al.* 2000, 2005; Ducea *et al.* 2003; Chan *et al.* 2009).

Models to explain the deformation history of the Tibetan Plateau can be grouped into four main types: (1) Argand-type underthrusting of India models (Argand 1924); (2) 'rigid block' models in which the crust behaves as a rigid or rigid–plastic cohesive unit (e.g. Molnar & Tapponnier 1975; Tapponnier & Molnar 1976, 1977; Tapponnier *et al.* 1982); (3) continuum models, in which the lithosphere is regarded as a continuum with a Newtonian or power-law rheology (e.g. England & McKenzie 1982, 1983; England & Houseman 1985, 1986; Houseman & England 1986); (4) crustal flow models. The last include (a) lower crustal flow models (e.g. Bird 1991; Royden *et al.* 1997;

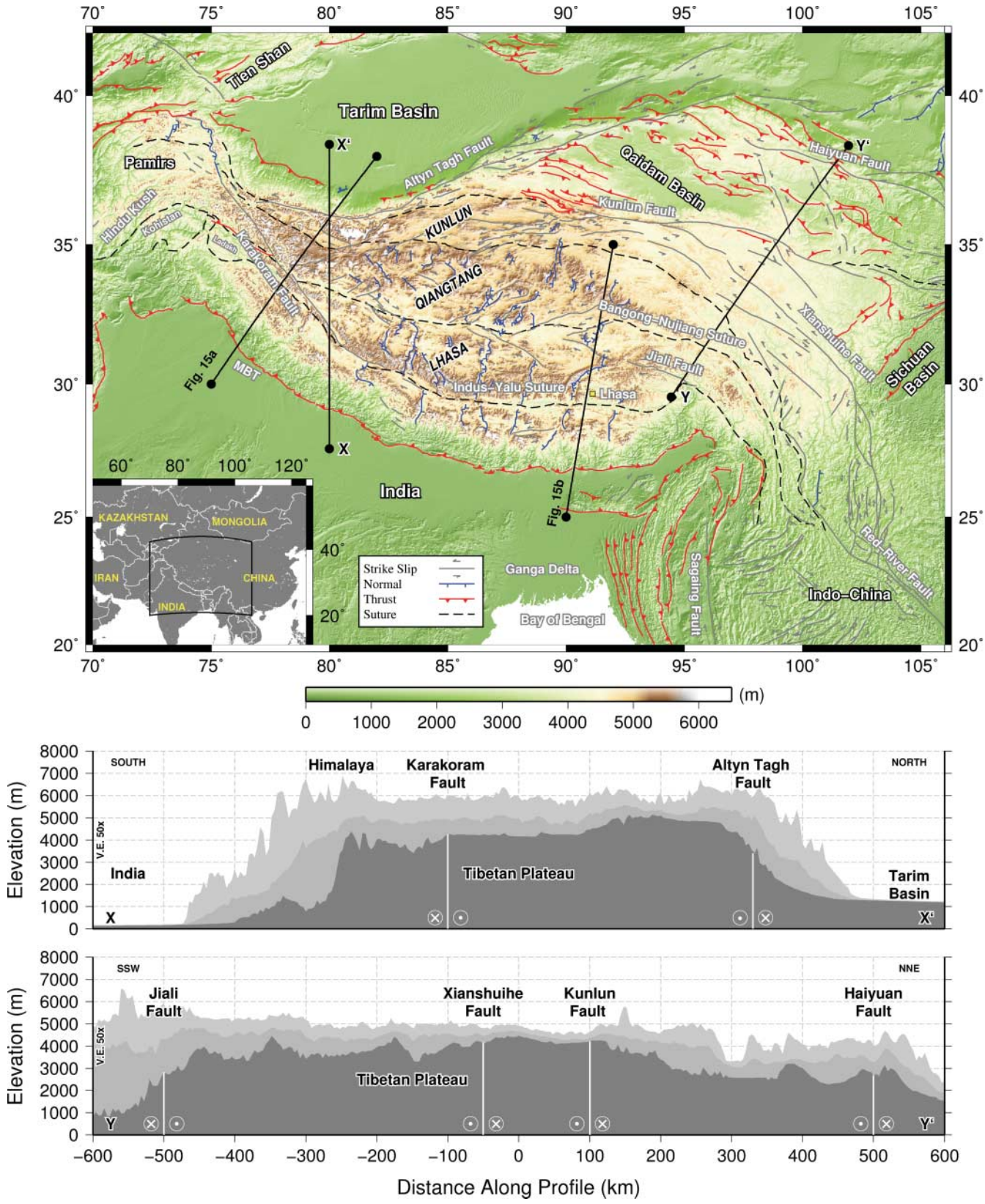

Fig. 1. Digital elevation map of the Tibetan Plateau region showing active and recent thrust faults (red), normal faults (blue) and strike-slip faults (grey) together with the major suture zones (black dashed) after Taylor & Yin (2009). Two topographic profiles (X–X' and Y–Y') across the major strike-slip faults are shown, with the three shades of grey representing maximum, mean and minimum elevations 100 km either side of the profiles. Lines of section of the two crustal profiles in Figure 15 are also shown.

Clark & Royden 2000; Haines *et al.* 2003) and (b) the Himalayan mid-crustal 'channel flow' model (e.g. Beaumont *et al.* 2001, 2004; Grujic *et al.* 2002; Searle *et al.* 2003, 2006, 2010*b*; Law *et al.* 2004, 2006; Godin *et al.* 2006).

In the first landmark paper on Tibetan tectonics, Argand (1924) proposed that the entire Tibetan Plateau was uplifted by underthrusting of the Indian plate from the south doubling the crustal thickness and increasing the surface elevation (Fig. 2). This foresightful suggestion preceded the plate-tectonic revolution by 40 years. Thirty-five years ago, in another landmark paper for continental tectonics, Molnar & Tapponnier (1975) first proposed the 'continental extrusion' or 'tectonic escape' model whereby large-scale (800–1000 km) eastward extrusion of Tibet was achieved by large (500–1000 km) horizontal motions along major intra-continental strike-slip faults, specifically the Karakoram–Jiale, Altyn Tagh, Kun Lun, Haiyuan and Xianshui-he Faults (Fig. 1). This 'rigid block' model requires large geological offsets (500–1000 km), high slip rates, synshearing metamorphism and melting as a result of shear heating, and deep faults cutting down into the mantle. This model has been vigorously promoted by many researchers working both in Tibet (e.g. Tapponnier *et al.* 1982, 2001*b*; Peltzer & Tapponnier 1988; Armijo *et al.* 1989; Avouac & Tapponnier 1993) and in SE Asia (Leloup *et al.* 1993, 1995, 2001; Lacassin *et al.* 2004*a*).

An alternative view of only a minor amount of eastward extrusion of Tibet during the Late Neogene has resulted from intensive geological mapping combined with precise U–Th–Pb dating of offset geological markers such as granites and exhumed metamorphic rocks offset along the strike-slip faults. This view suggests that the metamorphism and most of the granites were formed prior to strike-slip faulting and not by shear heating, and that the faults are purely crustal features where localized strain at the surface dissipates into a wide zone of distributed ductile shear at depth. This view has been promoted both for the Karakoram Fault in particular (Searle 1996; Searle *et al.* 1998; Murphy *et al.* 2000; Phillips *et al.* 2004; Phillips & Searle 2007; Searle & Phillips 2007; Robinson 2009*a*,*b*) and for the Red River Fault (Jolivet *et al.* 2001; Searle 2006, 2007; Yeh *et al.* 2008; Searle *et al.* 2010*c*).

In this paper we first review and discuss the merits and shortcomings of the various published models for the lithospheric structure of Tibet. We review the structural and seismic evidence for crustal thickness and structure across Tibet. We then discuss the evidence for timing of crustal thickening of Tibet and the present-day global positioning system (GPS) velocities. We review the volcanic history of the Tibetan Plateau, as the volcanic rocks of the region hold the key to interpreting mantle structure and evolution. We also review slip rates across geological, Quaternary and present time scales for the Karakoram and Altyn Tagh Faults as well as major strike-slip faults of eastern Tibet. We discuss models of crustal rheology, particularly the so-called 'jelly sandwich'–'crème brûlée' models (Jackson 2002; Burov & Watts 2006). Finally, we present a working model for the evolution of the Tibetan lithosphere over the last 50 Ma based on all geological and geophysical data.

Crustal deformation models for Tibet

Argand-type underthusting models

Argand (1924) first proposed that the thick crust of Tibet resulted from the underthrusting of the entire plateau by India (Fig. 2a

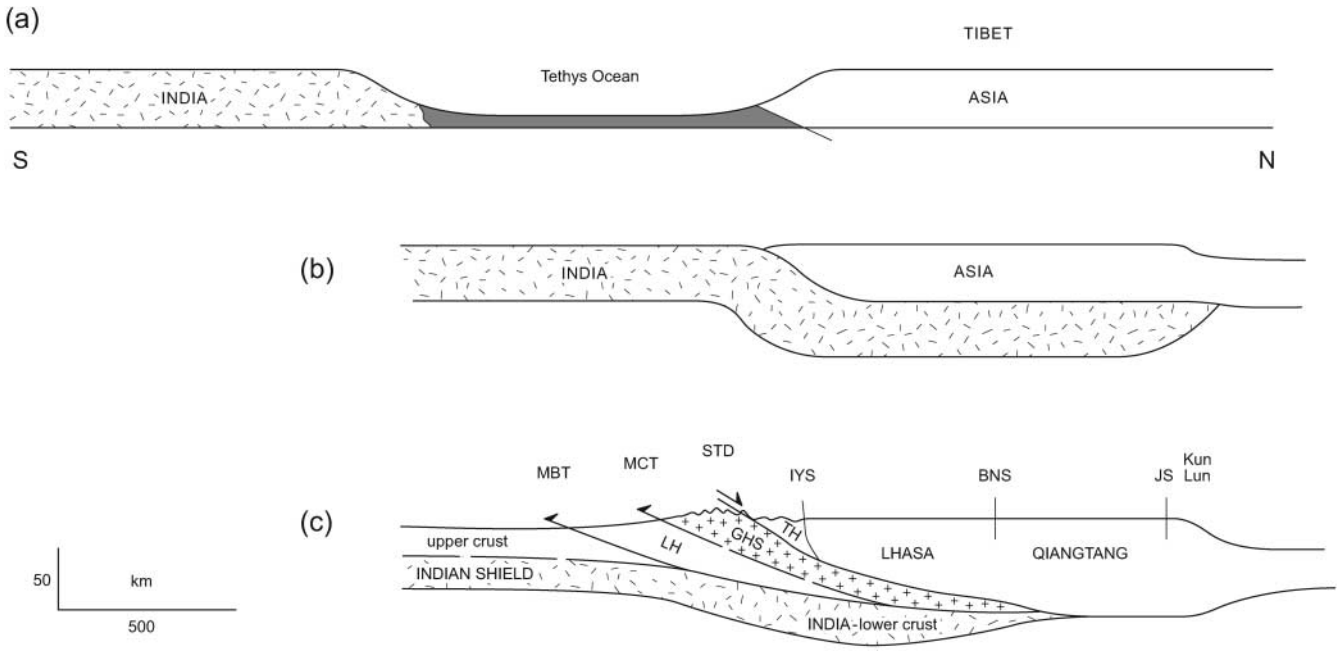

Fig. 2. (**a**) Simplified pre-collision disposition of India and Asia separated by the Tethyan Ocean. (**b**) The Argand model showing the Indian plate underthrusting the whole of the Tibetan Plateau following collision along the Indus–Yarlung suture (IYS) zone, after Argand (1924). This model implies *c.* 1000 km underthrusting of Indian crust beneath Asian crust resulting in the double thickness crust of Tibet. (**c**) An updated Argand-type model in which the upper Indian crust has been scraped off to form the Himalaya, and the Precambrian lower Indian crust has underthrust north as far as the Bangong–Nujiang suture (BNS) zone. In this model *c.* 500 km of crustal shortening across the Neoproterozoic–Phanerozoic rocks of the Himalaya is balanced by *c.* 500 km northward underthrusting of Archean–Mesoproterozoic Indian lower crust. MBT, Main Boundary Thrust; MCT, Main Central Thrust; STD, South Tibetan Detachment; JS, Jinsha suture; LH, Lesser Himalaya; GHS, Greater Himalaya Sequence; TH, Tethyan Himalaya.

and b). This model provided a plausible mechanism to explain both the double crustal thickness of Tibet and surface uplift of the plateau. Subsequent geological mapping and structural studies in the Himalaya showed that the Himalayan range is composed of folded and thrust Neoproterozoic to Palaeogene rocks that in the middle crustal levels were metamorphosed to Barrovian-facies metamorphic rocks during the Oligocene–Miocene (Searle *et al.* 1997*a*; Hodges 2000). The Archaean–Mesoproterozoic Indian plate lower crust that originally underlay the Phanerozoic passive margin sediments prior to the India–Asia collision is never exposed along the Himalaya and must therefore have underthrust the Tibetan Plateau to the north after the collision (Fig. 2c). Seismic experiments lend support the underthusting of at least the southern part of the plateau by Indian lithosphere (Owens & Zandt 1997; Tilmann *et al.* 2003; Hetényi *et al.* 2007; Nábelek *et al.* 2009). Although the Argand model does suggest rigid plate underthrusting of India beneath Asia it does not compare with the 'rigid plate' models (e.g. Molnar & Tapponnier 1975) that treat the entire Asian crust as a rigid plate.

'Rigid block' models

The 'rigid block' models in general propose that the Tibetan crust can be described in terms of a rigid or rigid–plastic medium indented by a rigid Indian plate. These 'plates', 'microplates' or 'blocks' are bounded by crustal-scale strike-slip faults that extend down to the mantle (Molnar & Tapponnier 1975; Tapponnier & Molnar 1976, 1977; Tapponnier *et al.* 1982; Avouac & Tapponnier 1993). Tapponnier & Molnar (1976) proposed that the great strike-slip faults correspond to α and β slip lines radiating out to the NW and NE away from the rigid Indian indenter. These models formed the basis of the continental extrusion model for Tibet whereby the indentation of rigid India resulted in extrusion of the Afghan block to the west, bounded by the dextral Herat fault and the sinistral Chaman fault, and the extrusion of the Indochina block to the SE, bounded by the (at present) dextral Red River Fault and the sinistral Sagaing Fault (Fig. 3a and b). Peltzer & Tapponnier (1988) used analogue plasticine models to explain the distribution of faults around Tibet and the eastward extrusion of Tibetan crust (Fig. 3c). They used a rigid Indian indenter and a free boundary to the east (SE Asia) but they placed a fixed floor and lid both below and above, inhibiting both crustal thickening and increasing elevation. As we can be certain that Tibet has both thick crust and high elevation, clearly these plasticine models are not particularly relevant to the real world. England & Molnar (1990) showed how the strike-slip faults of eastern Tibet could be interpreted in terms of right-lateral shear along the eastern margin and clockwise rotation (Fig. 4) instead of major eastward extrusion.

Peltzer & Tapponnier (1988) proposed large-scale continental extrusion of Tibet along the bounding faults of the plateau. They proposed *c*. 1000 km of right-lateral motion along the Karakoram Fault, and *c*. 500 km of left-lateral slip along the Altyn Tagh Fault. However, the granites they matched in the Pamirs to the Gangdese granites in southern Tibet were never part of the same batholith and have a different mineralogy, composition and age (Searle 1996; Searle *et al.* 1998, 2010*a*; Robinson *et al.* 2004, 2007). Estimates of geological offsets along the Karakoram Fault range from almost none (Jain & Singh 2008) through a minimum of 25 km (Searle *et al.* 2010*a*), 65 ± 5 km (Murphy *et al.* 2000), *c*. 120 km (Searle *et al.* 1998; Phillips *et al.* 2004) to 149–167 km (Robinson 2009*a*). Robinson (2009*b*) suggested that the northern part of the Karakoram Fault was no longer active based on detailed mapping of Quaternary deposits. The offsets of >400 km suggested by Lacassin *et al.* (2004*a*) and Valli *et al.* (2007, 2008) we regard as invalid correlation of offset geological markers (see Searle & Phillips 2004; Lacassin *et al.* 2004*b*, discussions). Evidence for larger offsets (*c*. 400 km) along the Altyn Tagh Fault, however, does appear to be more robust (Yue *et al.* 2003, 2005; Zhang *et al.* 2001; Cowgill *et al.* 2003).

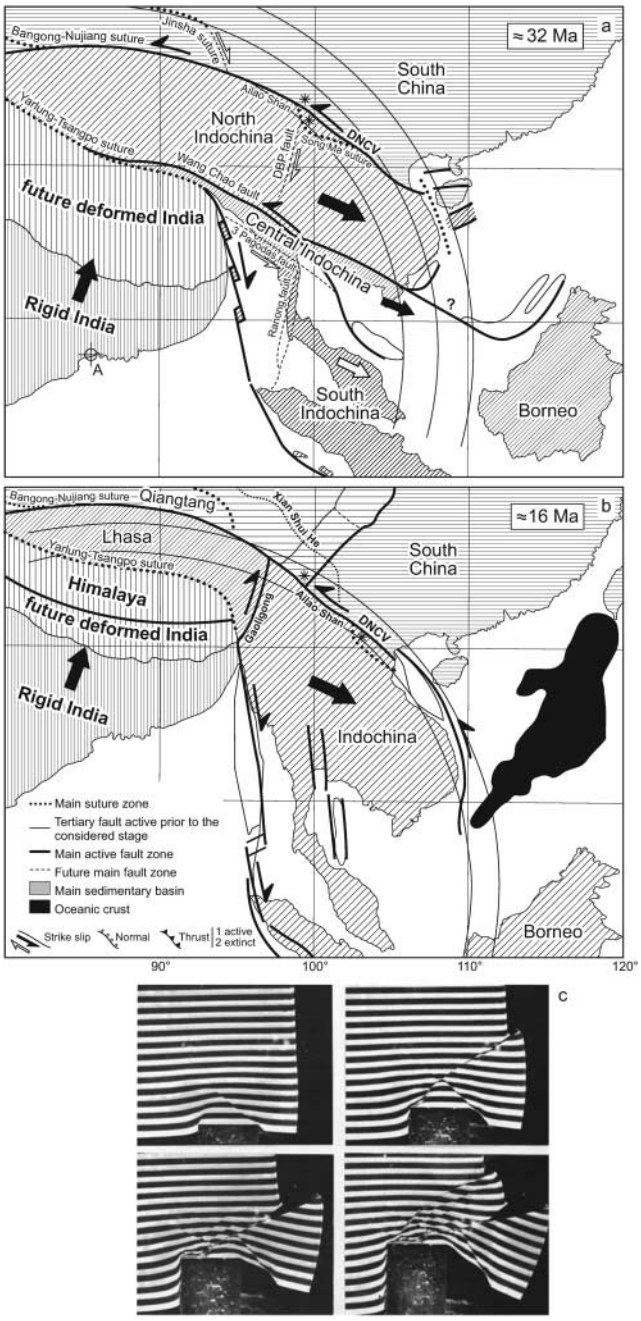

Fig. 3. Palaeogeographical reconstructions of SE Asia (**a**) at *c*. 32 Ma and (**b**) at *c*. 16 Ma, after Leloup *et al.* (2001) and Replumaz & Tapponnier (2003) illustrating the continental extrusion model. (**c**) Plasticine experiments showing plane strain indentation of a rigid Indian indenter into a layered plasticine block with a free boundary on the eastern side, after Tapponnier *et al.* (1982) and Peltzer & Tapponnier (1988).

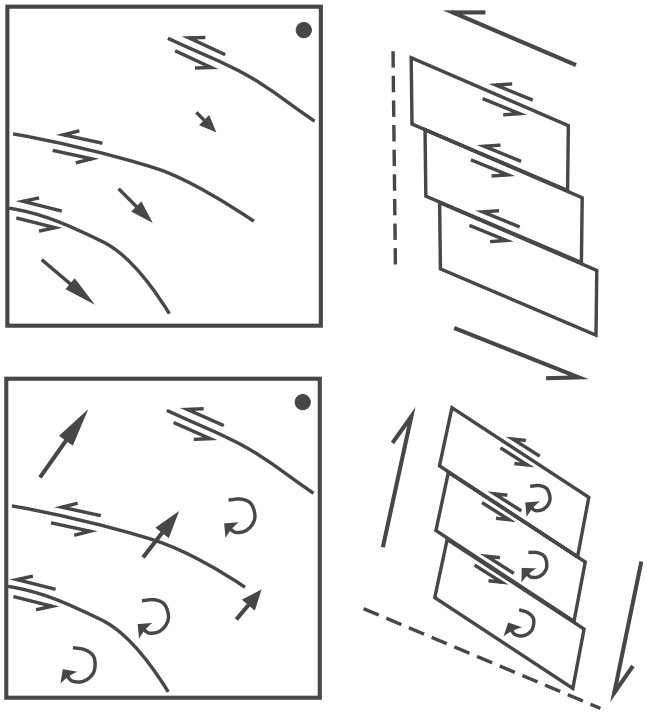

Fig. 4. Model of right-lateral shear along the eastern margin of the indenting Indian plate and clockwise rotation of crustal blocks around the Eastern Himalayan syntaxis, after England & Molnar (1990).

Avouac & Tapponnier (1993) compiled estimated slip rates for all the major faults of Tibet and concluded that the bounding faults all had fast slip rates and large amounts of offsets with as much as 50% of the total convergence absorbed by eastward extrusion of Tibet. However, many of these slip rates rely on poorly dated offset Quaternary features that were assumed to have formed during the last glacial maximum, an assumption that we now know to be incorrect (Brown *et al.* 2005). Tapponnier *et al.* (2001*b*) proposed a NE progressive growth of the plateau with large-scale eastward and southeastward extrusion facilitated by the east- and southward curving Kun Lun, Xianshui-he and Jiale faults.

The rigid body models for Tibet also imply that the major block-bounding strike-slip faults cut the entire thickened crust and extend down into the mantle, and that shear heating along the faults resulted in synshearing metamorphism and formation of crustal melt granites (e.g. Leloup & Kienast 1993; Rolland & Pêcher 2001; Lacassin *et al.* 2004*a*,*b*; Valli *et al.* 2007, 2008; Rolland *et al.* 2008). A simple test of this theory would be that U–Pb monazite ages for peak metamorphism and magmatism would all have to date strike-slip motion along the faults. U–Pb monazite ages obtained from metamorphic rocks along the Karakoram Fault are Cretaceous (Streule *et al.* 2009) and preliminary zircon ages from metamorphic rocks along the Red River Fault are Triassic in age (Searle *et al.* 2010*c*), strongly suggesting that metamorphism was earlier than, and unconnected to shearing along the fault. Because the crust beneath western Tibet is up to 90 km thick (Wittlinger *et al.* 2004; Rai *et al.* 2006), these faults would have to penetrate these depths and remain coherent, an unlikely scenario given the high geothermal gradient and great depth.

A more recent approach has been to increase the number of rigid blocks to explain the observed surface kinematics as measured by GPS observations, resulting in a micro-plate description of Tibetan active tectonics. Meade (2007) produced a kinematic model of the India–Asia collision zone based upon 554 GPS observations from Zhang *et al.* (2004) and Shen *et al.* (2005) in which they estimated slip rates on faults bounding 17 blocks. Estimates for the major strike-slip faults on the plateau are relatively low at *c.* 5–10 mm a^{-1}, but in western Tibet the model suggested a relatively large 15 mm a^{-1} right-lateral fault along a microplate boundary where there is no evidence for one. This is most probably due to the absence of GPS data in this region. Meade (2007) suggested that the optimal locking depth for the faults was 17 km, in good agreement with the seismic moment release from the historical catalogue. Thatcher (2007) produced a similar 11-microplate model for Tibet based upon 349 GPS measurements, and similarly proposed low slip rates of 5–12 mm a^{-1} for Tibet's major strike-slip faults, in contrast to the large slip rates from earlier studies consisting of larger blocks (e.g. Peltzer & Tapponnier 1988; Avouac & Tapponnier 1993). However, Thatcher (2007) acknowledged systematic misfits that point to internal deformation of the blocks, which he suggested could be smaller blocks within the larger blocks.

Continuum models

A contrasting description of continental deformation involves a continuum description of deformation distributed through a continuously deforming lithosphere driven at the boundary and by interior forces, and in which the brittle upper-crustal discontinuities are less significant. These models attempted to explain the observed patterns of crustal deformation in Tibet and proposed that crustal thickening could account for most of the deformation with only *c.* 10–20% of the India–Asia convergence taken up by lateral extrusion. Dewey & Burke (1973) proposed a model of homogeneous crustal shortening and thickening in Tibet without the need for major underthrusting of India. Continuum models describe the large-scale and long-term deformation of the continental lithosphere as a continuum with a Newtonian or power-law rheology (England & McKenzie 1982, 1983). The numerical model consists of flow of a thin sheet of power-law material over an inviscid substrate. The thickness of the viscous sheet is small compared with the loads on it, and the surface and base have zero shear stress. A major assumption in the formulation of the model is that any variation in the horizontal component of velocity with depth can be ignored. Flow in the material is in response not only to the boundary forces (e.g. the rigid indenter as an analogue of India's convergence), but also to the internal body forces owing to gradients in crustal thickness, resulting in a time dependence for the flow. The flow is controlled by two parameters: the power-law stress exponent, n, and the dimensionless Argand number, Ar, which is the ratio of stress resulting from crustal thickness contrasts to that required to deform the material (England & McKenzie 1982).

Using this approach, England & Molnar (1997*b*) produced a velocity field for Asia by estimating the stress field from observations of Quaternary faulting. They found that a large fraction (*c.* 85%) of India's convergence could potentially have been absorbed by crustal or lithospheric thickening and that the strains associated with the Altyn Tagh and Karakoram Faults slip rates of 20–30 mm a^{-1} are inconsistent with those calculated, having been overestimated owing to lack of accurate dating. Using the velocity field from England & Molnar (1997*b*), England & Molnar (1997*a*) calculated vertically averaged strains for a thin sheet of fluid in which gradients of stress point up

topographic gradients to the centre of Tibet where the gravitational potential energy is maximum and coincident with the greatest contrast in crustal thickness. Therefore the dynamics is one of creeping flow balancing gradients in stress and the gravitational body force. From this prediction, England & Molnar (1997*a*) estimated a lithospheric viscosity for Tibet of 10^{22} Pa s, and concluded that, as this is only 1–2 orders of magnitude greater than the convecting upper mantle, the continental lithosphere belongs to the fluid part of the solid Earth, rather than to the part that acts as rigid plates. England & Molnar (2005) produced an updated velocity field for Asia based upon GPS estimates as well as the Quaternary slip rates used previously (England & Molnar 1997*b*), and showed that the strain field is consistent across these time scales. They concluded that block-like behaviour is a useful descriptor for only the Tarim, South China and Amurian regions.

Molnar *et al.* (1993) proposed that convective removal of lower lithosphere beneath Tibet at *c*. 8 Ma coincided with initiation of east–west extension and volcanism, suggesting replacement of lithosphere with a hotter asthenosphere, and also coincident with major climate changes in South Asia, particularly strengthening of the Indian monsoon system. Since then, dating of over 50 volcanic samples across the plateau has shown that shoshonitic volcanism has occurred sporadically from the time of collision (50 Ma) to today (Chung *et al.* 2005, 2009), suggesting that no sudden delamination occurred at *c*. 8 Ma. North–south aligned normal faults in Tibet were initially assumed to be Pliocene–Pleistocene (Armijo *et al.* 1988) and *c*. 13.5 Ma in age (Blisniuk *et al.* 2001), but east–west extension is now known to have occurred across the entire plateau from *c*. 47 Ma to the present day based on dating of adakitic and ultrapotassic dykes (Wang *et al.* 2010). Early interpretations of a change from north–south compression to east–west extension in Tibet (e.g. Molnar *et al.* 1993) are now known to be incorrect as both are contemporaneous in time. Normal faults do not necessarily relate to crustal thinning or 'orogenic collapse' (Dewey 1988), as material was constantly being replaced by underthrusting from the south. Recent surface-wave tomography studies imply a high-velocity lithospheric mantle beneath the whole plateau (except the far north under the Kun Lun) to a depth of 225–250 km (Priestley & McKenzie 2006; Priestley *et al.* 2008), arguing strongly against any lithospheric delamination beneath Tibet. Thin viscous sheet models also ignore depth-dependent behaviour and do not allow for lateral shear or detachments between upper and lower crust or between lower crust and mantle (Royden *et al.* 1997).

Lower crustal flow models

Bird (1991) first suggested that under large plateau regions of thick crust such as Tibet, the lower crust would flow assuming power-law creep. Based mainly on GPS observations and using a 3D viscous model, Royden *et al.* (1997, 2008) proposed a model for eastern Tibet based on lower crustal flow around the Eastern Himalayan syntaxis and also around the rigid Sichuan basin (Fig. 5). This model proposed that the lower crust is very weak and is decoupled from both the upper crust and the upper mantle. Clark & Royden (2000) used the regional topographic gradients to model a Newtonian fluid flowing through a 15 km thick lower crust, estimating a viscosity of 10^{16} Pa s for beneath the plateau and 10^{18} Pa s for low-gradient margins and 10^{21} Pa s for a steep margin. Haines *et al.* (2003) also presented evidence from INDEPTH III seismic data that lower crustal ductile flow had destroyed evidence in the deep crust for earlier accretion of distinct terranes.

Surface-wave tomography and receiver function analysis from regional seismic arrays in east and SE Tibet show low shear-wave speed and presumably low mechanical strength (Yao *et al.* 2008). A sharp change in mantle anisotropy occurs beneath the SE margin of the Tibetan Plateau, with fast directions consistently east–west (Sol *et al.* 2010). Because of the coincidence between mantle anisotropy, surface strain and strike-slip faults in this region, Sol *et al.* suggested that deformation of the lithosphere was coupled across the crust–mantle boundary. If this was the case there should be evidence of a Himalayan-type crustal flow along the eastern margin of the plateau.

The eastern margin of the Tibetan Plateau along the Long Men Shan is almost as abrupt as the southern margin along the Himalaya, but the two show very different geology (Kirby *et al.* 2002). The eastern part of Tibet shows no evidence of major Late Cenozoic crustal shortening, no evidence of post-collisional metamorphism or middle–lower crustal flow as seen along the Himalaya, and no flexural foreland basin to the east. Most of the upper crustal deformation in eastern Tibet is Mesozoic but U–Pb dating of zircons in Barrovian-facies metamorphic rocks gives ages of *c*. 65 Ma (Wallis *et al.* 2003), suggesting that the crust was already thick before the India–Asia collision. North–south stretching lineations do not support the model of eastward lower crust flow. Cenozoic deformation is relatively minor with a steep thrust–fold belt, but although seismically active there is very little east–west shortening.

There is abundant evidence of upper crust clockwise rotations both in the GPS motions and the curved strike-slip faults (e.g. Xianshui-he and Jiale faults in particular), but there is no geological evidence that this deformation pattern is also present in the lower crust. Certainly there is no geological evidence that the upper or middle crust is flowing or thrusting significantly eastward from Tibet to Sichuan or Yunnan. As there are major detachments that are known to decouple the upper, middle and lower crust in southern Tibet and the Himalaya, the GPS patterns of rotation around the Eastern Himalayan syntaxis do not necessarily mimic the flow of the lower crust. The GPS motions in Yunnan and Burma (Fig. 6) are also surprising, being almost at right angles to the strike-slip fault motions along the active dextral parts of the Red River Fault and the active dextral Sagaing Fault (Gan *et al.* 2007).

Himalayan channel flow models

The channel flow model (Fig. 7) developed for the Greater Himalaya along the southern margin of the Tibetan Plateau was proposed initially from field geological mapping and strain data combined with *P–T* constraints and U–Pb dating of metamorphic rocks and leucogranites (Searle & Rex 1989; Grujic *et al.* 2002; Searle *et al.* 2003, 2006; Law *et al.* 2004, 2006; Searle & Szulc 2005; Godin *et al.* 2006). The channel flow model infers that a partially molten middle crust layer was extruded south from beneath southern Tibet to the Greater Himalaya during the Early Miocene, at *c*. 23–15 Ma. This is the span of U–Pb crystallization ages from the Himalayan leucogranites that provide evidence for melt-driven flow. The Himalayan channel flow model involves rocks wholly of Indian crustal origin that have been underthrust to the north, thickened, heated, metamorphosed and returned to the surface along a mid-crustal channel bounded by low-angle ductile shear zones below (Main Central Thrust) and above (South Tibetan Detachment).

These geological constraints were subsequently simulated in

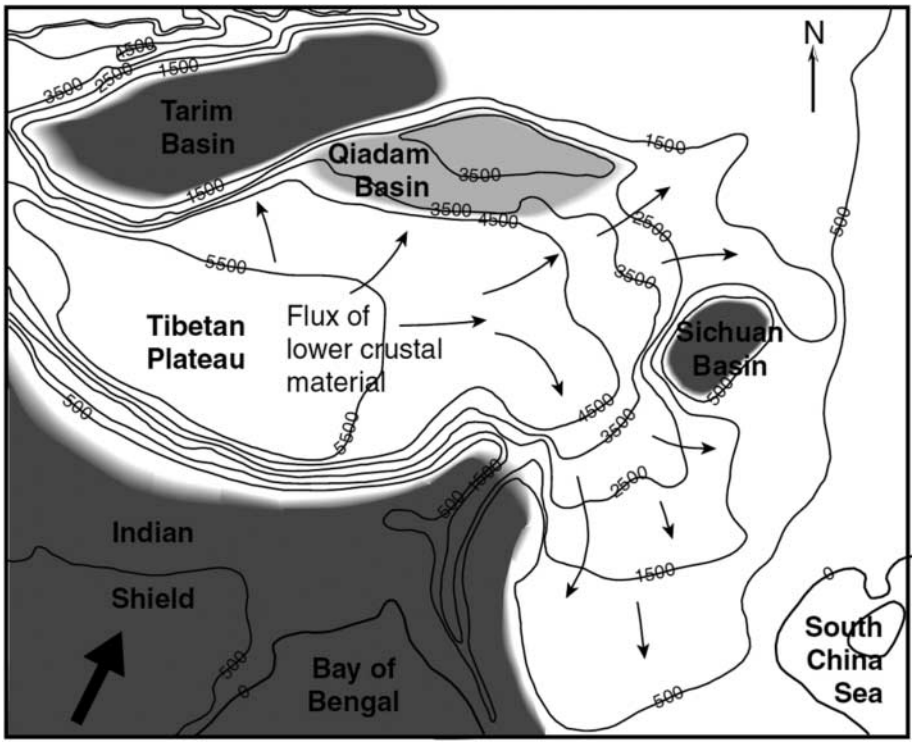

Fig. 5. Lower crustal flow model for eastern Tibet, after Royden *et al.* (1997) and Clark & Royden (2000), showing flow lines around the Eastern Himalayan syntaxis and also around the stable Sichuan basin.

the numerical models of Beaumont *et al.* (2001, 2004). In this model, partial melting occurs only in the middle crust beneath the seismogenic upper crust, but not in the lower crust, which is underthrust Indian Shield Precambrian granulites (Caldwell *et al.* 2009). In parts of the Karakoram–far west Tibet region where the Moho reaches depths of *c*. 80–90 km (Wittlinger *et al.* 2004; Rai *et al.* 2006), the lower crust must be in eclogite or high-pressure granulite fields today. The channel flow model is based on both geological constraints from the Greater Himalaya and geophysical constraints from the INDEPTH seismic experiments in southern Tibet (Zhao *et al.* 1993; Nelson *et al.* 1996). Intermediate-period Rayleigh and Love waves propagating across Tibet indicate a radial anisotropy in the middle–lower crust consistent with a 20–40% thinning of the middle crust and consistent with channel flow (Shapiro *et al.* 2004).

The geologically constrained parameters include a 10–20 km thick middle crust composed of sillimanite–K-feldspar grade gneisses, migmatites and leucogranites bounded by an inverted metamorphic sequence above the Main Central Thrust along the base and a right-way-up metamorphic sequence beneath a major low-angle normal fault, the South Tibetan Detachment, along the top (Searle *et al.* 2008, 2010*b*). From mapping of metamorphic isograds in western Zanskar and eastern Kashmir, Searle & Rex (1989) showed that the isograds are folded around a large-scale SW-verging recumbent fold with *c*. 100 km of SW displacement along both ductile shear zones along the top (South Tibetan Detachment zone) and bottom (Main Central Thrust zone). Both the Main Central Thrust and the South Tibetan Detachment are major ductile shear zones active synchronously during the Early Miocene (*c*. 24–15 Ma) when the partially molten middle crust was extruded southward at least 100 km beneath the brittle deforming upper crust of southernmost Tibet (Indian plate Tethyan or Northern Himalaya). It is possible that the 'bright spots' imaged by the INDEPTH profile, pockets of liquid at relatively shallow depth (*c*. 15–18 km) beneath southern Tibet today, are actually pockets of leucogranite magmas forming today at similar depths and *P–T* conditions as the Early Miocene leucogranites along the Himalaya (Searle *et al.* 2003, 2006; Gaillard *et al.* 2004).

Seismic constraints on the deep structure of Tibet

Lithospheric delamination or underthrusting?

Two interpretations of the lithospheric structure of Tibet are: (1) Tibet is underlain by relatively cold thickened lithospheric mantle; or (2) lithospheric delamination occurred, where, as a result of homogeneous lithospheric thickening, thickened lithospheric mantle dropped off to be replaced by hotter asthenospheric mantle at *c*. 7–8 Ma (Houseman *et al.* 1981; England & McKenzie 1982; England & Houseman 1989; Molnar *et al.* 1993; Hatzfeld & Molnar 2010). This purportedly resulted in the sudden and rapid rise of the plateau, which indirectly caused major climate and vegetation changes in South Asia (Molnar *et al.* 1993). Kosarev *et al.* (1999) presented seismic evidence for a detached Indian lithospheric mantle beneath Tibet. However, subsequent broadband seismic experiments showed variations in crustal–lithospheric structure across the plateau from shear-coupled teleseismic P waves (Owens & Zandt 1997; Schulte-Pelkum *et al.* 2005). These studies revealed a major difference in mantle structure beneath southern and northern Tibet.

Owens & Zandt (1997) interpreted the Indian continental crust and mantle lithosphere as underthrusting north as far as the Bangong suture (*c*. 32°N) and noted that the crust under northern Tibet was 10–20 km thinner than the crust under southern Tibet (Fig. 8a). The broadband seismic data show that southern Tibet is underlain by crust and relatively cold mantle of Indian continental affinity as far north as the Bangong suture, but that northern Tibet is underlain by anomalously hot, low-density upper mantle characterized by mantle anisotropy. This has been interpreted as representing significant underthrusting of strong

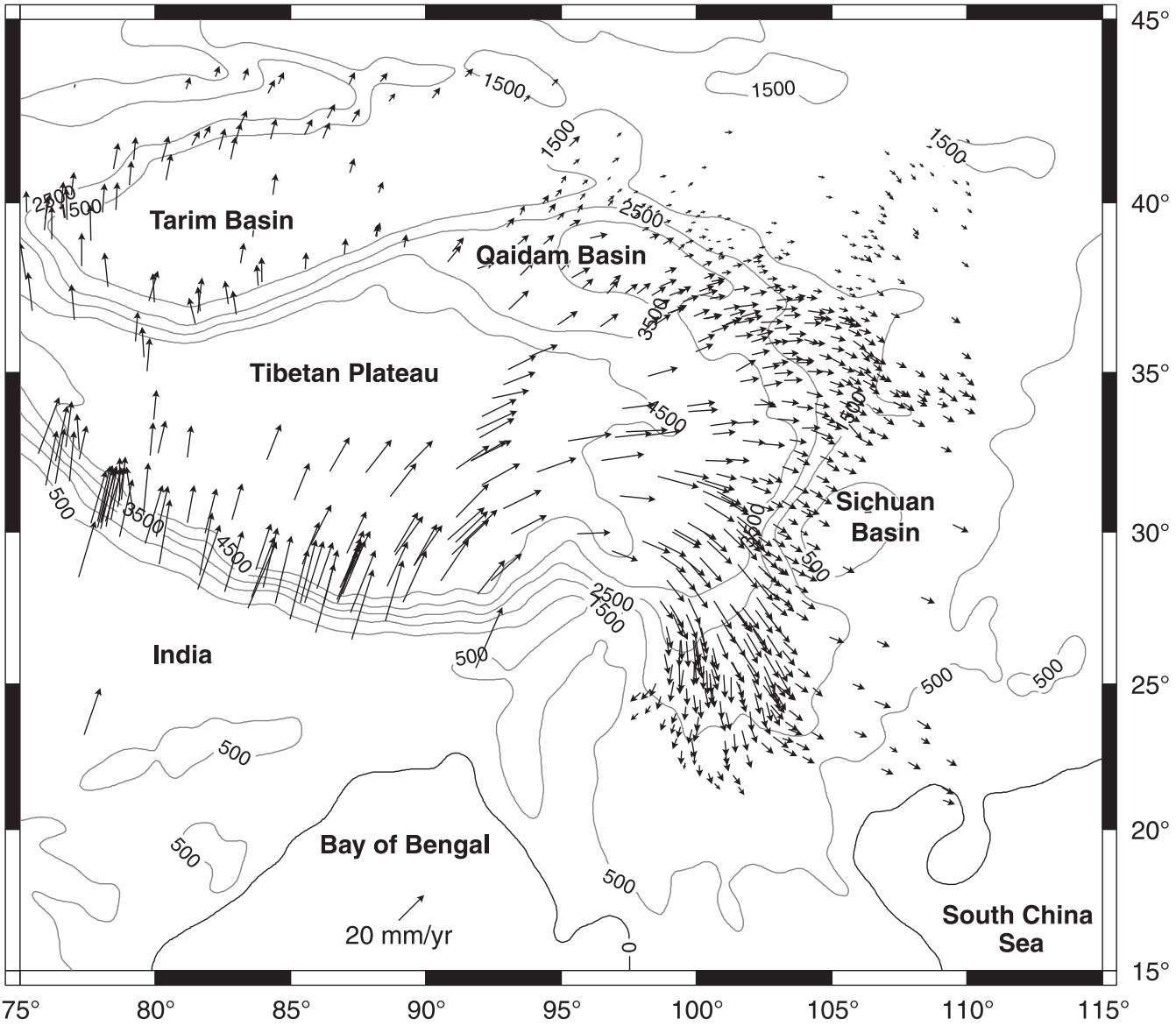

Fig. 6. GPS velocities across Tibet relative to a stable Eurasia, after Gan *et al.* (2007). Contour lines indicate smoothed surface elevations using a 200 km wide Gaussian filter.

Indian lithosphere into weaker and hotter Asian continental lithosphere (Owens & Zandt 1997). The advancing Indian lithospheric front provides a mechanism to form anisotropy in the mantle beneath northern Tibet, interpreted as lateral flow.

The INDEPTH seismic profiles (Zhao *et al.* 1993; Nelson *et al.* 1996; Haines *et al.* 2003; Tilmann *et al.* 2003) have also revealed major differences in lithospheric structure between northern and southern Tibet (Fig. 8b). The southern Tibet profiles have successfully imaged major reflectors corresponding the northerly down-dip extensions of the major Himalayan faults: the Main Boundary Thrust, the Main Central Thrust and the South Tibetan Detachment. The South Tibetan Detachment marks the upper limit of Himalayan metamorphic rocks and also the upper limit of the mid-crust zone of partial melting beneath the southernmost part of the plateau (Nelson *et al.* 1996). Tomographic images show a subvertical high-velocity zone from *c.* 100 to 400 km depth located immediately south of the Bangong suture zone that has been interpreted as representing downwelling Indian mantle (Tilmann *et al.* 2003). The INDEPTH III seismic profile extends north into the Qiangtang terrane, where the presence of crustal fluids in parts of eastern Tibet probably corresponds to low-viscosity ductile flow (Wei *et al.* 2001;

Fig. 7. The Himalayan channel flow model after Searle *et al.* (2006, 2008, 2010*b*) showing the southward extrusion of a ductile partially molten layer of middle crust. Inset diagrams show the condensed right-way isograds beneath the South Tibetan Detachment and the condensed inverted isograds above the Main Central Thrust. Photographs show the South Tibetan Detachment as exposed on Everest (top), and 70 km to the north of Everest at Dzakaa chu (Cottle *et al.* 2007). Bottom diagram shows the restored South Tibetan Detachment profile for the Everest section, after Searle *et al.* (2003, 2006) during early Miocene leucogranite formation, and the flow pathways for its exhumation beneath the Lhotse detachment (LD) and the Qomolangma detachment (QD) branches of the South Tibetan Detachment.


S
Everest
N
STD
GHS

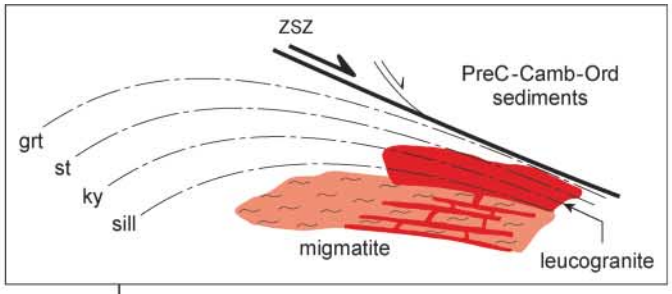
ZSZ
PreC-Camb-Ord sediments
grt
st
ky
sill
migmatite
leucogranite

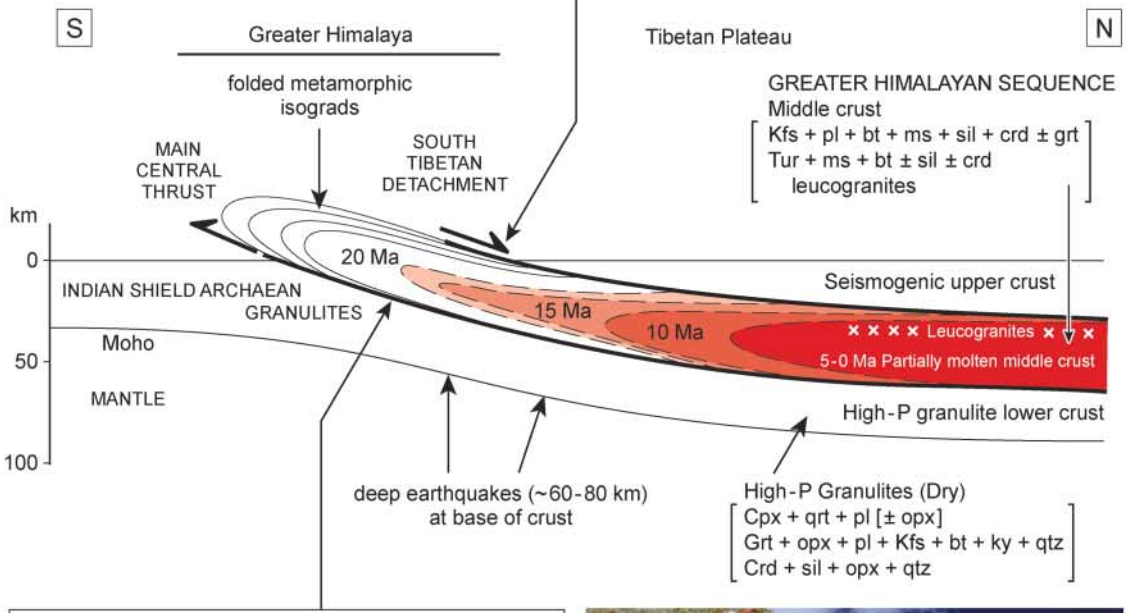
S
Greater Himalaya
Tibetan Plateau
N
folded metamorphic isograds
GREATER HIMALAYAN SEQUENCE
Middle crust
Kfs + pl + bt + ms + sil + crd ± grt
Tur + ms + bt ± sil ± crd
leucogranites
MAIN CENTRAL THRUST
SOUTH TIBETAN DETACHMENT
km
0
50
100
20 Ma
15 Ma
10 Ma
Seismogenic upper crust
INDIAN SHIELD ARCHAEAN GRANULITES
Moho
MANTLE
Leucogranites
5-0 Ma Partially molten middle crust
High-P granulite lower crust
deep earthquakes (~60-80 km) at base of crust
High-P Granulites (Dry)
Cpx + qrt + pl [± opx]
Grt + opx + pl + Kfs + bt + ky + qtz
Crd + sil + opx + qtz

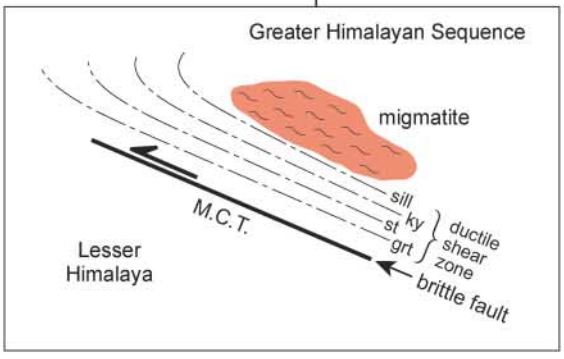
Greater Himalayan Sequence
migmatite
sill
ky
st
grt
ductile shear zone
M.C.T.
brittle fault
Lesser Himalaya

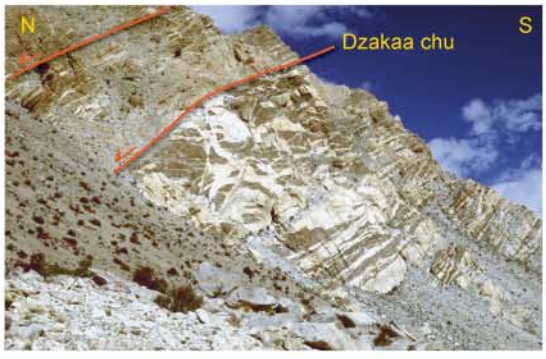
N
Dzakaa chu
S

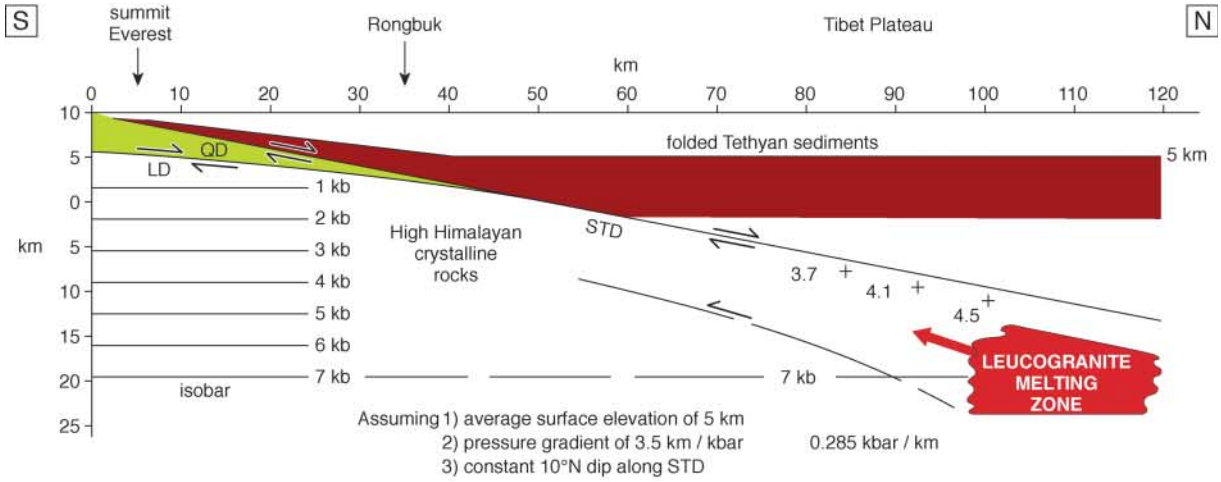
S
summit Everest
Rongbuk
Tibet Plateau
N
km
0 10 20 30 40 50 60 70 80 90 100 110 120
10
5
0
5
10
15
20
25
km
QD
LD
folded Tethyan sediments
5 km
1 kb
2 kb
3 kb
4 kb
5 kb
6 kb
7 kb
isobar
High Himalayan crystalline rocks
STD
3.7
4.1
4.5
LEUCOGRANITE MELTING ZONE
7 kb
Assuming 1) average surface elevation of 5 km
2) pressure gradient of 3.5 km / kbar
3) constant 10°N dip along STD
0.285 kbar / km

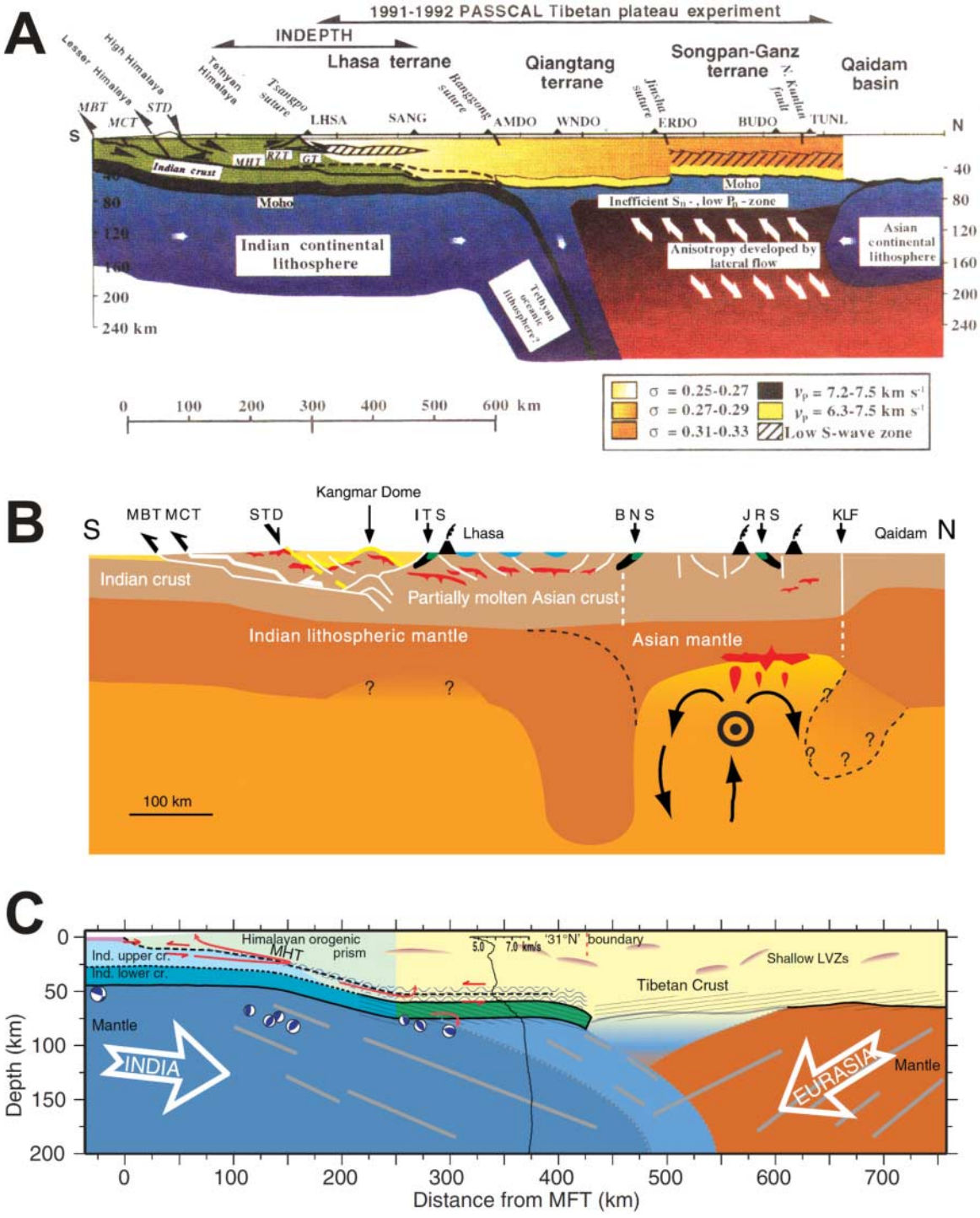

Fig. 8. Three interpretative profiles across the Tibetan Plateau as interpreted from deep seismic experiments. (**a**) Owens & Zandt (1997) profile at *c*. 92–93°E showing Indian crust (green) extending north beneath the southern part of the Lhasa Block. MHT, Main Himalayan Thrust imaged on seismic reflection data. Blue indicates mantle lithosphere. Red areas indicate region teleseismic tomography and suggest that mantle is lower velocity than southern Tibet. (**b**) Tilmann *et al.* (2003) profile showing the downwelling of Indian lithosphere beneath the Bangong suture (BNS). The convection cell beneath northern Tibet is superimposed on eastward extrusion. Red patches indicate pockets of partial melts. (**c**) Nábelek *et al.* (2009) interpretation of the receiver function profile, also showing underthrusting of Indian lithosphere as far as 31°N. The eclogitized lower crust of India is shown in green. Prominent lineations of the upper mantle fabric are shown in grey. Also shown are the possible mantle earthquake focal mechanisms, after Chen & Yang (2004). LVZ, low-velocity zone.

Haines *et al.* 2003). The INDEPTH IV line extends across northern Tibet to the Qaidam basin, along which a 15 km offset in the Moho has been detected across the northern boundary of the Tibetan Plateau from *c.* 65 km crustal thickness beneath Tibet to *c*. 48 km beneath the Qaidam basin (Vergne *et al.* 2002).

The 2002–2005 Hi-CLIMB receiver function experiment involved an 800 km long linear array of broadband seismometers extending from the Ganga basin across the central Himalaya and Lhasa block to about 34°N in the middle of the Qiangtang block (Hetényi *et al.* 2007; Nábelek *et al.* 2009). The results compare closely with the Owens & Zandt (1997) interpretation, with Indian crust underthrusting north as far as 32°N (Fig. 8c). The Moho was imaged at 40 km depth beneath the Ganga basin, dipping north to 50 km depth beneath the Himalaya and 70 km depth beneath the Indus–Yarlung suture zone. To the north the Moho remains at a constant depth beneath 200 km width of the Lhasa block but rises to a shallower depth of 65 km beneath the Qiangtang block (Nábelek *et al.* 2009). The thinner crust under the Qiangtang block is compensated by a lower density, lower velocity and hotter mantle. Recent surface-wave tomography studies imply a high-velocity lithospheric mantle beneath the whole plateau (except the far north under the Kun Lun) to a depth of 225–250 km (Priestley *et al.* 2008; Priestley & McKenzie 2006). These new data argue strongly against lithospheric delamination beneath Tibet.

Maggi *et al.* (2000), Jackson (2002), Priestley & McKenzie (2006) and Priestley *et al.* (2008) found no convincing evidence for substantial seismicity in the continental upper mantle, and proposed instead that the deep earthquakes in the eastern Himalaya occurred along the crust–mantle boundary or within the lowermost crust (Priestley *et al.* 2008, fig. 1, p. 347). Likewise in the western Himalaya, Rai *et al.* (2006) used teleseismic receiver functions to map the Indian Moho along a 700 km long profile across the Indian Himalaya as far as the Karakoram Fault and Wittlinger *et al.* (2004) used receiver functions to map the Moho NE of the Karakoram Fault. Combining these two studies shows that the Moho steepens to a depth of 75 km beneath the Karakoram Fault and reaches a maximum known depth of 90 km beneath far west Tibet. The Moho shallows to 50–60 km depth beneath the Altyn Tagh Fault and *c*. 50 km beneath the Tarim basin. The amount of underthrusting of Tarim plate material south beneath the Kun Lun and northern Tibet is debatable. Whereas the Himalaya has hundreds of kilometres of shortening of the upper crust, which must be balanced by a similar amount of northward underthrusting of Indian lower crust, there is very little Neogene shortening seen in eastern Tibet or the Kun Lun (Kirby *et al.* 2002).

The Pamir and Hindu Kush seismic zones are the deepest zones of seismicity known in the continents. The Hindu Kush shows a very narrow northward steepening zone of earthquakes down to a depth of *c*. 300 km whereas the Pamir seismic zone is a southward-dipping zone from the Alai valley (Tadjik basin crust) down to *c*. 60 km depth beneath the central Pamir (Burtman & Molnar 1993; Pegler & Das 1998). There is debate about whether the deep earthquakes are related to subduction of a small Black Sea type oceanic basin within the continental crust (Chatelain *et al.* 1980; Roeker 1982) or whether they are related to fast and deep subduction of thinned Indian continental crust since *c*. 11 Ma (Searle *et al.* 2001). As there is no geological evidence of any oceanic crust since at least the mid-Cretaceous anywhere in the Central Asia region we favour the latter option of deep and fast subduction of thinned Indian continental crust. Continental material is known to have subducted to depths as much as 300 km from several ultrahigh-pressure terranes throughout the Phanerozoic and the Hindu Kush seismic zone provides an excellent example of how this can be achieved in a continental collision zone setting.

GPS measurements in Tibet

Since the advent of the GPS in the early 1980s it has become possible to measure horizontal surface motions over hundreds of kilometres to an accuracy of a few millimetres. Wang *et al.* (2001) compiled local GPS networks occupied between 1991 and 2001 consisting of 354 stations and showed that 90% of the India–Asia relative motion (measured to be 38 mm a^{-1}) is absorbed through deformation in Tibet and its margins. Zhang *et al.* (2004) updated this dataset to include 533 stations on and around the plateau in which 36-40 mm a^{-1} India–Asia convergence was measured, with 15–20 mm a^{-1} N20°E shortening across the Himalaya, 10–15 mm a^{-1} across the Tibetan Plateau interior, and 5–10 mm a^{-1} across the northern margin. Relatively low slip rates (4–11 mm a^{-1}) were subsequently inferred for the Karakoram, Altyn Tagh and Kun Lun faults.

The latest GPS measurements from Gan *et al.* (2007) consist of *c*. 726 stations around the plateau occupied during 1998–2004. Overall, the present-day GPS rates show north–south shortening of 40 mm a^{-1} across the plateau with almost 20 mm a^{-1} east–west motion with respect to India and stable Asia (Fig. 6). GPS data tell us only about active relative motions of the surface. They do not give us any information on motion direction or shortening rates back in time, and if, as we know for southernmost Tibet and the Himalaya, the upper, middle and lower crust are decoupled along large-scale detachments, then surface GPS motions also will tell us nothing about motion of the middle or lower crust. Only if the crust and mantle are completely coupled will GPS data give us information on potential lower crust flow.

GPS measurements are used in a variety of ways to try to constrain modern slip rates for the major faults of Tibet on a decadal time scale. They are either used to directly calculate a rate based upon a profile across the fault (Bendick *et al.* 2000) or used in larger plateau-wide studies (Zhang *et al.* 2004; Gan *et al.* 2007). Additionally, they are used in block or continuum models for the plateau (e.g. the microplate models of Meade (2007) and Thatcher (2007)) or are combined with Quaternary-derived fault slip estimates to provide far-field constraints to lithospheric deformation models (England & Molnar 2005; He & Chery 2008). At present the distribution of GPS stations presents a problem in measuring the interseismic strain accumulation because of the relatively large spacing of stations compared with the fault spacing, even in the more densely sampled eastern plateau. Large regions of western Tibet are unsurveyed, making constraints on the northern Karakoram and westernmost Altyn Tagh difficult, as well as making it hard to identify whether any internal deformation of the plateau occurs in this region. The increasing spatial coverage and longer time series of satellite-derived InSAR observations could potentially fill this geodetic shortcoming in future years. Estimates of the more difficult to determine vertical component of deformation of the plateau from GPS are not yet available but will place an important constraint on models for orogenic growth versus collapse.

Timing of crustal thickening in Tibet

Pre-collision thickening

There is an increasing body of evidence that substantial crustal thickening and, by inference, surface uplift of Tibet may have

occurred prior to the India–Asia collision (England & Searle 1986; Searle 1995; Murphy *et al.* 1997; Kapp *et al.* 2005, 2007*a*,*b*; Spurlin *et al.* 2005). Crustal thickening, folding and thrusting along the Bangong suture across central Tibet occurred during Early Cretaceous times. Geological mapping along the Qiangtang terrane shows mid-Cretaceous volcanic flows and continental red beds unconformably overlying upper Palaeozoic and Triassic–Jurassic rocks and early Mesozoic blueschist-bearing mélange (Kapp *et al.* 2005, 2007*a*). Geological evidence shows that west and central Tibet must have been above sea level since the mid-Cretaceous. In the Long Men Shan along the eastern border of Tibet, U–Pb ages of zircon from Barrovian-facies metamorphic rocks are *c*. 65 Ma (Wallis *et al.* 2003) showing that crustal thickening and metamorphism must have occurred prior to the India–Asia collision. There is also abundant evidence from the Karakoram in North Pakistan (geologically the western extension of the Qiangtang terrane) that crustal thickening, kyanite- and sillimanite-grade regional metamorphism occurred episodically or semi-continuously since 65 Ma (Searle *et al.* 2010*a*).

The youngest marine sedimentary rocks in the Lhasa block are Aptian–Albian shallower marine limestones of the middle Takena Formation (Leier *et al.* 2007). After this time only continental red-bed deposition occurred, indicating that the entire region was subaerial. During the Late Cretaceous to Early Eocene (*c*. 120–50 Ma), the Lhasa Block formed the southern margin of Asia and was an Andean-type margin with a 2500 km long, up to *c*. 100 km wide, subduction-related I-type granite batholith (Gangdese granites) comprising abundant hornblende- and biotite-bearing granodiorites and granites with an extensive calc-alkaline volcanic suprastructure (Linzizong volcanic rocks; Mo *et al.* 2007, 2008; Wen *et al.* 2008*a*,*b*; Chiu *et al.* 2009). The oldest U–Pb zircon age from the Gangdese granites is 188.1 ± 1.4 Ma (Chu *et al.* 2006) suggesting a long-lasting I-type batholith from Early Jurassic to Early Eocene time. $^{40}Ar/^{39}Ar$ ages from the calc-alkaline Linzizong volcanic rocks show two discrete stages of volcanism, a widespread Cretaceous stage and an intense magmatic 'flare-up' in the Palaeocene *c*. 50 Ma when compositions vary from low-K tholeiitic through calc-alkaline to shoshonitic magma suites (Lee *et al.* 2009).

The Lhasa block must have had a high, but unquantified, topography and thick crust associated with this massive magmatic addition to the crust in addition to some pre-collision crustal shortening (Kapp *et al.* 2007*a*,*b*). The area and volume of the Trans-Himalayan Gangdese batholith is similar in proportion to the Andean batholith of Peru and Chile today, but not as long-lasting. A prominent regional unconformity has been mapped across the whole of southern Tibet where folded Takena Formation sedimentary rocks are abruptly truncated by a major unconformity beneath flat-lying Linzizong volcanic rocks dated at 60–45 Ma (Fig. 9a). There appears to be good geological evidence for crustal thickening in Tibet at least pre-mid-Cretaceous and also pre-60 Ma Linzizong volcanic successions. This deformation phase predates the India–Asia collision and the final closure of the Neo-Tethys Ocean between the two continental masses at 50.5 Ma (Green *et al.* 2008). We define the final India–Asia collision as the timing of the final marine sedimentation (planktonic foraminifera zone P8; shallow benthic zone SBZ10; Green *et al.* 2008) in the suture zone and along the north Indian plate margin (Garzanti *et al.* 1987; Searle *et al.* 1988, 1997*b*; Rowley 1998; Zhu *et al.* 2005; Green *et al.* 2008). Ophiolite obduction southward onto the passive margin of Indian preceded India–Asia collision and most probably occurred during the Late Cretaceous–Palaeocene (Searle *et al.* 1988, 1997*b*).

Post-collision thickening

One of the most enigmatic features of Tibetan geology is that despite having double normal thickness crust, there is remarkably little evidence (e.g. folding, thrusting) of post-Middle Eocene shortening across the plateau. This observation lends support for the Argand-type underthrusting of India models, but would not support the Dewey & Burke (1973) or Houseman & England (1996) pure shear thickening type models. Doubling the crustal thickness of Tibet by pure shear thickening could only be achieved by internal folding and thrusting in the homogeneous shortening model, whereas in the Argand (1924) model the Lhasa block could be simply preserved without post-collision folding and thrusting, jacked-up by underplating of India beneath (Fig. 2b). Much of the Lhasa block shows relatively undeformed granites of the Gangdese–Ladakh and other related Transhimalayan batholiths with flat-lying or gently folded Linzizong volcanic rocks. Although the Lhasa and Qiangtang blocks appear not to have undergone much shortening following the India–Asia collision, major Palaeocene to Miocene shortening has been documented in northern Tibet along the Fenghuo Shan–Nanqian thrust belts (Coward *et al.* 1988; Horton *et al.* 2002; Spurlin *et al.* 2005).

There must have been some considerable relief in the plateau during the Neogene, with a series of 1–2 km deep basins developed (e.g. Lunpola basin) especially along the Indus–Yarlung suture zone and the Bangong suture zone in central Tibet. Up to 4 km thickness of fluvial and lacustrine sediments filled the Nima basin along the Bangong suture zone during the period 27–23 Ma (Kapp *et al.* 2005). Oxygen isotope data suggest that the central part of the plateau had reached high elevation as early as Eocene–Oligocene time whereas northern Tibet became elevated only later (Rowley & Currie 2006; DeCelles *et al.* 2007). However, between 2.6 and 3 km thickness of post-collisional Eocene to Miocene red beds were deposited across extensive areas of north and NE Tibet and the Qaidam basin suggesting that the plateau has been elevated since the Eocene.

Recently, important high-grade metamorphic rocks have been discovered in SE Tibet in the Lhasa Block. A belt of eclogites with Permian sensitive high-resolution ion microprobe (SHRIMP) zircon ages (*c*. 291–242 Ma) and disrupted ultramafic rocks has been discovered in the middle of the Lhasa block (Yang *et al.* 2009). Regional kyanite- and sillimanite-grade metamorphic rocks also occur in the southeastern part of Tibet, but it is unclear if these rocks are related to deep parts of the Lhasa terrane or to the Namche Barwa syntaxis (Greater Himalayan Sequence). On the basis of petrological and geochronological data, Zhang *et al.* (2010) proposed an early granulite-facies event at *c*. 90 Ma and a later post-collision amphibolite-facies event at 36–33 Ma. In SE Tibet deeper levels of the Gangdese arc may be exposed with high-grade Nyinchi gneisses intruded by the Bayi two-mica granite at 22 ± 1 Ma and the Lunan granite–granodiorite at 25.4 ± 0.3 Ma (Zhang *et al.* 2009). These may be the only record so far of the deep crustal evolution of the Lhasa Block. It seems more probable, however, that these kyanite- and sillimanite-bearing gneisses and migmatites are actually more closely related to the Namche Barwa rocks (Indian plate Greater Himalayan Sequence) than the Gangdese batholith (Asian plate) in which case the western margin of the Eastern Himalayan syntaxis has been mis-mapped

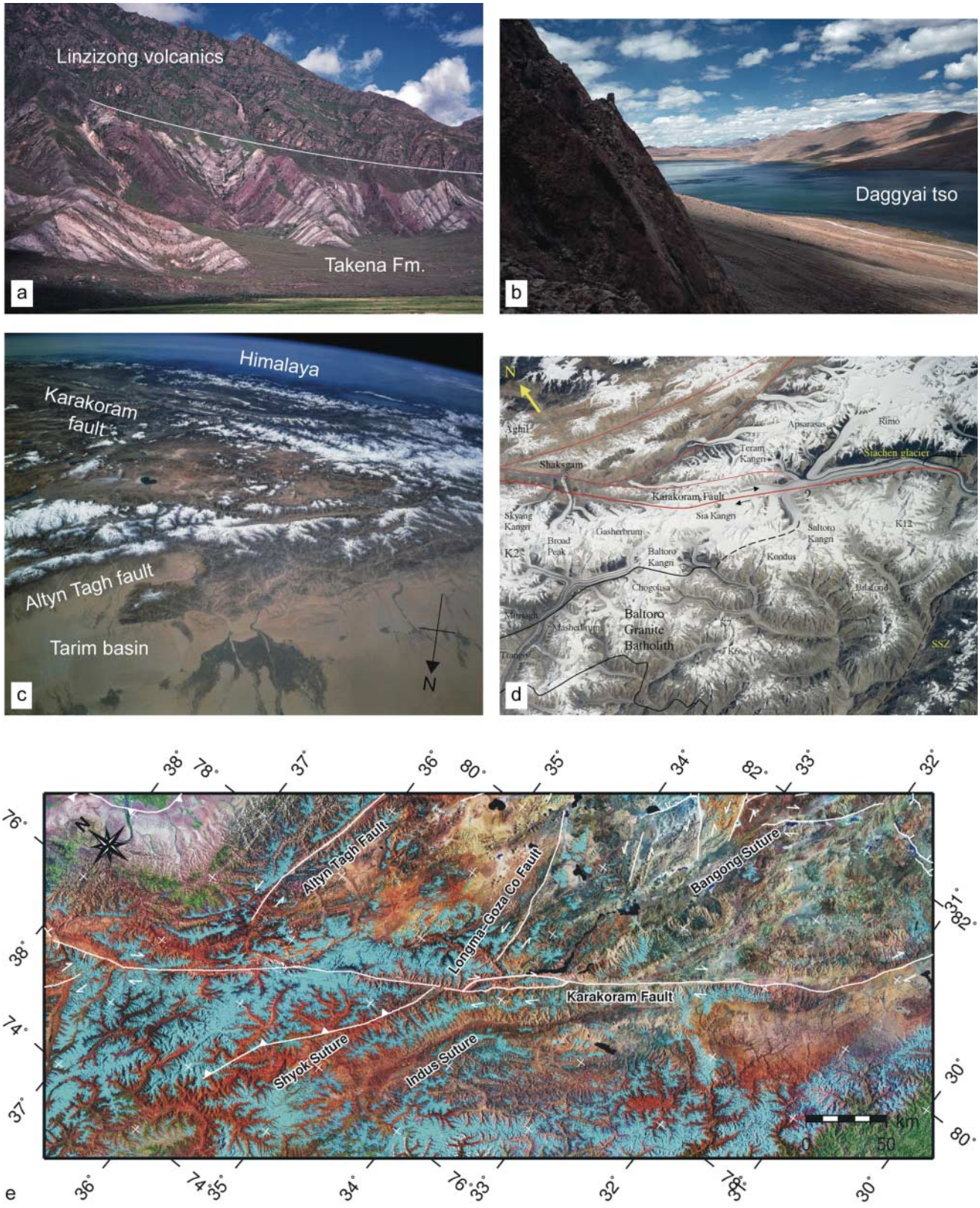

Fig. 9. (**a**) Photograph showing folded Cretaceous Takena Formation red beds beneath a prominent unconformity above which are flat-lying Linzizong volcanic rocks dated at 60–50 Ma. (**b**) North–south-aligned normal fault along the Daggyai tso graben in south–central Tibet. (**c**) NASA shuttle photograph of western Tibet; view towards SE showing the Karakoram and Altyn Tagh Faults converging towards the west in the Pamir region. (**d**) NASA shuttle photograph showing a part of the Karakoram ranges of north Pakistan and SW Tibet; view to NE. The Karakoram Fault runs along the Siachen glacier and offsets mapped vertical northern margins of the Baltoro granite in Pakistan (Searle 1991) and the Siachen batholith in Ladakh (Phillips 2008). The total geological offsets are only *c*. 17–25 km. (**e**) Landsat composite image (courtesy of Global Land Cover Facility (GLCF)) of the Karakoram Fault, Ladakh and SW Tibet.

and actually occurs further to the west of the Bayi–Linzi area. It is also likely that deeper structural levels occur in the SE Lhasa block where structural interleaving of Himalayan-type regional metamorphic crust and Gangdese-type deformed diorite–granodiorite–tonalite type Asian crust have occurred.

Volcanism in Tibet

Post-collisional volcanic rocks are widespread across Tibet and mapping, geochemical characterization and dating have revealed systematic variations in space and time (Fig. 10a and b). These volcanic rocks also allow us to make assumptions about the mantle source region beneath Tibet, and entrained xenoliths of granulite, eclogite and ultramafic rocks sourced from the lower crust and upper mantle allow us to construct a model of the crustal composition of Tibet (Fig. 11). Potassium-rich shoshonitic lavas and subordinate sodium-rich lavas were erupted across the Qiangtang terrane between *c*. 50 and 30 Ma (Chung *et al.* 1998, 2003, 2005; Ding *et al.* 2007; Wang *et al.* 2010). Ultrapotassic (lamproite) volcanic rocks requiring a hot enriched mantle lithosphere source, and adakititic lavas requiring a garnet-bearing eclogitic lower crust source were erupted coevally across the Lhasa block during the period *c*. 30–10 Ma (Chung *et al.* 2003, 2009; Guo *et al.* 2007). The Tibetan adakites consist of intermediate to felsic lithologies, lack any mafic members, are generally Na-rich and have geochemical characteristics (e.g. high MgO and Sr, low Y and heavy REE) similar to modern adakites from highly evolved island arcs above circum-Pacific subduction zones (e.g. Martin 1998). Ultrapotassic lamproites were emplaced from *c*. 25 to 10 Ma and the adakites from *c*. 30 to 10 Ma (Chung *et al.* 2003, 2005, 2009; Nomade *et al.* 2004). We can deduce from these data that the Lhasa block must have had thick crust, thick enough to have an eclogitic root, an elevated geotherm and a hot mantle during this period.

In the Qiangtang block, central Tibet, both peraluminous rhyolites and dacites and metaluminous andesitic porphyrys have adakitic geochemical characteristics. North–south-trending diabase and andesitic porphyry dykes have been dated by $^{40}Ar/^{39}Ar$ as ranging from 47 to 38 Ma, implying that Qiangtang crust was already thick by *c*. 47 Ma and that east–west extension occurred since that time (Wang *et al.* 2010). Geochemical and Nd–Sr isotopic data suggest that the dykes were derived from partial melting of enriched lithospheric mantle with some metasomatism related to subducted continental crust. Some extremely alkaline intrusive rocks including aegerine–riebeckite–sodalite–feldspathoid (leucite–nosean–nepheline-phyric) syenites and porphyrys have ages *c*. 30–29 Ma (Wang *et al.* 2010). In the Karakoram terrane (western equivalent of the Qiangtang block) numerous lamprophyric dykes (mainly biotite-bearing minettes and amphibole-bearing vogesites, with similar Oligocene–early Miocene ages intrude the northern Karakoram terrane (Searle *et al.* 1992, 2010*a*).

Chan *et al.* (2009) sampled both mafic UHT–UHP granulite and hornblende + biotite restitic xenoliths formed at 1130–1330 °C and 22–26 kbar as well as felsic granulites formed at 870–900 °C and 17 kbar from a 12.7 Ma shoshonitic dyke in SW Tibet. U–Pb zircon and monazite ages from the granulite xenoliths span 14.4 ± 0.4 to 16.8 ± 0.9 Ma. These data suggest that southern Tibet must have had a very thick crust (70–90 km) at this time. Turner *et al.* (1993) related the shoshonitic volcanism in Tibet to convective thinning of the lithosphere and its replacement by hot asthenosphere. However, recent surface-wave tomography studies imply a high-velocity lithospheric mantle beneath the whole plateau today (except the far north under the Kun Lun) to a depth of 225–250 km (Priestley *et al.* 2008; Priestley & McKenzie 2006), arguing against lithospheric detachment or sinking. Instead, we suggest that northward underthusting of cold Indian lithosphere beneath the Lhasa block from 50 Ma collision progressively shut off the hot Asian mantle source from south to north so that ages young northward across the Qiangtang terrane toward the Kun Lun.

The youngest magmatic rocks recorded in northern Tibet are potassium-rich shoshonitic volcanic rocks erupted during the Middle Miocene to Quaternary across the far north along the Kun Lun–Songpan–Ganze terrane (Chung *et al.* 2005; Wang *et al.* 2010). These shoshonites are generally less K-rich than the Eocene to Oligocene lavas in the Qiangtang terrane but still require a hot mantle source region. Also present in the far northern Tibetan Plateau in the Ulugh Muztagh region are uncommon peraluminous two-mica tourmaline-bearing leucogranites dated by the $^{40}Ar/^{39}Ar$ method at 11–4 Ma (Molnar *et al.* 1987*b*; McKenna & Walker 1990). Most recently, similar rocks were discovered from nearby regions and have been dated using $^{40}Ar/^{39}Ar$ and zircon U–Pb methods at 9–1.5 Ma (Wang *et al.* 2010; in preparation). These rocks have geochemical and isotopic characteristics (e.g. high SiO_2 contents, evolved compositions, high Sr isotope initial ratios) similar to crustal melts or S-type granites. Thus we can infer that from *c*. 10 Ma to the present time northern Tibet has had thick crust and hot mantle in the region north of the Bangong suture and south of the Kun Lun. It is possible that the Ulugh Muztagh peraluminous leucogranites are much more abundant at depth, and some of the 'bright spots' identified at high mid-crust levels in the INDEPTH III seismic profile (Tilmann *et al.* 2003) and magnetotelluric studies (Wei *et al.* 2001) may be pockets of Ulugh Muztagh type melts forming today.

Normal faults in Tibet

There are two distinct types of normal faults in Tibet: (1) north–south-aligned, steep normal faults flanking actively rifting grabens across the high plateau north of the Himalaya (Fig. 9b), some of which are seismically active; (2) east–west-striking (or NW–SE-striking in the western Himalaya), low-angle, north-dipping normal faults that bound the upper part of the Greater Himalayan Sequence with a southward extruding layer of partially molten middle crust (channel flow) that show no evidence of being currently seismically active.

North–south-aligned normal faults

Seven north–south-trending rift systems in Tibet were first identified by Tapponnier & Molnar (1977), Molnar & Tapponnier (1978) and Ni & York (1978) from seismicity and Landsat imagery. Field investigations by Tapponnier *et al.* (1981) and Armijo *et al.* (1988, 1989) confirmed that north of the Himalaya in southern Tibet, east–west extension was occurring on north–south normal faults, with rifts post-dating compressional structures. These observations led to the idea of 'orogenic collapse' (Dewey 1988). It is now known, however, that normal faults in the upper crust of Tibet were active synchronously with compressional structures and, because of the continuous underthrusting of Tibet by Indian lower crust (and to a lesser extent Tarim crust in the north), do not require a lowering of surface elevation or a decrease in crustal thickening. Armijo *et al.* (1988, 1989) noted the kinematic link between the north–south rifts terminating in the north with NW–SE-trending right-lateral strike-slip faults. They explained the rifting as due to right-lateral shear in south-

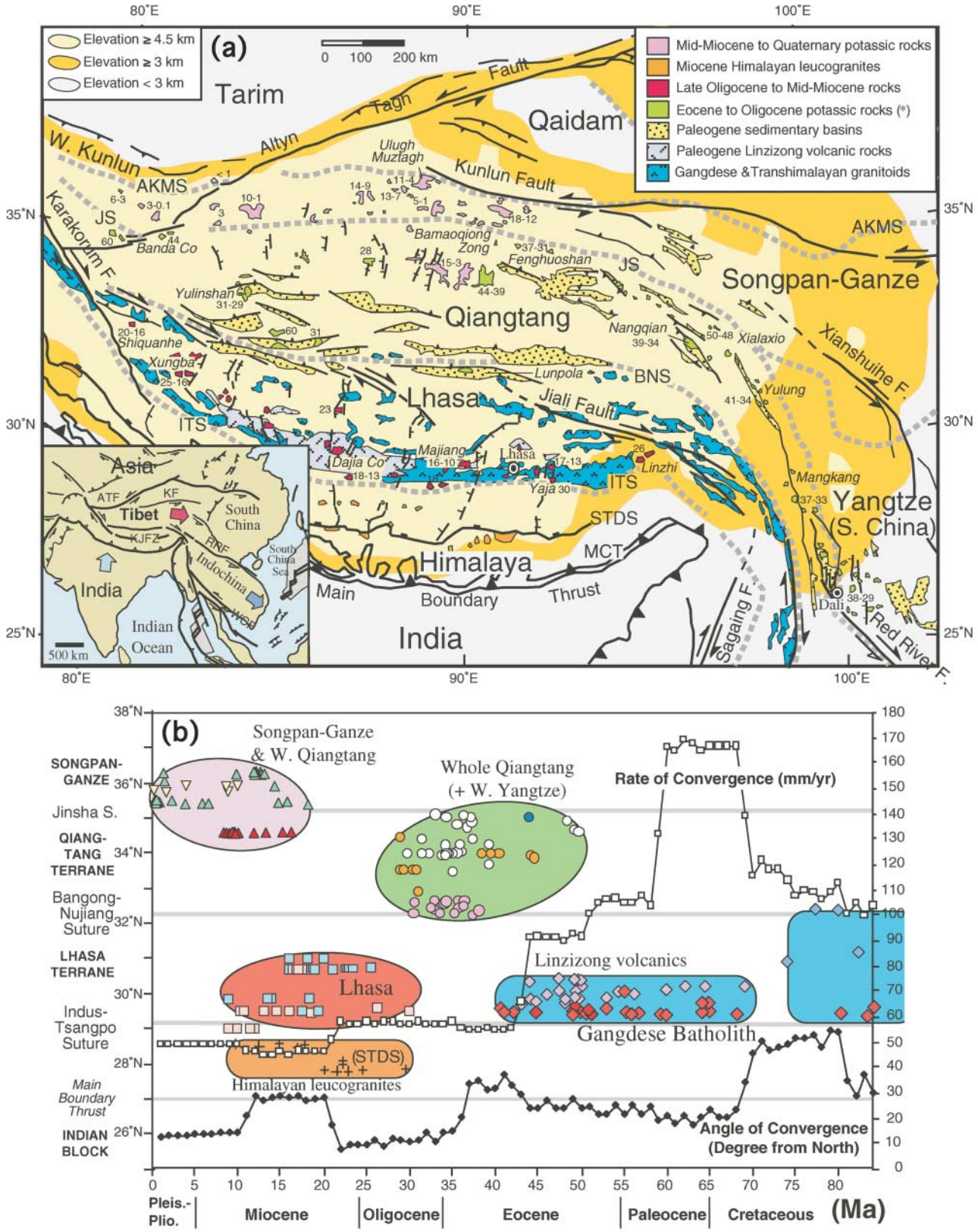

Fig. 10. (**a**) Simplified geological map of the Tibetan Plateau and surrounding areas, modified after Chung *et al.* (2005) showing distribution of post-collisional (potassic) magmatism across Tibet with their age ranges in numerals (see text and Chung *et al.* 2005, 2009; Lee *et al.* 2009; Wang *et al.* 2010, for sources of data). MCT, Main Central Thrust; STDS, South Tibetan Detachment system; ITS, Indus Tsangpo suture zone; BNS, Bangong Nujiang suture; JS, Jinsha suture; AKMS, Anyimaqin, Kun Lun, Muztagh suture; ATF, Altyn Tagh Fault; KF, Kun Lun Fault; KJFZ, Karakoram, Jiale fault zone; RRF, Red River Fault; WCF, Wang Chao Fault. (**b**) Spatial variation in Tibetan magmatism across Tibet, showing geographical distribution of volcanic rocks (left margin) against time, after Chung *et al.* (2005). (See text and Chung *et al.* (2005, 2009) for sources of data.)

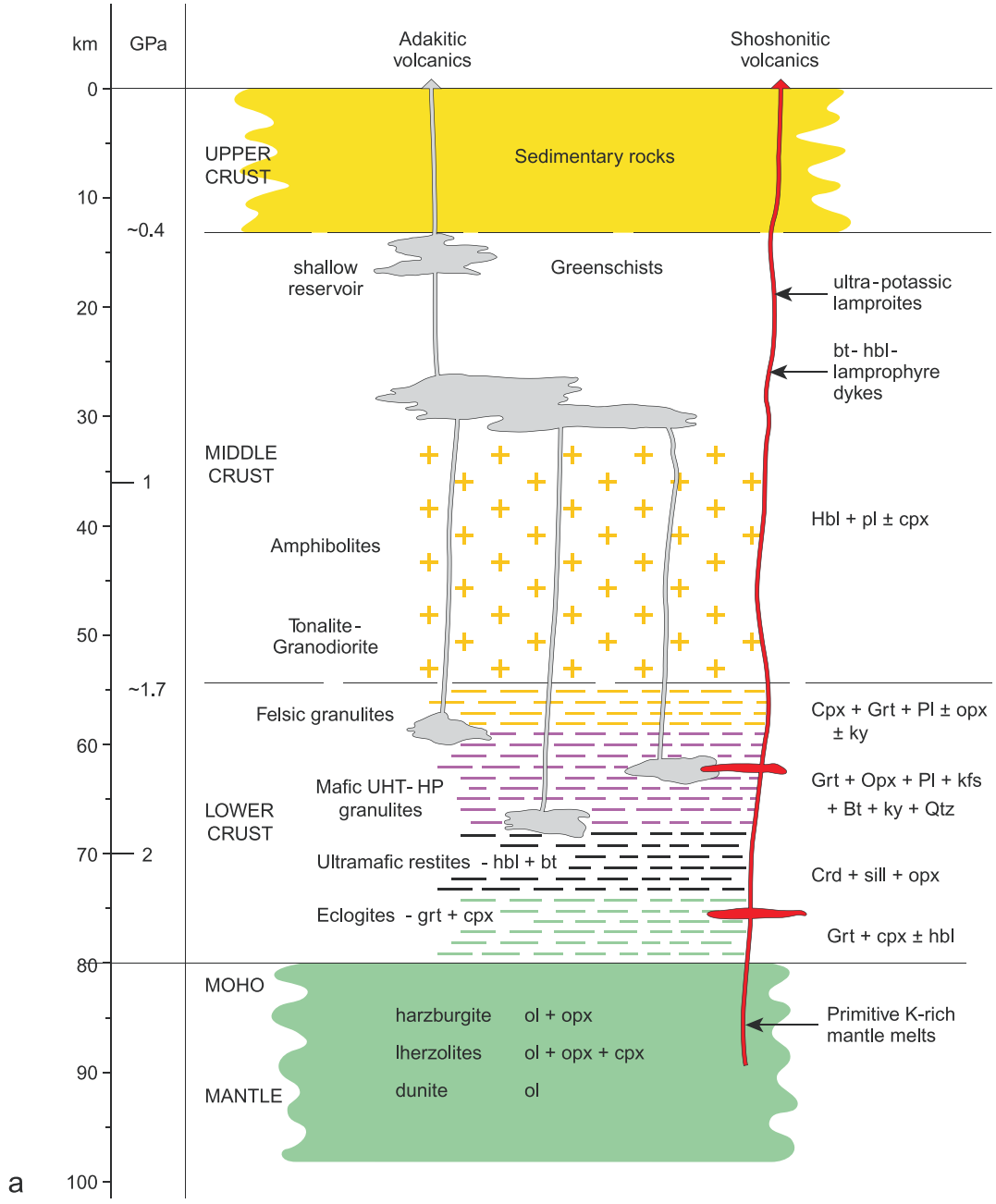
km
GPa
Adakitic volcanics
Shoshonitic volcanics
0
10
20
30
40
50
60
70
80
90
100
~0.4
1
~1.7
2
UPPER CRUST
Sedimentary rocks
shallow reservoir
Greenschists
ultra-potassic lamproites
bt- hbl- lamprophyre dykes
MIDDLE CRUST
Amphibolites
Hbl + pl ± cpx
Tonalite- Granodiorite
Felsic granulites
Cpx + Grt + Pl ± opx ± ky
Mafic UHT- HP granulites
Grt + Opx + Pl + kfs + Bt + ky + Qtz
LOWER CRUST
Ultramafic restites - hbl + bt
Crd + sill + opx
Eclogites - grt + cpx
Grt + cpx ± hbl
MOHO
harzburgite ol + opx
lherzolites ol + opx + cpx
dunite ol
MANTLE
Primitive K-rich mantle melts
a


b


c

ern Tibet along the Karakoram–Jiale fault zone, a series of WNW–ESE-aligned strike-slip faults roughly along the Bangong suture zone that terminated in the south in the north–south-aligned grabens. They proposed that the Karakoram–Jiale fault system accommodated large-scale eastward extrusion of the Tibetan rigid block. This would decouple northern Tibet from southern Tibet and allow for the eastward extrusion of the northern plateau with respect to India, but not the Lhasa block.

Previous knowledge on the more northern rifts had been based upon earthquake fault plane solutions and limited Landsat imagery interpretation (Armijo *et al.* 1988; Molnar & Lyon-Caen 1989). However, more recent field observations from northern Tibet (Yin *et al.* 1999) found significant north–south-striking active normal faults, similar to those in the south, with up to 4–8 km displacements. The age of slip onset is uncertain, but Yin *et al.* (1999) estimated a minimum slip rate of 2 mm a^{-1}. This is similar to estimates from Armijo *et al.* (1988) of several kilometres of offset with slip rates of 1–4 mm a^{-1} for faults in southern Tibet. In a mirror image to the connection of strike-slip faults to the southern Tibet rifts, the rifts of northern Tibet are connected at their southern end to left-lateral strike slip faults (Taylor *et al.* 2003). This forms a set of conjugate strike-slip faults that accommodates the coeval north–south shortening and east–west extension of the plateau (Taylor *et al.* 2003; Taylor & Peltzer 2006).

McCaffrey & Nabelek (1998) suggested that the driving force for the extension seen in southern Tibet was basal shear from the oblique sliding of the Indian plate beneath the plateau. They noted the similarities to subduction along a curved boundary and the radial vergence of slip vectors along the Himalaya. However, the India–Asia collision is widely thought to have been orthogonal and not oblique and there is no evidence of diachroneity in the timing of major events along the strike of the Himalaya (collision, peak metamorphism, anatexis, etc.) to suggest a diachronous or oblique collision.

By noting that the strikes of the rifts approximately fan outwards from the Himalayan front, Kapp & Guynn (2004) showed that the collisional stress of India punching the Himalayan arc causes the orientation of stress axes to be such that the intermediate stress σ_2 fans outward, suggesting that the strikes of normal faults will be similarly oriented. Kapp *et al.* (2008) noted low-angle normal faults flanking the Yadong–Gulu rift near Lhasa, and the Lunggar rift in west–central Tibet, but suggested that these originated as high-angle faults and were passively rotated with increased extension. Yin *et al.* (1999) observed similar normal faulting in northern Tibet as for the south, leading them to suggest that a regional boundary condition for the whole of eastern Asia was responsible for extension for the last 10 Ma, such as may be responsible for the Baikal rift. By making comparisons on the rift spacing in the Basin and Range being smaller than in Tibet and the similar onset ages for rifts across eastern Asia, Yin (2000) further supported the argument for a regional boundary condition being necessary, rather than topographic collapse or convective removal localized to the plateau. Because the regional boundary forces would be expected to die out exponentially to the north, it seems unlikely that the Baikal rift could be directly related to the Indian collision.

Using InSAR-derived measurements and body-wave seismology of eight recent moderate to large earthquakes across the plateau, Elliott *et al.* (2010) recalculated the contribution of normal faulting to the extension of the plateau to be 15–20%. By re-examining the relationship of the location of different faulting mechanisms with plateau elevation, they found that 85% of the moment release in normal faulting over the past 43 years is constrained to regions above 5 km, lending weight to the suggestion that this widespread faulting across the plateau is a result of variations in the gravitational potential energy of the lithosphere.

East–west-aligned low-angle normal faults

East–west-aligned low-angle (<30°) normal faults are restricted to the South Tibetan Detachment series of faults that form the northern upper boundary of the Greater Himalayan Sequence metamorphic rocks (Fig. 7). Originally discovered by Burg *et al.* (1984), the South Tibetan Detachment low-angle normal fault and associated ductile shear zone beneath is now known to occur along the entire length of the Greater Himalaya and form the geomorphological southern boundary of the Tibetan Plateau (e.g. Burchfiel *et al.* 1992; Searle *et al.* 1997*a*, 2003; Cottle *et al.* 2007, 2009). The South Tibetan Detachment faults form the passive roof fault of the southward extruding Greater Himalayan Sequence partially molten mid-crust during the Early Miocene (*c*. 23–15 Ma). The South Tibetan Detachment faults have a cumulative geological offset of *c*. 100 km or more and link north with the folded normal fault detachments that bound the tops of the North Himalayan domes (Lee *et al.* 2000). There is no evidence that these faults are active today, although they must have been at low angles during their Miocene slip, or that they have been rotated from steeper faults (Searle 2010).

Strike-slip faults in Tibet

The interpretation of motion along strike-slip faults relies on three different time scales: (1) active deformation over decadal time scales can be inferred from GPS and InSAR measurements, which record the accumulation of elastic strain; (2) Late Quaternary slip rates can be inferred from dating of offset surface features using *in situ* cosmogenic nuclides and radiocarbon dates; (3) long-term geological slip rates can be inferred from U–Th–Pb dating of offset granitoids or metamorphic rocks. We now review the active, Late Quaternary and long-term geological record of each of the major strike-slip faults associated with Tibetan extrusion. In the original extrusion model for Tibet (Molnar & Tapponnier 1975; Tapponnier *et al.* 1982, 2001*b*) the boundaries of the extruding Tibetan crust were thought to be the right-lateral Karakoram–Jiale fault system along the SW and south and the left-lateral Alyn Tagh fault along the north (Fig. 9c). The Altyn Tagh and Kun Lun faults both extend east beyond the topographic boundary of Tibet, and bound the transpressional Qaidam basin. The Kun Lun and Xianshui-he fault systems curve around the eastern and south-

Fig. 11. (**a**) Schematic crustal section through Tibet illustrating a model showing the proposed origin and emplacement of post-collision adakites and shoshonites. Crustal thickness is from Owens & Zandt (1997), Schulte-Pelkum *et al.* (2005) and Nábelek *et al.* (2009). Depths of adakite reservoirs and sources are from Guo *et al.* (2007). Mineral compositions of lower crust granulites and eclogites and ultramafic restites are from xenoliths entrained in shoshonitic dykes (Hacker *et al.* 2000; Chan *et al.* 2009). (**b**) Field photograph of a typical adakitic dyke intruding Lhasa block. (**c**) Shoshonitic dyke from near Xigase, SW Tibet.

eastern margins of Tibet, cutting across the eastern topographic margin of the plateau.

Karakoram Fault

The *c*. 700 km long NW–SE-aligned (*c*. 140°) vertical Karakoram Fault runs from the Tashkurgan region of the northeastern Pamir to the Kailas region of SW Tibet (Fig. 1). The fault cuts obliquely across the geological terranes of the Pamir, Karakoram–Qiangtang and Ladakh–Gangdese Ranges. The northwestern end terminates in a series of contractional faults in the central Pamir where mapping has demonstrated that major gneiss domes (e.g. Kongur, Muztagh Ata) are not offset across the fault (Robinson *et al.* 2007; Robinson 2009*a*,*b*). The southeastern end of the Karakoram Fault merges into the Indus–Yarlung Tsangpo suture zone south of Mount Kailas, where north-directed backthrusting occurs along the northern margin of the Indian plate (Searle 1996; Searle *et al.* 1997*b*) and north–south extensional faulting occurs in the Purang graben (Murphy *et al.* 2000; Murphy & Yin 2003). The Karakoram Fault forms one major strand along the Nubra Valley but in the Tangtse region the fault splays into two branches, the main strand, the Tangtse Fault strand, to the SW and the Pangong Fault strand to the NE, both of which display spectacular mylonites (Fig. 12). Stretching lineations along the Nubra valley sector plunge between 0 and 20° NW and at Tangtse plunge *c*. 30° NW. Between the two strands the Pangong Range is an exhumed metamorphic complex comprising amphibolites, hornblende–biotite diorites, orthogneisses, migmatites and abundant leucogranite dykes.

Debate centres around two end-member models. One model suggests that metamorphic rocks and leucogranites exhumed along the Karakoram Fault zone are synkinematic with regard to strike-slip shearing, with heat advection by magmatic ascent along a lithospheric-scale fault. The second model suggests that metamorphism and most leucogranites exhumed along the fault were pre-kinematic with respect to strike-slip shearing. Critical to the discussion concerning the age, offsets and slip rates along the Karakoram strike-slip fault are the following three factors.

(1) Did the metamorphism along the Karakoram Fault result from shear heating (Rolland & Pêcher 2001; Lacassin *et al.* 2004*a*,*b*; Valli *et al.* 2007, 2008; Rolland *et al.* 2008), or was it earlier and unrelated to shearing motion along the fault (Searle *et al.* 1990, 1998; Phillips *et al.* 2004; Searle & Phillips 2004; Phillips & Searle 2007)?

(2) Are the deformed leucogranites along the Karakoram Fault synkinematic with respect to strike-slip shearing (Rolland & Pêcher 2001; Lacassin *et al.* 2004*a*,*b*; Valli *et al.* 2007, 2008; Rolland *et al.* 2008; Weinberg & Mark 2008), or pre-kinematic (Searle *et al.* 1998; Phillips *et al.* 2004; Searle & Phillips 2004; Phillips & Searle 2007)?

(3) What are the precise geological offsets along the Karakoram Fault?

Relationship between metamorphism, melting and strike-slip shearing

Deep crustal metamorphic rocks have been exhumed along the fault in the K2 region of northern Pakistan (Searle & Phillips 2007), in the Ladakh sector, north India (Searle 1996; Searle *et al.* 1998; Phillips *et al.* 2004; Phillips & Searle 2007) and also in the Ayilari Range in SW Tibet (Lacassin *et al.* 2004*a*; Valli *et al.* 2007, 2008). Field relationships of sheared leucogranites along the Karakoram Fault are remarkably similar in both Tangtse, Ladakh (Searle *et al.* 1998; Phillips *et al.* 2004; Searle & Phillips 2004; Phillips & Searle 2007; Streule *et al.* 2009) and at Zhaxikang in Tibet (Lacassin *et al.* 2004*a*,*b*; Valli *et al.* 2007, 2008). Within the mylonite zone, early leucogranites display an early shear-parallel fabric with later cross-cutting dykes that intruded obliquely or orthogonal to the mylonite foliation. Outside of the mylonite zones within the Pangong Range a network of leucogranite dykes intrudes earlier orthogneisses and amphibolites with larger sheets of garnet two-mica leucogranite rotated into parallelism with the fault.

The Tangtse leucogranite is a garnet two-mica leucogranite that contains spectacular dextral S–C fabrics and crops out adjacent to the Tangste branch of the Karakoram Fault. Searle *et al.* (1998) published a $^{206}Pb–^{238}U$ SHRIMP U–Pb zircon age of 18.0 ± 0.6 Ma from this granite with inherited zircons of *c*. 106 Ma and 63 Ma. The age was more precisely refined by isotope dilution thermal ionization mass spectrometry (ID-TIMS) age dating of Phillips *et al.* (2004) to 15.55 ± 0.74 Ma. Despite assertions that the Tangtse granite is synkinematic with the strike-slip shear fabrics (Lacassin *et al.* 2004*a*,*b*; Valli *et al.* 2007; Weinberg & Mark 2008) it has been demonstrated that the S–C fabrics were superimposed on the granite at temperatures of *c*. 550–500 °C after the granite crystallized and that the dextral strike-slip shear fabrics die out away from the fault (Searle *et al.* 1998; Phillips *et al.* 2004; Phillips & Searle 2007) so the age of the leucogranite must be a maximum age of initiation of ductile shear at this locality.

Phillips (2008), Phillips *et al.* (2004) and Phillips & Searle (2007) carried out detailed mapping combined with numerous U–Pb ID-TIMS age-dating of granitoids along the shear zone. They concluded that ductile shearing along the Tangtse strand of the fault occurred between 15.68 and 13.73 Ma, the U–Pb ages being determined from both early deformed leucogranites parallel to the mylonite foliation that shows a protomylonite fabric and from late leucogranite dykes that cross-cut the ductile mylonite fabric. All granites and metamorphic host rocks within the Ladakh sector of the Karakoram Fault mylonite zones have been affected by dextral shear S–C fabrics imposed after metamorphic peak P–T conditions and after crystallization of the granites. Brittle faults along the margins of the shear zone cut all rocks and prominent pseudotachylytes within the ductile shear zone indicate palaeo-earthquake ruptures. Using $^{40}Ar–^{39}Ar$ dating, Dunlap *et al.* (1998) showed that two phases of rapid exhumation between *c*. 17 and 13 Ma and between 9 and 7 Ma corresponded to a switch from dominantly transpressional exhumation to dominantly strike-slip motion.

Lacassin *et al.* (2004*a*) worked along the southernmost part of the Karakoram Fault in SW Tibet in the Zhaxigang and Gar regions. In contradiction to the interpretations of Searle *et al.* (1998) and Phillips *et al.* (2004), they suggested that 'KFZ leucogranites resulted from shear-induced melting' and therefore that ages of the granites (*c*. 23 Ma, U–Pb zircon) would date shear movement along the fault. Lacassin *et al.* (2004*a*) stated that 'dextrally sheared gneisses [were] intruded by syn-kinematic leucogranites whose age (~23 Ma) indicates that right-lateral motion was in progress at that time' (Lacassin *et al.* 2004*a*, p. 255) and that the 'implications of syn-kinematic granite emplacement are inescapable. Our conclusion that the onset of dextral motion along the Karakoram shear zone (KSZ) occurred prior to 23 Ma is therefore robust' (Lacassin *et al.* 2004*b*, p. 161). Those workers also stated that 'the Tangtse granite, whose age (~17 Ma) was taken by Searle *et al.*, to provide a lower bound for the onset of right-lateral slip, could have formed as a result melting during shear, like the leucogranite we dated at Zhaxikang' (Lacassin *et al.* 2004*b*, p. 264).

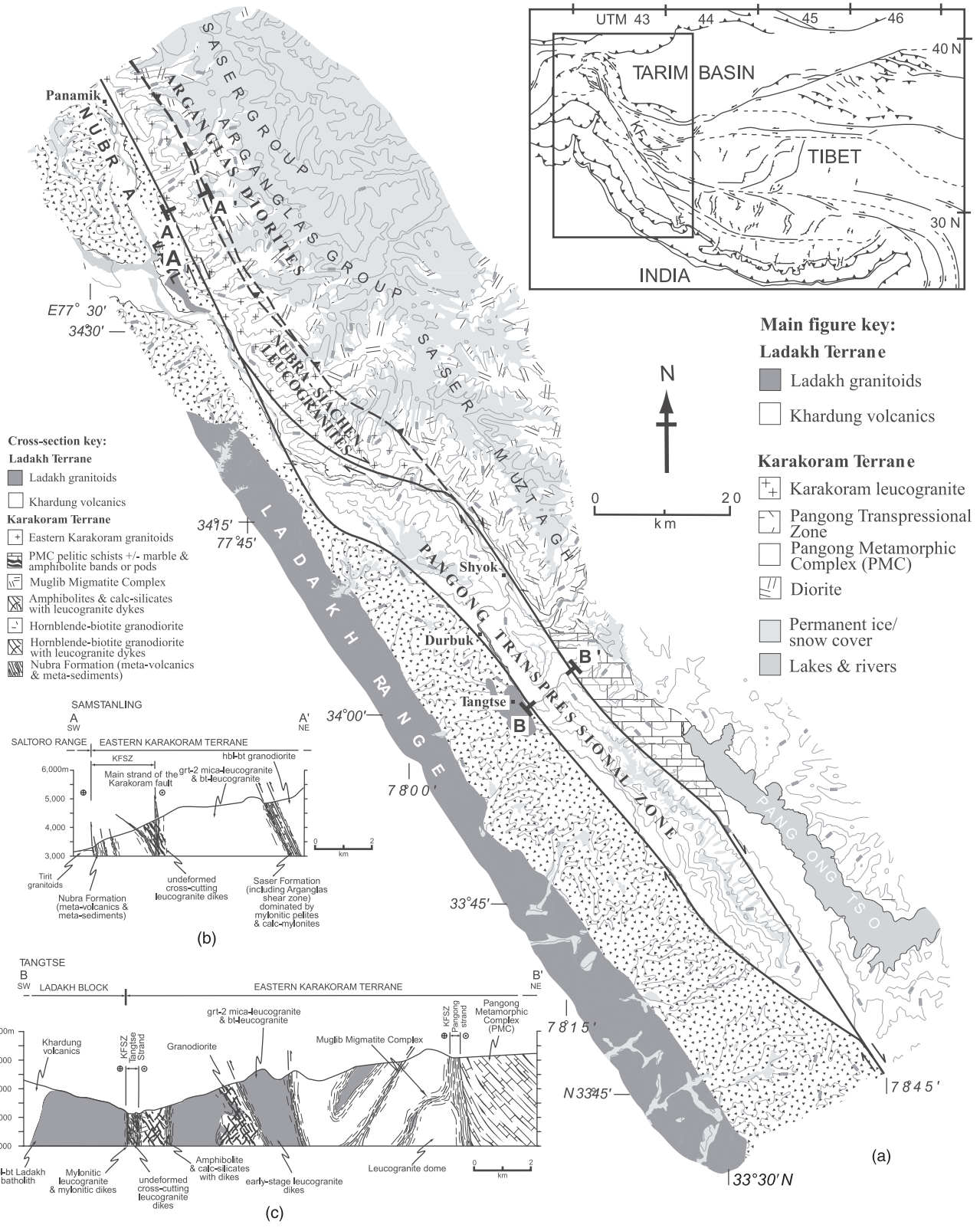

Fig. 12. Structural architecture of the Karakoram Fault in the Ladakh region: (**a**) map of the Eastern Karakoram including key sample localities; (**b**) cross-section across the Nubra valley; (**c**) cross-section across the Pangong transpressional zone, after Searle & Phillips (2007), Phillips & Searle (2007) and Phillips (2008).

Valli *et al.* (2007, 2008), also working in SW Tibet, proposed that minimum estimates for the initiation of the Karakoram shear zone were the oldest $^{40}Ar–^{39}Ar$ ages of 21.2 ± 10 Ma in agreement with their U–Th/Pb ages of >25–22 Ma. They interpreted the dated granites as being synkinematic with right-lateral shear with heat and fluid advection along the active fault, despite all the dated minerals ($^{40}Ar–^{39}Ar$ and U–He on K-feldspars, muscovite, biotite, apatite) having 'closure' temperatures lower than the granite solidus. U–Th/Pb ages of zircon and monazite are generally interpreted as dating crystallization of the magma and any ductile fabrics must obviously be formed after crystallization from the melt. Valli *et al.* (2007, p. 22) stated that 'Several lines of evidence suggest that the Tangtse granite is synkinematic to the KFZ and thus that ~18 and ~16 Ma [U–Pb ages from Phillips *et al.* 2004] are only lower bounds, not upper bounds, for the age of this fault.' They also suggested that 'Host rocks [to the Tangtse granite] were penetratively deformed in a dextral transpressive environment at temperatures ranging from >800 °C, thus above the Tangtse granite solidus temperature (750 °C) to surface conditions, suggesting synkinematic emplacement of the granite'. Phillips & Searle (2007) refuted these claims and showed that all strike-slip related fabrics were superimposed on earlier formed metamorphic and granitic rocks at temperatures less than *c*. 550 °C. Only a few late leucogranite dykes cross-cut the ductile mylonites along both the Tangtse and Pangong strands of the Karakoram Fault, and none of these dykes cut the brittle faults.

Rolland *et al.* (2008) proposed that granulite (*c*. 800 °C, 5.5 kbar)–amphibolite (700–750 °C, 4–5 kbar) to greenschist facies assemblages were developed within the Karakoram Fault zone during strike-slip shearing and suggested that the 'Tangtse granite was emplaced syn-kinematically at the contact between a LT and the HT granulite facies'. They further suggested that 'Microstructures observed within the Tangtse granite exhibit a syn-magmatic dextral S–C fabric' and that 'the Tangtse granite is not offset by, but is rather emplaced within the Karakoram Fault'. Sillimanite-grade metamorphism in graphitic pelites of the Pangong metamorphic complex was superseded by the preserved *P–T* conditions of a Bt + Ms + St + Grt + Qtz + Fsp assemblage at 585–605 °C and 6.05–7.25 kbar, equivalent to *c*. 20–25 km of burial (Streule *et al.* 2009). Laser ablation monazite U–Pb geochronology reveals that sillimanite-grade metamorphism occurred at 108.0 ± 0.6 Ma in rocks immediately adjacent to the Pangong strand of the Karakoram Fault, implying that most metamorphic rocks along the Karakoram Fault formed earlier than strike-slip shearing and cannot have formed by shear heating during Miocene strike-slip faulting (Streule *et al.* 2009).

Weinberg *et al.* (2009) reported a U–Pb zircon SHRIMP age of 15.0 ± 0.4 Ma from a two-mica leucogranite north of Satti and suggested correctly that the Karakoram Fault must have been initiated after this age. Weinberg & Mark (2008), however, implied that anatexis occurred in the Karakoram Fault shear zone during transpressive deformation and that the fault zone provided a magma transfer and production zone to the Baltoro batholith. They interpreted the spectacular S–C fabrics in the Tangtse migmatites as magma-assisted fold transposition where magma migrated into layer-parallel and axial planar sheets forming stromatic migmatites. Axial planar foliation planes acted as melt conduits forming layer-parallel leucosomes, and the migmatite textures show pervasive magma flow through a crust that was regionally hot at the time (Weinberg & Searle 1998). Although many features do clearly show syn-melting features with melt leucosomes flowing into fold hinges (Weinberg & Mark 2008, figs 5 and 6) these structures are all clearly overprinted or truncated by the later strike-slip fabrics along the Tangtse and Pangong strands of the fault. In our view, the melt textures exposed in the migmatites along the Tangtse gorge are earlier than, and unrelated to the strike-slip deformation. Similar melt textures are present in numerous locations along the southern margin of the Baltoro batholith (e.g. Masherbrum migmatite complex; Searle *et al.* 1992, 2010*a*) where they are located a long way from the Karakoram Fault and are clearly nothing to do with strike-slip deformation.

Geological offsets along the Karakoram Fault

Initial estimates of 1000 km dextral offset along the Karakoram Fault (Peltzer & Tapponnier 1988, plate 2) were proposed by matching granites in the Pamir with the Gangdese granites in SW Tibet. However, Searle (1996) and Searle *et al.* (2010*a*) showed that these granites were completely different in age, and mineralogical and isotopic composition, and were never part of the same belt. Lacassin *et al.* (2004*a*,*b*) proposed *c*. 400 km of offset along the Karakoram Fault by matching the Bangong suture zone in western Tibet with the Rushan–Psart zone in the central Pamir. However, the Rushan–Psart zone is much older than the Bangong suture and the correlation has been shown to be invalid (Searle & Phillips 2007; Robinson 2009*a*,*b*). Table 1 shows a summary of all the geological offsets proposed in the literature.

Since the India-China border region in Ladakh was first opened to non-Indian nationals in 1995, the first field studies and detailed mapping along the Tangtse and Pangong branches of the Karakoram Fault was carried out by Searle (1996), Weinberg & Searle (1998) and Dunlap *et al.* (1998). Searle (1996) proposed that geological markers such as the Shyok suture zone, the Baltoro–Karakoram granites and the course of the antecedent Indus River all showed right-lateral offsets up to 120 km maximum along the Karakoram Fault. Searle *et al.* (1998) concluded that maximum right-lateral offsets were *c*. 150–120 km, and that the fault was initiated after 18.0 Ma based on U–Pb zircon ages of a dextrally sheared leucogranite, the Tangtse granite that was cut by the fault. Murphy *et al.* (2000) proposed 66 km of right-lateral offset along the Karakoram Fault using the north-verging 'Great Counterthrust' or Main Zanskar backthrust as a pinning point. The mapping of Searle (1991), Phillips (2008) and Searle *et al.* (2010*a*) suggests that right-lateral offsets of the Early–Middle Miocene Baltoro and Siachen leucogranites could be as little as 17–25 km (Fig. 9d).

Robinson (2009*a*) suggested 149–167 km of right-lateral offset along the Karakoram Fault by matching the Late Triassic–Early Jurassic Aghil Formation carbonates across the fault in western Xinjiang. This geological offset is debatable because of the large amount of erosion in the northern Karakoram that may have wiped out the evidence. However, what is clear is that there has been no Quaternary slip along this part of the Karakoram Fault. Robinson (2009*b*) showed by detailed mapping that multiple generations of Quaternary glacial and fluvial deposits at least 150 ka old, and older Pliocene loess deposits, overlie all strands of the fault with no offset. These results are consistent with the apparent lack of neotectonic activity along the Nubra valley (Brown *et al.* 2002) and the general lack of seismicity along the fault today.

Jain & Singh (2008) interpreted the undeformed Tirit granodiorite as intruding the main penetrative shear fabric of the KSZ and therefore proposed that motion along the Karakoram Fault occurred between 75 and 68 Ma. However, the calc-alkaline Tirit granodiorite is petrologically, geochemically and structurally part

Table 1. *Published ages, offsets and slip rates for the Karakoram Fault, with brief details on the source of the estimate*

Age (Ma)	Offset (km)	Slip rate (mm a^{-1})	Data source	Reference
–	1000[a]	–	[a]Offset Ladakh–Gangdese granodiorite batholith	Peltzer & Tapponnier (1988)
–	–	$<9 \pm 4$[a]	[a]Analysis of earthquake slip-vectors	Molnar & Lyon-Caen (1989)
–	115[a]	–	[a]Offset of Indus river	Gaudemer *et al.* (1989)
–	115[a]	32 ± 8[b]	[a]Offset of Indus river [b]Inferred Quaternary slip rate based on assumed age and calculated offset of glacial moraine	Liu (1993)
–	–	32 ± 8[a]	[a]Inferred Quaternary slip rate based on assumed age and calculated offset of glacial moraine	Avouac & Tapponnier (1993)
–	200[a]	–	[a]Offset Indus–Yarlung suture	Ratschbacher *et al.* (1996)
11[a]	300[b]	30[c]	[a]Ar–Ar mica age in shear zone [b]Extrapolated offset [c]Inferred Quaternary rate from assumed age and glacial moraine offset	Matte *et al.* (1996)
4[a]	120[b]	–	[a]Extrapolated age [b]Offset of Karakoram leucogranites	Searle (1996)
–	–	*c*. 10[a]	[a]Modelled regional strain field	England & Molnar (1997*b*)
–	–	20[a]	[a]Analogue block model	McCaffrey & Nabelek (1998)
18[a]	150[b]	8[c]	[a,b]Age and offset of pre-kinematic leucogranites [c]Calculated long-term geological slip rate	Searle *et al.* (1998)
–	–	11 ± 4[a]	[a]Geodetic measurements from southwest Tibet	Banerjee & Bürgmann (2002)
–	–	*c*. 10[a]	[a]Modelled regional strain field	Holt *et al.* (2000)
–	–	4[a]	[a]Calculated Quaternary slip rate based on dated age and offset of glacial moraine	Brown *et al.* (2002)
13[a]	66[b]	4[c]	[a]Ar–Ar mica age in Kailas thrust [b]Offset of Kailas thrust [c]Inferred slip rate since 13 Ma	Murphy *et al.* (2000)
23–32[a]	250–400[b]	10–13[c]	[a]Age of 'synkinematic' granites [b]Offset of sutures [c]Inferred slip rate since 23 Ma	Lacassin *et al.* (2004*a*)
–	–	1 ± 3[a]	[a]InSAR across SW Tibet	Wright *et al.* (2004)
–	–	3 ± 5[a]	[a]Geodetic measurement from Ladakh	Jade *et al.* (2004)
16–14[a]	40–150[b]	3–10[c]	[a]Age of offset leucogranites [b]Minimum-maximum offset range [c]Inferred slip rate range since *c*. 15 Ma	Phillips *et al.* (2004)
–	–	4–10[a]	[a]Plateau wide GPS measurements	Zhang *et al.* (2004)
–	–	*c*. 10[a]	[a]Calculated Quaternary slip rate based on dated age and offset of glacial moraines	Chevalier *et al.* (2005)
–	–	5[a]	[a]Reinterpretation of Chevalier *et al.* (2005)	Brown *et al.* (2005)
–	–	3–4[a]	[a]Continuum modelling with GPS and Quaternary constraints	England & Molnar (2005)
21.2[a]	120[b]	7–10[c]	[a]Ar–Ar age gives minimum for fault imitation [b]Offset of the Indus river [c]Inferred minimum slip rate range	Valli *et al.* (2007)
		0–6[a]	[a]Microplate model with GPS constraints	Meade (2007)
–	–	14–18[a]	[a]3D mechanical model with far-field GPS and Late Quaternary slip rate constraints	He & Chery (2008)
15–21[a]	480[b]	21–32[c]	[a]Compilation of age constraints along strike [b]Offset of Bangong suture [c]Slip rate using a,b	Valli *et al.* (2008)
13–25[a]	200–240[b]	8–19[c]	[a]Compilation of age constraints along strike [b]Matching Shyok suture to Shiquanhe suture [c]Slip rate using a,b	Valli *et al.* (2008)
10–23[a]	>220[b]	>10–22[c]	[a]Compilation of age constraints along strike [b]Offset of Indus suture [c]Slip rate using a,b	Valli *et al.* (2008)
	149–167[a]	6–12[b]	[a]Exposure limits of Late Triassic–Early Jurassic limestone Aghil formation [b]Inferred slip rate using initiation ages from Phillips *et al.* (2004) and Valli *et al.* (2007)	Robinson (2009*a*)
	0[a]	0[b]	[a]No offset observed in 150 ka Quaternary fans [b]Quaternary slip rate for the northern Karakoram Fault	Robinson (2009*b*)

of the Ladakh batholith (Weinberg *et al.* 2009) and, furthermore, is entirely SW of the trace of the Karakoram Fault in the Nubra valley. Interestingly, Jain & Singh (2008) reported physical continuity of the Baltoro granite batholith across the Karakoram Fault in the Nubra valley region, implying no Tertiary offset. They stated: 'Cross-cutting granite and later pegmatitic granite dykes characterize the southern front and appear to have intruded even the KSZ between ~20–14 Ma, thus precluding any large-scale strike-slip movements along the KSZ' (Jain & Singh 2008, p. 13). Furthermore, they wrote: 'Our field observations from upper reaches of the Nubra valley beyond Panamik document the presence of undeformed Karakoram Batholith that support the physical continuity of this batholith with the Baltoro-type granitoids in western Karakoram' (Jain & Singh 2008, p. 15).

Quaternary and Holocene offsets

Measurement of *in situ* cosmogenic nuclides (e.g. ^{10}Be and ^{26}Al) is widely used to date offset Quaternary surface features within a time span of 10–100 ka in addition to ^{14}C dating where suitable organic material is available. The cosmogenic isotope technique is based upon the fact that cosmogenic nuclides accumulate *in situ* from exposure of, for example, quartz grains to cosmic rays at or near the land surface (e.g. Nishiizumi *et al.* 1986, 1989). Therefore it is possible to date the time at which an alluvial fan containing the measured sample was abandoned and left exposed, and, in principal, if a fan offset is measurable in that fan as it crosses the fault, then a slip rate can be determined. Although the technique is routinely used, factors such as surface production rate, erosion rate and inheritance may be poorly constrained or unknown. In addition, site selection and sampling techniques appear variable. Consequently, attributing a surface age to an offset alluvial fan is not always straightforward and can have a large effect on the inferred slip rate. There is an uncertainty associated with the reconstruction of offset risers of alluvial fans when assigning an age to the initiation of offset to the upper or lower terrace age, which can result in slip rates varying by a factor of 1.2–5 (Cowgill 2007).

The high Quaternary slip rates initially defined for the Karakoram Fault were based on assumed postglacial ages of 10 ± 2 ka of displaced moraines by Liu (1993), who carried out a detailed study of offset geomorphological features along the southern strand of the Karakoram Fault in SW Tibet. Twenty-four sites were examined using SPOT images, with offsets varying from 50 to 350 m. These offsets, coupled with an assumed postglacial age of formation, allowed Liu (1993) and Avouac & Tapponnier (1993) to infer a rapid slip rate of 32 ± 8 mm a^{-1}. Despite an accepted offset determination, if their assumed postglacial age were incorrect, then a significant cornerstone of the extrusion hypothesis would be untenable. The assumed moraine age of 10 ± 2 ka by Liu (1993) was supported by lacustrine sedimentary records from western Tibet (Gasse *et al.* 1991, 1996), central and eastern Tibet (Lister *et al.* 1991) and northern Xinjiang (Rhodes *et al.* 1996). Significantly, none of the sedimentary cores provided a climatic record that extended beyond *c*. 20 ka. Although valley glaciers in northern and eastern Tibet may have reached their maximum extent during the Last Glacial Maximum (LGM) at 20 ka, the maximum extent of glaciation in SW Tibet may have occurred earlier (e.g. Shroder *et al*. 1993; Gillespie & Molnar 1995; Lehmkuhl & Haselein 2000). To examine the possibility of early maximum glacial advance in Ladakh, Brown *et al.* (2002) used cosmic ray exposure dating on a terminal moraine near Leh, Ladakh. Their samples yield a mean ^{10}Be age of 90 ± 15 ka and this clearly indicates that the maximum extent of glaciation occurred well before the LGM at 20 ka. The results by Brown *et al.* (2002) are supported by an optically stimulated luminescence (OSL) date of 78 ± 12 ka from Zanskar, *c*. 50 km south of Leh (Taylor & Mitchell 2000). Therefore, the OSL and the ^{10}Be age data for Ladakh suggest that the last glacial expansion in the Eastern Karakoram occurred during Marine Isotope Stage 4, a date inconsistent with the assumed 10 ± 2 ka age for an offset moraine along the Karakoram Fault at the nearby Pangong Lake (Liu 1993). Importantly, Brown *et al.* (2002) also dated debris flow, tributary stream valleys and alluvial fans associated with highstand outflow from Pangong Lake in the Tangtse valley. These landforms yielded a ^{10}Be age of 10 ± 2 ka and, given that they are offset by the Karakoram Fault by up to 40 m, these ages provide a Holocene slip rate of 4 ± 1 mm a^{-1}. If the moraine at Pangong Lake is associated with Marine Isotope Stage 4, then its 300–350 m offset determined by Liu (1993) implies a Holocene slip rate of *c*. 4 mm a^{-1}, consistent with that determined by Brown *et al.* (2002) and an order of magnitude less than that inferred by Avouac & Tapponnier (1993).

More recently, Chevalier *et al.* (2005) suggested a slip rate of 10.7 ± 0.7 mm a^{-1} based upon ^{10}Be dating of quartz cobbles taken from offset glacial moraines. By deriving both a surface age and a displacement they concluded that, as the millenial slip rate is an order of magnitude greater than that determined by InSAR (Wright *et al.* 2004), then it implies secular variation in slip. Brown *et al.* (2005) contested these data on the basis that the scattered ^{10}Be dataset reflected a strong influence of post-depositional processes. This implies that only the oldest boulder ages should be used to conservatively assess moraine age and in this case the slip rate would concur with that of Brown *et al.* (2002) and the published geodetic rates. Although Chevalier *et al.* (2005) conceded that interpretation of a dispersed dataset is complex, and that the degree to which surface exposure ages are affected by surface reworking is 'not solidly established', they concluded that their glaciotectonic model represents the simplest and most likely interpretation.

Earthquakes along the Karakoram Fault

One of the most enigmatic aspects of the geology of the Karakoram Fault is that despite it being one of the largest and most prominent strike-slip faults in all Tibet, there appears to be little or no seismic activity along it. Either the earthquake repetition time span is very large, or we must conclude that the Karakoram Fault is barely active. One deep earthquake, the 13 February 1980 Karakoram earthquake, involved oblique thrusting at *c*. 90 ± 4 km depth but its epicentre is located to the NE of the fault (Fan & Ni 1989). The depth is consistent with the earthquake rupturing the base of the crust, and is consistent with the compressional state of stress beneath the Karakoram today, but similar to the deep earthquakes beneath Nepal–southern Tibet, it is likely that elevated temperatures in the middle crust preclude earthquakes beneath the Karakoram. Jade *et al.* (2004) suggested that active right-lateral slip along the Karakoram Fault could be no more than 3.4 mm a^{-1} based on GPS measurements.

Altyn Tagh Fault

The Altyn Tagh Fault is a major left-lateral strike-slip fault that bounds the northern part of the thickened Tibetan crust. It runs for at least 2000 km along the southern margin of the Altun Shan to the northwestern end of the Qilian Shan (Fig. 13a and b). The fault separates the high plateau to the south from the low Tarim Basin in the north, and trends ENE–WSW between 82°E and 100°E before changing strike at the southern end of the Tarim Basin, where it becomes known as the Karakax Fault and trends WNW–ESE. In the east, the fault runs north of the transpressional Qaidam basin and then splays into a series of east–west- to ENE–WSW-striking faults within the Alxa block (Darby *et al.* 2005). Unlike the Karakoram Fault, no deep crustal metamorphic rocks or granites have been exhumed along the fault, which cuts through Proterozoic–Palaeozoic rocks and Lower and Middle Jurassic non-marine sedimentary rocks (Ritts & Biffi 2000). A spectacular 200 m wide gouge zone is exposed along the Altyn Tagh Fault (Fig. 13c).

Recent estimates of slip along the Altyn Tagh Fault define three distinct time intervals: (1) long-term geological rates primarily determined from correlating geological piercing points across the fault, and therefore some also yielding a possible total

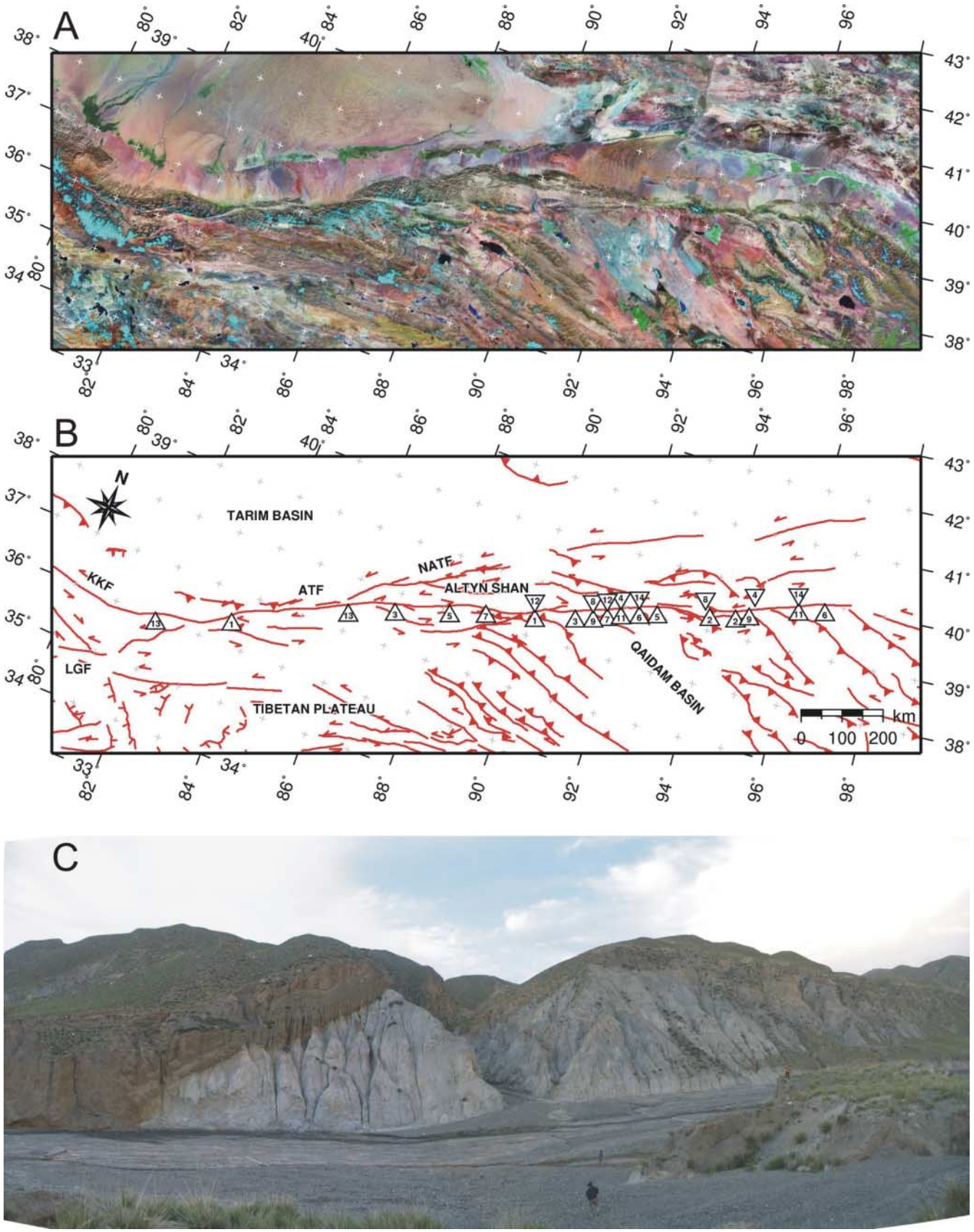

Fig. 13. (**a**) Landsat composite image (courtesy of Global Land Cover Facility (GLCF)) of the Altyn Tagh Fault in northern Tibet and (**b**) showing main active faults and offset geological markers (see Tables 2 and 3 for details). (**c**) Panorama of the wide fault gouge zone on the Altyn Tagh Fault.

offset (e.g. Cowgill *et al.* 2003; Yue *et al.* 2003); (2) Quaternary estimates derived from alluvial terrace ages and geomorphological offsets (e.g. Meriaux *et al.* 2005; Gold *et al.* 2009); (3) modern decadal geodetic measurements of interseismic strain from GPS and InSAR (e.g. Wright *et al.* 2004; Zhang *et al.* 2007). In addition to these three observation-derived slip-rate estimates, attempts have been made to model the deformation of Asia and infer slip rates from these, although many are constrained by GPS observations or Quaternary faulting (e.g. England & Molnar 2005; Meade 2007).

Geological offsets and slip rates

There are few accurately determined geological slip rates for the Altyn Tagh Fault and those that exist are predominantly restricted to observations east of 90°E. However, there are a number of geologically constrained fault total offsets. Table 2 lists measurements of offset piercing points across the Altyn Tagh Fault for the Phanerozoic. The first estimate of total offset across the Altyn Tagh Fault was from Tapponnier *et al.* (1982), who proposed 500–700 km of Tertiary offset but provided no details on offset geological markers. Peltzer & Tapponnier (1988) measured a *c.* 500 km displacement of Palaeozoic granodiorites between the western and eastern Kun Lun Shan based upon a Chinese geological map. Wang (1997) proposed a late Cenozoic left-slip offset of 69–90 km at 94°E, but owing to a poorly constrained initiation of major faulting, the range of slip rate values covers the interval 7–45 mm a^{-1}. However, Ritts *et al.* (2004) argued that this measurement was inaccurate owing to mismatches of offsets. Yin & Harrison (2000) calculated an average slip rate of 7–9 mm a^{-1} from an estimated left slip of *c.* 280 ± 30 km since the early Oligocene (*c.* 30 Ma) based on a piercing point defined by Cenozoic thrusts (Tables 2 and 3, and Fig. 14).

Ritts & Biffi (2000) proposed *c.* 400 km of left-lateral offset along the Altyn Tagh Fault based on an offset north–south-aligned Jurassic palaeo-shoreline and *c.* 360 km offset of Palaeozoic felsic plutons. Those workers and Yue *et al.* (2001, 2003) suggested a long-term Cenozoic slip rate of 12–16 mm a^{-1}, calculated from these stratigraphically correlated basin units. These offsets and slip rates are similar to the *c.* 425 km proposed by Cowgill *et al.* (2003) for early Palaeozoic piercing points. Initiation of slip along the Altyn Tagh Fault is thought to have been late Oligocene–earliest Miocene (*c.* 23 Ma) from strata in the Xorkol Basin bounding the Altyn Tagh Fault at 92°E (Yue *et al.* 2001, 2003). However, Yin *et al.* (2002) estimated a significantly earlier age of fault initiation at 49 Ma with a total slip of *c.* 470 ± 70 km, yielding a rate of 9 ± 2 mm a^{-1}. Provenance matching using zircon dating of Miocene conglomerate clasts constrains the long-term slip rate to <10 mm a^{-1} (Yue *et al.* 2003). However, this requires an accelerated slip rate between 25 and 17 Ma of 300 km offset (*c.* 40 mm a^{-1}). Therefore a two-stage evolution in fault kinematics has been suggested with fast slip and extrusion during the Late Oligocene–Early Miocene changing to slow slip and crustal thickening up to the present (Yue & Liou 1999; Yue *et al.* 2003; Ritts *et al.* 2008).

Quaternary slip rates

Estimates for the Altyn Tagh Fault slip rate over assumed Late Quaternary time scales were first made by Peltzer *et al.* (1989) and placed the rate relatively high at 2–3 cm a^{-1} (Table 3; Fig. 14). These estimates were made from satellite-measured stream offsets of 100–400 m along most of the length of the fault and assuming the offset occurred since the beginning of the Holocene. Tapponnier *et al.* (2001*a*) summarized a number of Quaternary slip rate estimates from ^{14}C and cosmogenic exposure dating from points along the entire length of the Altyn Tagh Fault (in addition to some from the Kun Lun and Haiyuan Faults). The values from Tapponnier *et al.* (2001*a*), although decreasing at either end of the Altyn Tagh Fault, show a slip rate along the central portion between 83 and 94°E of 20–30 mm a^{-1}. At 94°E, dated offset risers yield a rate of 23 ± 8 mm a^{-1} in the last 6 ka and 31 ± 6 mm a^{-1} at 87°E, which was constant over the last 110 ka (Fig. 14). Ryerson *et al.* (2006) reviewed applications of morphochronology to Tibetan active tectonics including a summary of fault slip rate determinations for major strike-slip faults of Tibet.

Examination of the available data for slip on the Altyn Tagh

Table 2. *Published estimates of the geological offsets on the Altyn Tagh Fault through the identification of piercing points across the fault*

Number	Piercing point type	Longitude (°E)	Age	Offset (km)	Reference
1	Magmatic belts (granodiorites)	84–90	Late Palaeozoic	*c.* 500	Peltzer & Tapponnier (1988)
2	Basin offset	94–95	Mid-Miocene (16 Ma) to Recent	69–90	Wang (1997)
3	Lacustrine shoreline	87–92	Mid-Jurassic (post-170 Ma)	400 ± 60	Ritts & Biffi (2000)
4	Cenozoic thrusts	92–95	Late Eocene–Oligocene (*c.* 40–32 Ma)	280 ± 30	Yin & Harrison (2000)
5	Eclogite facies	88–93	Early Palaeozoic *c.* 500 Ma	400	Zhang *et al.* (2001)
6	Ophiolite and blueschist facies	92–97	Early Palaeozoic *c.* 500 Ma	350	Zhang *et al.* (2001)
7	Cooling zones ($^{40}Ar/^{39}Ar$ and AFT)	89–92	Early–Mid-Jurassic	350 ± 100	Sobel *et al.* (2001)
8	Basin offset	91–94	Early Miocene	320 ± 20	Yue *et al.* (2001)
9	Basin offset	91–95	Oligocene	380 ± 60	Yue *et al.* (2001)
10	Palaeomagnetic rotation	86–95	Late Oligocene (24 Ma)	500 ± 130	Chen *et al.* (2002)
11	Magmatic arc rocks	92–96	490–480 Ma	370	Gehrels *et al.* (2003)
12	Clast provenance analysis	90–92	Early Miocene (23–16 Ma)	0–165	Yue *et al.* (2003)
13	Tectonic boundary and batholiths	82–86	Early–Mid-Palaeozoic (518–384 Ma)	475 ± 70	Cowgill *et al.* (2003)
14	Sandstone clast (zircon age) provenance	92–96	Oligocene	360 ± 40	Yue *et al.* (2005)

Piercing points are numbered and refer to labels of estimates used in Figure 13. The type of piercing point is given, in addition to the current longitudinal range over which the feature is offset. The age and offset (km) are listed with error estimates provided by the relevant researcher. Estimates of total offset span the Phanerozoic and appear to be consistent around 400 km for much of this time-span, indicating no early initiation of slip along the Altyn Tagh Fault in the Mesozoic. However, relatively recent motion has occurred as recorded by the reduced offset of Miocene sediments. Additionally, these relatively small offsets imply a low slip rate of the Altyn Tagh Fault since the Mid-Miocene, with a maximum around 10 mm a^{-1} (Yue *et al.* 2003).

Table 3. *Published estimates of slip rate on the Altyn Tagh Fault*

Number	Method	Longitude (°E)	Estimate (mm a^{-1})	Reference
	Geological			
1	Thrust offsets	92–95	7–9	Yin & Harrison (2000)
2	Facies offset	92–95	12–16	Yue *et al.* (2001)
3	Sedimentary offset	90–94	7–11	Yin *et al.* (2002)
4	Palaeomagnetic rotations	86–95	27–45	Chen *et al.* (2002)
5	Zircon date granite clasts	91–92	<10	Yue *et al.* (2003)
6	Tectonic belt and batholith offsets	82–86	10–16	Cowgill *et al.* (2003)
	Late Quaternary			
7	Stream, terrace and moraine offset	78–96	20–30	Peltzer *et al.* (1989)
8	Stream, fan and terrace offset	96	2–6	Meyer *et al.* (1996)
9	Cosmogenic dated offsets	78	12–23	Ryerson *et al.* (1999)
10	Cosmogenic and ^{14}C dated offsets	78	10–14	Tapponnier *et al.* (2001*a*)
11	Cosmogenic and ^{14}C dated offsets	87	25–37	Tapponnier *et al.* (2001*a*)
12	Cosmogenic and ^{14}C dated offsets	90	36–34	Tapponnier *et al.* (2001*a*)
13	Cosmogenic and ^{14}C dated offsets	94	15–31	Tapponnier *et al.* (2001*a*)
14	Palaeoseismology	90–93	10–20	Washburn *et al.* (2003)
15	Cosmogenic and ^{14}C dated offsets*	87	20–34	Meriaux *et al.* (2004)
16	Cosmogenic and ^{14}C dated offsets	94	14–20	Meriaux *et al.* (2005)
17	Cosmogenic and TL dated offsets†	85–86.5	15.5–19.5	Xu *et al.* (2005)
18	Cosmogenic and TL dated offsets†	94–95	7.5–14.5	Xu *et al.* (2005)
19	Cosmogenic and TL dated offsets†	96	3.8–5.8	Xu *et al.* (2005)
20	Cosmogenic and TL dated offsets†	97	2–2.4	Xu *et al.* (2005)
21	Offsets reinterpreted from *	86.4	7–12	Cowgill (2007)
22	Offsets reinterpreted from †	85	8–12	Zhang *et al.* (2007)
23	Offsets reinterpreted from †	86.5	5–10.5	Zhang *et al.* (2007)
24	Offsets reinterpreted from †	94–95	6–13	Zhang *et al.* (2007)
25	Offsets reinterpreted from †	96	5–9	Zhang *et al.* (2007)
26	Offsets reinterpreted from †	96.5	2–6	Zhang *et al.* (2007)
27	Offsets reinterpreted from †	96.5–97	1–2.5	Zhang *et al.* (2007)
28	Cosmogenic and ^{14}C dated offsets	86.7	8–17	Gold *et al.* (2009)
29	^{14}C dated offsets	88.5	9–14	Cowgill *et al.* (2009)
	Geodetic			
30	GPS 1994–1998	89–91	4–14	Bendick *et al.* (2000)
31	GPS 1991–1998	92	7–11	Chen *et al.* (2000)
32	GPS 1991–1998	93	4–8	Chen *et al.* (2000)
33	GPS 1993–1998	*c.* 80	4–10	Shen *et al.* (2001)
34	GPS 1993–1998	*c.* 90	7–11	Shen *et al.* (2001)
35	GPS 1994–2002	88–91	5–13	Wallace *et al.* (2004)
36	InSAR 1992–1999	79–80	0–10	Wright *et al.* (2004)
37	GPS synthesis	90	4–7	Zhang *et al.* (2004)
38	GPS synthesis	95	3–7	Zhang *et al.* (2004)
39	GPS 1998–2004	84–93	15.9	Gan *et al.* (2007)
40	GPS 1998–2004	93–95	10.8	Gan *et al.* (2007)
41	GPS 1998–2004	95–97	4.3	Gan *et al.* (2007)
42	GPS 1998–2004	97–100	1.6	Gan *et al.* (2007)
43	GPS 1998–2004	83–86	12–20	Zhang *et al.* (2007)
44	GPS 1998–2004	89–91	8.6–15.2	Zhang *et al.* (2007)
45	GPS 1998–2004	93–95	6.5–11.1	Zhang *et al.* (2007)
46	GPS 1998–2004	96	1.6–6.2	Zhang *et al.* (2007)
47	InSAR 1995–2006	94	8–10	Jolivet *et al.* (2008)
48	InSAR 1992–2000	86	6–16	Elliott *et al.* (2008)
	Plateau-scale modelling			
49	Block model	80–100	16–46	Armijo *et al.* (1989)
50	Block model (Quaternary constraint)	82–90	27–30	Avouac & Tapponnier (1993)
51	Block model (Quaternary constraint)	75–82	20–25	Avouac & Tapponnier (1993)
52	GPS constraints	80–96	6.4–8.4	Xiong *et al.* (2003)
53	Continuum model (GPS and Quaternary constraints)	80–93	8–9	England & Molnar (2005)
54	Microplate model (GPS constraint)	76–84	2–3	Meade (2007)
55	Microplate model (GPS constraint)	84–94	5–6	Meade (2007)
56	Microplate model (GPS constraint)	94–97	3	Meade (2007)
57	Microplate model (GPS constraint)	86–92	8–9	Thatcher (2007)
58	GPS and Quaternary constraints	86	5–14	He & Chery (2008)
59	GPS and Quaternary constraints	93	14–18	He & Chery (2008)
60	GPS and Quaternary constraints	96	5–14	He & Chery (2008)

The estimates are grouped by geologically constrained offsets, Quaternary dated offsets, geodetically derived rates (GPS and InSAR) and also estimates from modelling calculations of plateau-wide deformation models. Within each category, estimates are listed by ascending publication date. TL, thermoluminescence dating.

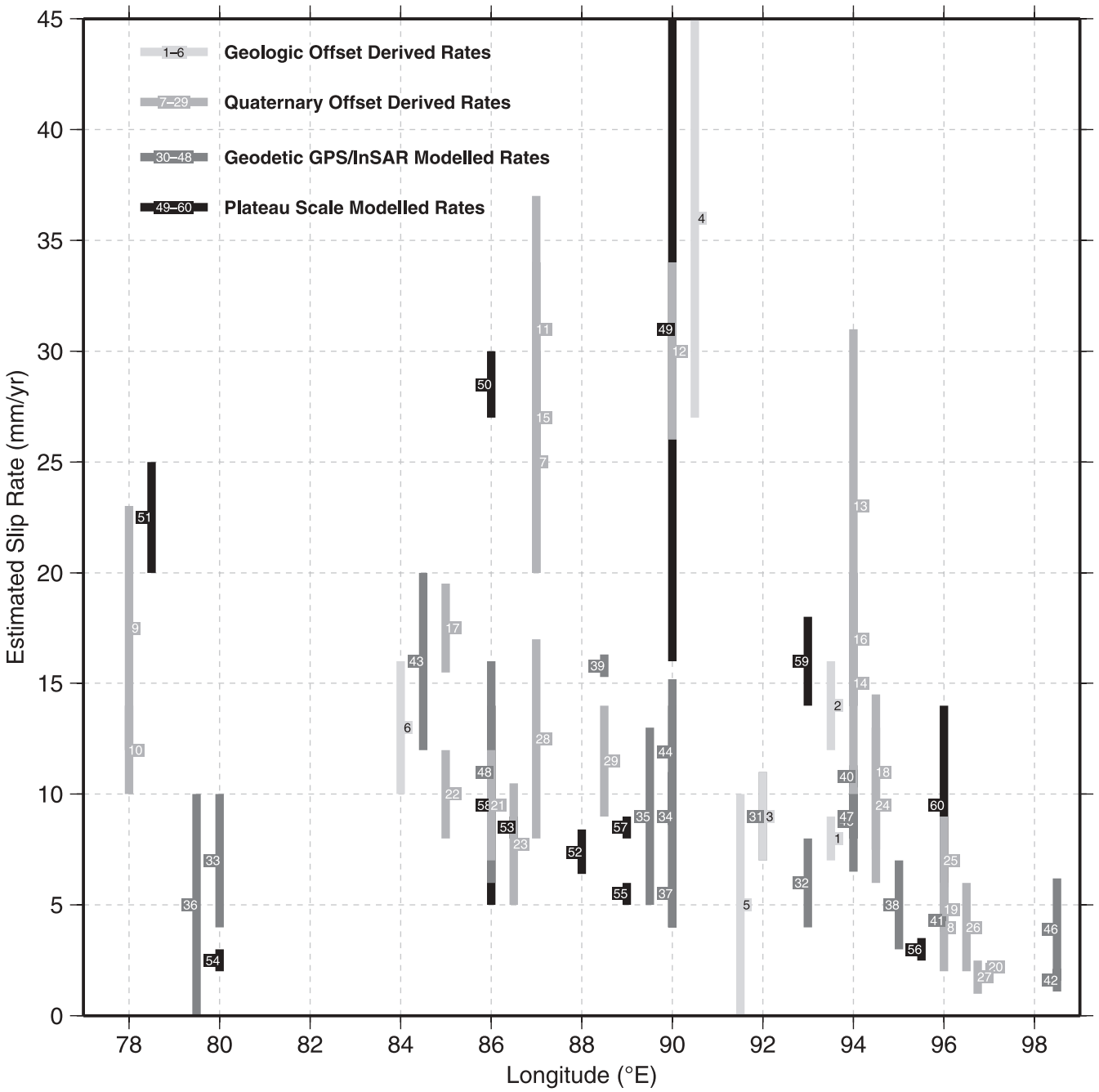

Fig. 14. Published slip rates for the Altyn Tagh Fault plotted against the longitudinal position on the fault to which the estimate refers. Rates are shaded according to the method and time scale over which the estimate is applicable. Estimates are numbered to match those given in Table 3.

Fault (Table 3; Fig. 14) suggests that there is a possible discrepancy between the geodetic or InSAR measurements and many of the millennial geological investigations that aim to quantify slip. All but the most recent rates (e.g. Gold *et al.* 2009) constrained by cosmogenic exposure dating of displaced surface features indicate that the Altyn Tagh Fault has an average millennial slip of 20–30 mm a^{-1} (e.g. Meriaux *et al.* 2004). This high rate contrasts with many of the longer-term geological or decadal rates that indicate a slip of 5–10 mm a^{-1}. Wallace *et al.* (2004) interpreted the inconsistency between slip rates as evidence of a slowing in slip rate over time or a systematic error in all Quaternary geological velocities. Palaeoseismology along the Altyn Tagh Fault indicates a slip of 10–20 mm a^{-1} over 2–3 ka (Washburn *et al.* 2001, 2003), supporting the possibility of a long-term reduction in slip rate. Wallace *et al.* (2004) noted that a likely mechanism for the slowing of the Altyn Tagh Fault may relate to increased slip along subparallel faults such as the Kun Lun Fault or a slowing of the entire northern plateau, although current datasets do not corroborate these hypotheses. The suggestion that the Altyn Tagh Fault and Kun Lun are kinematically linked is not supported by either geological or geodetic measurements for the Kun Lun; Van der Woerd *et al.* (2000)

reported a long-term uniform rate of 11.5 mm a^{-1} since 40 ka, whereas Zhang *et al.* (2004) estimated a geodetic rate of 8–11 mm a^{-1}.

Although Wallace *et al.* (2004) conceded that there is little evidence to support a widespread slowing of rates across the entire northern plateau, they suggested that a recent reduction in clockwise rotation may explain the observed disparity between long-term and recent slip rates for the Altyn Tagh Fault. Without such supporting data, Wallace *et al.* (2004) concluded that systematic errors in all cosmogenic ages may have biased the slip to higher rates and there is some validity to this point. The selection of the 'correct' age from a distributed dataset is a very real limitation of the cosmogenic dating technique and many published single ages are determined from skewed or non-Gaussian datasets that are not supported by additional independent datasets. For investigations that utilize an assumed age for postglacial landforms, recent data suggest that geomorphological features in central Asia may be an order of magnitude older than previously envisaged (e.g. Brown *et al.* 2002; Hetzel *et al.* 2002).

An alternative approach to interpreting the large discrepancy between geodetic and millennial rates was taken by Cowgill (2007). By exploring the technique of slip rate calculation, including error analysis and geomorphological interpretation, they noted that a number of uncertainties were largely overlooked in published Altyn Tagh Fault studies. Consequently, previous cosmogenic age data of displaced fluvial risers would carry such large errors that the derived slip rate will inevitably be within error of geodetic slip estimates for the Altyn Tagh Fault. Rapid slip has been suggested to occur at 20–34 mm a^{-1} (Meriaux *et al.* 2004) and 14–20 mm a^{-1} (Meriaux *et al.* 2005) from such riser offset dating at 87°E and 94°E. By applying newly derived geomorphological indices to the Cherchen He sites of Meriaux *et al.* (2005), Cowgill (2007) suggested a revised slip rate of 9.4 ± 2.3 mm a^{-1} (Table 3), one-third of the original interpretation and within error of those derived from GPS and palaeoseismic studies for this region.

At an additional site on the central Altyn Tagh Fault, Cowgill *et al.* (2009) determined well-constrained age data for offset fluvial risers, providing a millennial slip rate of 14–9 mm a^{-1} since 4–6 ka. As for Cherchen He, these data are inconsistent with previously published millennial slip rates but agree with geodetic, palaeoseismic and geological measurements. Cowgill *et al.* (2009) therefore concluded that there is no discrepancy between geological, millennial or geodetic slip rates along the Altyn Tagh Fault. Similarly, a range of slip rate estimates from Xu *et al.* (2005) based upon cosmogenic, carbon and thermoluminescence (TL) dated offset landforms yielded a rate along the central Altyn Tagh Fault of 17.5 ± 2 mm a^{-1}, which was subsequently reinterpreted in light of epistemic uncertainty in dating the terrace riser to be 5–12 mm a^{-1} (Zhang *et al.* 2007). More recent Quaternary observations by Gold *et al.* (2009) and Cowgill *et al.* (2009) at 86.7–88.5°E yielded slip rate estimates of 8–17 mm a^{-1} and 9–14 mm a^{-1} respectively, which lend support to the idea that the previously high Quaternary estimates were due to inaccuracies in interpretation of offset features, rather than pointing to secular variation (Cowgill *et al.* 2009).

Geodetically modelled slip rates

Geodetic slip rates are primarily dominated by GPS surveys consisting of data collected from both campaign and permanent measurements (e.g. Zhang *et al.* 2004; Gan *et al.* 2007), and are determined from fitting the horizontal velocities to a locked fault elastic model. The first GPS measurement for the Altyn Tagh was made by Bendick *et al.* (2000) and consisted of a transect of GPS observations on the east–central portion of the fault and the North Altyn Tagh Fault. The result pointed towards a low slip rate of 4–14 mm a^{-1} (as well as a small convergent component of 2–4 mm a^{-1}). This was subsequently updated by Wallace *et al.* (2004) and yielded an estimate of 5–13 mm a^{-1} (Table 3). Further GPS campaign measurements by Chen *et al.* (2000), Shen *et al.* (2001), Zhang *et al.* (2004) and Gan *et al.* (2007) gave estimates of 4–16 mm a^{-1} covering 89–100°E, with a decrease in slip rate from west to east (Zhang *et al.* 2007; Fig. 14). However, owing to the remote location of NW Tibet and the high plateau in the south, there are no GPS observations within 500 km to the south of the fault between 80 and 90°E. Therefore no accurate estimate of slip rate can be made in this region currently with GPS.

There is, however, an increasing number of measurements based on InSAR as a larger archive of data is accumulated. The slip rates estimated from these studies are all relatively low (Table 3; Fig. 14), with a range of 0–10 mm a^{-1} for the western portion of the Altyn Tagh Fault (Wright *et al.* 2004), 6–16 mm a^{-1} nearer the centre (Elliott *et al.* 2008) and 8–10 mm a^{-1} for the eastern portion (Jolivet *et al.* 2008). These geodetic datasets encompass measurements on the yearly to decadal scale and have been undertaken over most of the length of the Altyn Tagh Fault between 80°E and 100°E. The vast majority are in very close agreement (as is the agreement between the two geodetic methods) and cluster around 5–15 mm a^{-1}, but with a decrease towards the east (Fig. 14).

Plateau-scale models

Another approach to estimating the slip rate of the Altyn Tagh Fault comes from plateau-wide models of deformation. However, these are not direct determinations of slip rate and are not independent measurements as they are usually constrained by GPS data (e.g. Meade 2007) and sometimes additionally by the Quaternary estimates on faults (e.g. England & Molnar 2005). Using a simple block model, Armijo *et al.* (1989) calculated an approximate slip rate estimate of 31 ± 15 mm a^{-1}, given the convergence rate of India, and the assumed eastward expulsion of northern Tibet as a rigid block. Avouac & Tapponnier (1993) produced a kinematic model with four rotating blocks, and predicted a *c*. 30 mm a^{-1} left-lateral slip along the Altyn Tagh Fault, in good agreement with the apparent observed rate of 30 mm a^{-1} at the time (Peltzer *et al.* 1989).

By using GPS baseline length changes and Quaternary fault slip rates, England & Molnar (2005) calculated a crustal velocity field and strain rate in Asia, from which block-like behaviour is seen only in the Tarim and south China. They estimated a slip rate of 8–9 mm a^{-1} along the length of the Altyn Tagh Fault based upon their calculated velocity field from Quaternary faulting and GPS, which matches well their thin viscous sheet model.

Meade (2007) and Thatcher (2007) both presented similar microplate models for the deformation in Tibet, and estimated a slip rate of 5–6 mm a^{-1} and 8–9 mm a^{-1} respectively, based upon minimizing the misfit with GPS observations using a number of *a priori* delineated rotating blocks (Table 3). These models use a larger number of blocks (11–17) than the earlier models by Armijo *et al.* (1989) and Avouac & Tapponnier (1993), leading to lower slip rates. However, this trend to an increasing number of microplates to fit the observations is approaching the idea of a continuum behaviour (Thatcher 2009).

Using a mechanical model constrained by far-field GPS measurements and Quaternary slip rates, with an elastoplastic upper

crust, viscoelastic lower crust and faults embedded in the model, He & Chery (2008) attempted to determine the long-term slip rates for the Altyn Tagh, Kun Lun and Karakoram Faults. Depending upon the assumed effective fault friction, they predicted long-term slip rates on the Altyn Tagh Fault of up to 13.7–17.8 mm a^{-1} along the central portion of the fault. This rate is at the slightly higher end of the GPS-determined slip rates and is for an assumed low fault friction.

Discussion of Altyn Tagh Fault slip rates

Comparisons made between recent geodetically and geologically determined rates show broad agreement with estimates of the order of 10 mm a^{-1} (e.g. Yue *et al.* 2003; Zhang *et al.* 2007). However, many Quaternary-derived estimates from cosmogenic and radiocarbon dating of offset terraces have resulted in estimates 2–3 times greater (e.g. Meriaux *et al.* 2004). Furthermore, many of these latter observations have been subsequently reinterpreted (e.g. Cowgill 2007), and as a result Quaternary-derived estimates have also reduced to similar values. However, the disparity still leaves open the question whether differences are due to interpretation of measurements or whether they imply a secular change in fault slip rates over decadal, millennial and million-year time scales.

If early block models with high slip rates using assumed Holocene ages for offsets are neglected and the reinterpretation of Quaternary slip rates to lower values discussed above is taken as correct, then the slip rate for the Altyn Tagh for the central portion at 84–94°E lies in the range 5–15 mm a^{-1} across the three time scales (Table 3 and Fig. 14). There are fewer measurements west of 84°E, where the Altyn Tagh Fault becomes the Karakax Fault, but these point to rates $<$15 mm a^{-1}. East of 94°E, the slip rate decays to $<$5 mm a^{-1} by 99°E. Zhang *et al.* (2007) stated that this gradual decrease in slip rate to the east indicates that the Altyn Tagh Fault does not separate two effectively rigid lithospheric plates. Therefore, the overall relatively low slip rate and eastward decrease suggest that a significant proportion of the India–Asia convergence is not transferred into northeastward extrusion of the Tibetan Plateau (Zhang *et al.* 2007). The low slip rates support the notion of a Tibetan Plateau that deforms internally on a distributed network of faults in the shallow brittle crust and as a continuum at depth (England & Molnar 2005).

Earthquake history

Relatively little is known about the Altyn Tagh's earthquake history. Two of the largest recorded earthquakes on the fault occurred a fortnight apart and were a pair of M_w 7.2 events in 1924 at 84°E (Molnar *et al.* 1987*a*; Washburn *et al.* 2003). The current levels of seismicity recorded in the very limited period of the last 33 years of the GCMT catalogue show only a couple of small oblique events recorded along its entire length. There appears to have been no major ($M > 7.6$) earthquakes since at least 1911 along the Altyn Tagh Fault (Chen & Molnar 1977). A traverse across the Altyn Tagh Fault and Kun Lun by Molnar *et al.* (1987*a*,*b*) revealed evidence for relatively recent faulting from 10 m offset ridges and fresh mole tracks 0.4 m high, the freshness of which they considered to point to an earthquake in the last few hundred years. Comparing these features with those from the 1920 $M_w = 8.0$ Haiyuan earthquake (Deng *et al.* 1984), which occurred on the left-lateral strike-slip Haiyuan Fault east of the Altyn Tagh Fault in northeastern Tibet, Molnar *et al.* (1987*a*) suggested that they are comparable and represent a similarly major earthquake capable of *c*. 8 m slip over *c*. 220 km. From this, they also suggested that a poorly constrained fast slip rate of 30 ± 20 mm a^{-1} is possible, and that the Altyn Tagh Fault can absorb a significant proportion (11 ± 7 mm a^{-1}) of the India–Eurasia convergence.

Palaeoseismic rupture mapping indicates that the Altyn Tagh Fault has produced major earthquakes as large as M_w 7.8 in the Holocene (Washburn *et al.* 2001, 2003). Using palaeo-trenches along the central Altyn Tagh Fault at 38.9°N, 91.8°E, Washburn *et al.* (2003) recorded two clear earthquakes with ^{14}C ages of AD 1456–1775 and AD 60–980. From records at three trenches, they recorded earthquake repeat intervals of 0.7–0.9 ka, similar to those given for the Kun Lun Fault (Van der Woerd *et al.* 1998), and supporting a relatively low slip rate.

Strike-slip faults in eastern Tibet

Haiyuan Fault

The Haiyuan Fault is a vertical left-lateral strike-slip fault than runs for *c*. 1000 km from the northeastern part of the Tibetan Plateau, north of the Qaidam basin across to the Ordos Block (Fig. 1). The Haiyuan Fault has a large seismic potential, as observed by the 1920 M_c 8.0–8.6 earthquake, which occurred near the town from which it derived its name and which resulted in the deaths of over 220 000 people (Deng *et al.* 1984). The Qilian Shan range to the north has also been affected by several, equally large (M 8–8.3) historical earthquakes along its NE-vergent fold–thrust belt in 1927 (Gaudemer *et al.* 1995). Palaeoseismic trenching along the central portion of the fault reveals four major events in the last 3.5–4 ka, yielding an earthquake recurrence time of almost 1000 years (Liu-Zeng *et al.* 2007).

Burchfiel *et al.* (1989, 1991) suggested that only 10.5–15.5 km offset had occurred along the Haiyuan Fault by matching geological markers across the fault. They showed that progressively smaller offsets occurred on younger rock units and proposed an average Pleistocene slip rate of 5–10 mm a^{-1} assuming that faulting started at the end of the Pliocene. In contrast, Gaudemer *et al.* (1995) estimated an offset of 95 km with a much older initiation age of 10 Ma, but which also suggests a slip rate of *c*. 10 mm a^{-1}. Ding *et al.* (2004) estimated the total amount of sinistral strike-slip offset along the Haiyuan Fault zone since the late Miocene as *c*. 60 km, summing the offsets of three classes of pull-apart basins developed during different periods, giving an average rate of 6.5 mm a^{-1}.

An early estimate of Holocene slip rate for the Haiyuan Fault by Zhang *et al.* (1988) from stream offsets and radiocarbon dating was 6–7 mm a^{-1} (although with some estimates as low as 3 mm a^{-1}). Late Holocence estimates of slip rate from Lasserre *et al.* (1999) gave a post-glacial slip rate of 12 ± 4 mm a^{-1} based upon alluvial terrace and riser offsets dated with ^{14}C ages. Lasserre *et al.* (2002) constrained the Late Pleistocene slip rate as 19 ± 5 mm a^{-1}, from ^{10}Be and ^{26}Al cosmogenic dating of offset moraines, although this has been recently challenged by Li *et al.* (2009), who derived a Quaternary estimate of 4.5 ± 1 mm a^{-1}.

The current slip rate as estimated geodetically is 4–8 mm a^{-1} (Cavalie *et al.* 2008) based upon InSAR observations and is in near agreement with that derived from GPS observations of 8.6 mm a^{-1} (Gan *et al.* 2007). Microplate models for Tibet from Meade (2007) and Thatcher (2007) estimated fault slip rates of 9 mm a^{-1} and 6 mm a^{-1} respectively.

Kun Lun Fault

The left-lateral Kun Lun Fault marks the northern boundary of the high-elevation, low-relief main part of the Tibetan Plateau for nearly 1500 km (Fig. 1). Timing of initiation of strike-slip shearing is poorly constrained but thought to be coeval with Miocene extension *c*. 15 Ma (Jolivet *et al.* 2003). Finite displacement along the fault is also poorly constrained although some workers have suggested 85 km of apparent deflection of the Yellow River along the eastern segment of the fault (Gaudemer *et al.* 1989). Fu & Awata (2007) suggested that maximum offset of basement rocks was *c*. 100 km, and that maximum timing of shearing was 10 ± 2 Ma, giving a long-term slip rate of *c*. 10 mm a^{-1}. In contrast, Jolivet *et al.* (2003) suggested that strike-slip motion in the western Kun Lun ranges started at least in the Late Eocene simultaneously with Eocene to Oligocene SW–NE compression. At *c*. 15 Ma extension resulted in pull-apart basins possibly concomitant with subduction of Tarim–Qaidam lithosphere southward beneath the Kun Lun.

As with the Altyn Tagh Fault, slip rates along the Kun Lun Fault vary considerably between short-term geodetic and long-term geological rates. Quaternary slip rates along the Kun Lun Fault are, however, better constrained. Kirby *et al.* (2007) suggested that slip rates decrease systematically eastwards along the eastern segment of the fault from >10 to <2 mm a^{-1}. Those workers also showed that slip along the fault ends in the thickened crust of the plateau and therefore any eastward extrusion must be absorbed by internal deformation in the plateau. This is supported by further observations east of 99°E, showing a lower slip rate of 2–6 mm a^{-1} for the easternmost portion of the fault (Harkins *et al.* 2010). The decrease in slip rate from *c*. 10 mm a^{-1} to near zero over the last *c*. 200 km of the eastern portion of the fault mirrors that observed for the eastern portion of the Altyn Tagh Fault at 95–97°E (Zhang *et al.* 2007).

Recent large earthquakes on this fault include the M_w 8.1 Kokoxili event, which ruptured a 300 km portion of the western end of the fault in 2001 (Lasserre *et al.* 2005), and two earlier earthquakes along the central segment in 1963 (M_w 7.1) and 1937 (M_w 7.5). Therefore the central and western segments of the fault have had at least four large earthquakes in the past century whereas the eastern segment appears to have had little historical seismicity (Kirby *et al.* 2007). Geodetic observations from GPS are in agreement for the western portion of the fault, with estimates of 8–11 mm a^{-1} (Zhang *et al.* 2004). More recent GPS measurements also show a decrease in slip rate from 96 to 106°E, from 14 to 2 mm a^{-1}. The microplate model of Thatcher (2007) suggests a uniform slip of 6–7 mm a^{-1} along the fault, whereas that of Meade (2007) suggests 10–11 mm a^{-1} for the western portion and 6–7 mm a^{-1} for the eastern segment. He & Chery (2008) in their mechanical model obtained consistent slip rates between 92 and 101°E of 8–12 mm a^{-1}, assuming a low effective fault friction.

Xianshui-he Fault

The left-lateral active Xianshui-he Fault cuts diagonally through the Songpan–Ganze terrane, south of the Qaidam basin in NE Tibet SW of the Long Men Shan and Sichuan Basin and curves around to north–south strike in western Yunnan (Fig. 1). The fault is called the Xiaojiang Fault in Yunnan north of the Red River and may also align with the Dien Bien Phu Fault in northwestern Vietnam, south of the Red River. It appears to be one of the most active of all Tibetan faults, with several large earthquakes along it and eight M 7+ events since 1725 (Allen *et al.* 1991). West of 100°E this activity appears to step left onto the Ganzi–Yushu Fault, which is also the locus of historical M_c 7+ earthquakes including the recent 2010 Yushu event.

The Xianshui-he Fault cuts the eastern margin of the large Konga Shan (7756 m) granite, a two-mica crustal melt granite that has a U–Pb zircon crystallization age of 12.8 ± 1.4 Ma (Roger *et al.* 1995), suggesting that the fault must have initiated after this time. A series of strike-slip faults splay off the Xianshui-he Fault forming a duplex system. Together with a few isolated young crustal melt leucogranitic intrusions in northern Tibet (e.g. Ulugh Muztagh granites; Molnar *et al.* 1987*b*) these rocks may be the only surface geological evidence for lower crustal melting within the high plateau.

Geological offsets of *c*. 60 km for the last 2–4 Ma imply a long-term slip rate of 15–30 mm a^{-1} (Wang & Burchfiel 2000). However, from thermochronology measurements dating the onset of fault activity at 13 Ma, Wang *et al.* (2009*b*) derived a long-term slip rate of 5.4 ± 0.8 mm a^{-1} based upon the 60–80 km offset and an older age of initiation (*c*. 13 Ma) based on K–Ar mica and apatite fission-track ages. Holocene slip rates from radiometric dating are estimated to be 15 ± 5 mm a^{-1} in the NW and 5 mm a^{-1} in the SE (Allen *et al.* 1991), with re-estimates of the data yielding 14 ± 2 mm a^{-1} and 9.6 ± 1.7 mm a^{-1} respectively (Xu *et al.* 2003). GPS measurements suggest a *c*. 10 mm a^{-1} slip rate along the fault between 29 and 32°N with the rate decreasing to 4–7 mm a^{-1} as it runs north–south (Shen *et al.* 2005). Wang *et al.* (2009*a*) found a joint GPS and InSAR geodetic rate across the left-lateral fault at 101°E of 9–12 mm a^{-1} with a locking depth of 3–6 km.

Jiale Fault

The right-lateral Jiale Fault is the most prominent strike-slip fault of SE Tibet, running for at least 800 km WNW–ESE from the Bangong suture zone to the Burma–Yunnan border (Fig. 1). North of the Eastern Himalayan syntaxis the fault splays into two branches, the northern Parlung Fault, which continues southeastward into the Gaoligong Fault, and the southern Puqu Fault, which swings right around the syntaxis to align north–south and eventually connect with the northern Sagaing Fault in Burma. The active deformation and GPS patterns (Fig. 6) suggest a clockwise rotation around the Eastern Himalayan syntaxis with extruding crust bounded by the right-lateral Jiale, Gaoligong and Sagaing faults in the west, and the left-lateral Xianshui-he, Xiaojiang and Dien Bien Phu faults in the east.

The Jiale Fault cuts obliquely though the eastern Gangdese belt and cuts Cretaceous granites with U–Pb zircon ages of 136–113 Ma (Chiu *et al.* 2009). $^{40}Ar/^{39}Ar$ ages suggest that the main phase of strike-slip shearing was *c*. 18–12 Ma (Lee *et al.* 2003; Lin *et al.* 2009). This age range overlaps with active shearing along ductile shear zones along the Gaoligong Fault (Akciz *et al.* 2008; Lin *et al.* 2009) and the Sagaing Fault in Burma (Searle *et al.* 2007). It is also similar to main strike-slip phase of motion along the Karakoram Fault (Dunlap *et al.* 1998; Searle *et al.* 1998). Therefore all the dated strike-slip faults in southern Tibet dated appear to have initiated over 30 Ma after the India–Asia collision. Armijo *et al.* (1989) proposed *c*. 450 km of right-lateral offset along the Jiale Fault but they had no accurately dated markers or pinning points. Precise dating and mapping of offset geological markers along the Jiale Fault remains poorly defined.

Conjugate strike-slip faults of central Tibet

Relative to the strike-slip faults at or towards the edges of the plateau discussed above, the strike-slip faults of central Tibet have been less well studied. This high plateau region contains no active thrust faulting, with only north–south normal faulting and approximately east–west strike-slip faulting present (Molnar & Tapponnier 1978; Armijo *et al.* 1989; Taylor & Yin 2009; Fig 1). Early studies focused on the NW–SE-oriented, right-lateral strike-slip faults of southern–central Tibet, which were mapped between the Karakoram and Jiali faults, forming an en echelon fault zone that was thought to accommodate the rigid eastward extrusion of northern Tibet between this zone and the Altyn Tagh and Kun Lun faults (Armijo *et al.* 1989).

The seismological record shows a distributed pattern of normal and strike-slip earthquakes across this region (Molnar & Lyon-Caen 1989), with the largest event in the last century being an M 8 right-lateral strike-slip event in 1951 on the Beng Co Fault (Armijo *et al.* 1989). The most recent seismicity consists of moderate to large normal faulting earthquakes, but with T-axes for both types of normal and strike-slip faulting consistently aligned ESE–WNW (Elliott *et al.* 2010). GPS measurements indicate that 19–25 mm a^{-1} of east–west extension and 7–17 mm a^{-1} of north–south contraction is accommodated across the central plateau, north of the Himalaya and south of the Kun Lun and Altyn Tagh faults (Zhang *et al.* 2004).

The right-lateral SE–NW strike-slip faults lie largely south of the Bangong–Nujiang suture in the Lhasa terrane and are terminated in the south by north–south normal faults (Taylor *et al.* 2003; Fig. 1). These are reflected along a slight relative east–west topographic low by NE–SW left-lateral strike-slip faults that lie just north of the Bangong–Nujiang suture in the Qiangtang terrane and are also kinematically linked to the north with further north–south-oriented normal faults (Yin *et al.* 1999). This pattern of faulting indicates a 250 km by 1500 km east–west-trending zone of conjugate strike-slip faulting across central Tibet that simultaneously accommodates north–south contraction and east–west extension (Taylor *et al.* 2003). By mapping three of the fault systems, Taylor *et al.* (2003) found average offsets in Tertiary thrusts and Palaeozoic–Mesozoic lithological units of only 12 km. This supports a model of coeval east–west extension and north–south contraction on multiple faults in a distributed pattern rather than the Qiangtang terrane behaving as a rigid block translating eastward, the latter requiring larger offsets on these faults.

Taylor & Peltzer (2006) attempted to measure the current slip rates of some of these faults using InSAR observations for the period 1992–1999. For the Riganpei Co, Gyaring Co and Lamu Co faults, they estimated rates of 5–10, 10–18 and 1–7 mm a^{-1} respectively, similar in magnitude to the other strike-slip faults discussed here. When taken with small total offsets (Taylor *et al.* 2003), these relatively high slip rates imply that these structures have not been active for the entire period of the Indo-Asia collision, and possibly have been active only in the last 2–3 Ma (Taylor & Peltzer 2006). This is in contradiction to geochronological constraints of the onset of east–west extension at *c.* 8 Ma (Harrison *et al.* 1995) or earlier at *c.* 13.5 Ma for normal faulting (Blisniuk *et al.* 2001), or the initiation of slip on the Jiali Fault at between 18 and 12 Ma (Lee *et al.* 2003), which suggests that movement on the central Tibetan faults may have accelerated through time. Meade (2007) did not attempt to resolve each of the conjugate faults on the plateau with the 17-microplate model, particularly in western Tibet where an arbitrary boundary was modelled as taking up 15 mm a^{-1} of right-lateral slip. However, 7 mm a^{-1} of left-lateral and 4 mm a^{-1} of right-lateral slip is predicted in the model for the east–central plateau. Thatcher (2007) did not attempt to resolve microplate boundaries for the western part of the plateau where there is an absence of GPS constraint.

Discussion: lithospheric structure and rheology

Jelly sandwich–crème brûlée models

The conventional view of continental lithospheric structure was that strong seismogenic layers in the upper crust and upper mantle are separated by a weak and aseismic lower crust, the so-called 'jelly sandwich' model (Chen & Molnar 1983; Burov & Watts 2006). Jordan & Watts (2005) estimated the elastic thickness of the Indian plate and concluded that the upper mantle was strong enough to support the load of the Himalaya–southern Tibet. The alternative model suggests that the strength of the lithosphere lies entirely within the crust, the so-called 'crème brûlée' model (Jackson 2002; Jackson *et al.* 2008). Earthquakes occur by frictional sliding in the brittle parts of the lithosphere, and so the depth distribution of earthquakes in the Tibetan crust is critical to our interpretation of the rheology. Almost all earthquakes within the main plateau region in Tibet occur in the upper crust at depths $<$18 km and show east–west extension within the high plateau (Molnar & Lyon-Caen 1989). These earthquakes are linked to the seven or so north–south-aligned grabens that cut across the entire plateau from the Himalaya north to the Kun Lun (Armijo *et al.* 1988). The grabens are most prominent in southern Tibet north of the South Tibetan Detachment system but the normal faults do extend into northern Tibet (Yin *et al.* 1999; Kapp *et al.* 2008; Taylor & Yin 2009).

Significantly, there are no earthquakes in the middle crust of southern Tibet, which is interpreted by both geological extrapolation from the Himalaya and from the INDEPTH seismic profiles to be partially molten and therefore too hot and ductile for earthquakes. Thus neither the 'jelly sandwich' nor the 'crème brûlée' model is compatible for southern Tibet. For this region a model showing that both the upper crust and lower crust are strong and relatively 'rigid' separated by a hot, ductile deforming partially molten middle crust would be more appropriate ('custard cream' model; Fig. 7). The strength of the upper mantle is open to debate but a strong viscosity and rheological contrast at the Moho between a plagioclase-dominated lower crust and an olivine-dominated upper mantle support a model of crust–mantle decoupling.

There is controversy about whether the cluster of earthquakes at *c.* 80–90 km depth in SE and NW Tibet (Chen & Molnar 1983; Molnar & Chen 1983) occurs within the lower crust (Maggi *et al.* 2000; Jackson 2002; Jackson *et al.* 2004; Priestley *et al.* 2008) or in the upper mantle (e.g. Burov & Watts 2006; Monsalve *et al.* 2009). A cluster of deep earthquakes at *c.* 60–90 km depth also occurs beneath the Greater Himalaya and southernmost Tibet roughly at the position of the ramp where the Indian plate flexes down from *c.* 40 km under the Ganga foreland basin to *c.* 75 km depth beneath southern Tibet. Monsalve *et al.* (2009) concluded from finite-element modelling that earthquakes in the upper mantle beneath the Himalayan collision are consistent with loading of a viscoelastic plate where the main forces are the weight of the orogenic wedge (Himalaya) and horizontal forces associated with plate convergence. However, as earthquakes can occur only in regions where temperatures are less than 600 °C (Priestley *et al.* 2008) it is difficult to envisage

temperatures as low as this beneath the thickened crust of the Himalaya or Tibet.

Proposed model for lithospheric structure of Tibet

Our model for the crustal structure of the western Himalaya–western Tibet and central Himalaya–central Tibet is shown in Figure 15a and b. The major faults and ductile shear zones associated with both the Main Central Thrust and South Tibetan Detachment along the Himalaya dip at low angles to the north and have been successfully imaged on the southern INDEPTH seismic profiles (Zhao *et al.* 1993; Nelson *et al.* 1996). The South Tibetan Detachment has been folded around the North Himalayan gneiss domes, the northern extension of the Greater Himalayan metamorphic rocks, and is not active today. The active southern front of the Himalaya is the Main Boundary Thrust, which dips to the north and merges with the Main Himalayan Thrust as imaged on seismic profiles (Nelson *et al.* 1996; Schulte-Pelkum *et al.* 2005) The Indus–Yarlung suture zone is a narrow and near-vertical feature containing remnant ophiolites and Tethyan sedimentary rocks. At about 18 km depth a horizontal band of dense ophiolite has been imaged beneath the Indus–Yarlung suture zone (Makovsky *et al.* 1999). Because at least 300 km of shortening has occurred across the upper crust Cambrian to Eocene rocks of the Tethyan Himalaya in the Himalaya to the south (Corfield & Searle 2000), and between 500–700 km of shortening across the Lesser–Greater Himalaya (DeCelles *et al.* 2002; Robinson 2008), simple balancing requires a similar amount of underthrusting to the north of Indian lower crust comprising Precambrian granulites of the Indian Shield. As the rocks of the lower crust of India underthrust the Himalaya and southern margin of Tibet they extend to depths of *c*. 60–80 km and enter the high-pressure granulite or eclogite fields. This strong, dry granulite crust might just be at low enough temperatures (<600 °C) to host the deep earthquakes. These earthquakes might alternatively be within the upper mantle (Monsalve *et al.* 2009) but, if so, then the temperatures in the mantle must be <600 °C, which seems rather unlikely beneath the thick Himalayan crust.

North of the Indus–Yarlung suture, the crust reaches the thickest known, *c*. 70–90 km, under the Karakoram and far west Tibet (Fig. 15a). The Asian plate in this profile consists of the Karakoram metamorphic sequence, a series of kyanite- and sillimanite-grade metamorphic rocks, migmatites and an extensive Miocene granite batholith with U–Pb zircon and monazite ages spanning *c*. 24–13 Ma (Searle *et al.* 2010*a*). We interpret the Karakoram strike-slip fault as purely a crustal structure. Temperatures in the deep crust beneath the Karakoram are far too high to support brittle faulting and the crustal melt granites in the Karakoram have a different mineralogy and isotopic composition from the Himalayan leucogranites (Searle *et al.* 1992, 2010*a*). Crustal thickness is also the same on either side of the Karakoram Fault, suggesting that the fault does not penetrate into the mantle. There is an apparent 10–15 km step in Moho depths across the northern boundary of west Tibet where thinner crust underlies the Precambrian stable Tarim block (Wittlinger *et al.* 2004).

In the Nepal–central Tibet profile (Fig. 15b) a similar Himalayan structure is present with shallow north-dipping structures extending beneath southern Tibet. The major difference lies in the structure of the Asian side of the collision zone. Unlike the Karakoram, in Tibet low exhumation and low erosion has not exhumed the deep crust metamorphic rocks to the surface. We are reliant on lower crustal xenoliths entrained in Miocene ultrapotassic volcanic rocks and dykes to infer the composition of the lower crust. Chan *et al.* (2009) and Hacker *et al.* (2000, 2005) described high-pressure granulite xenoliths from southern Tibet and the Qiangtang terrane respectively. *P–T* conditions of these Miocene granulites indicate a thick (60–80 km), hot (>900–1000 °C) and dry lower crust. In addition to the high-pressure granulites, eclogite-facies rocks and ultramafic restitic xenoliths support the eclogitized lower crust model (Fig. 15b).

Helium isotopes analysed from geothermal springs reveal two distinct zones. In southern Tibet helium isotopes are consistent with radiogenic heat production in the crust whereas in northern Tibet a ^{3}He anomaly is consistent with a mantle contribution (Hoke *et al.* 2000). The east–west divide is roughly 100–150 km to the north of the Indus suture zone, consistent with underthrusting of Indian lower crust north at least as far as this. There is no clear association between mantle helium domains and crustal structures in southern Tibet.

The surface velocity field as determined by GPS appears to be most consistent with relatively slow slip rates along the boundaries of elastic, rotating blocks under which relatively high-viscosity lower crust and mantle are present (Hilley *et al.* 2009). Based upon these data, and coupled with detailed field observations, we conclude that continental extrusion of Tibet was not a dominant controlling factor at any stage of the Himalayan–Tibet orogeny. Despite the geomorphological prominence of large strike-slip faults such as the Karakoram Fault, they actually show very limited geological offsets, they initiated long (>30 Ma) after the India–Asia collision, they were not the cause of metamorphism, and are not responsible for large-scale continental extrusion of the thickened crust of the Tibetan Plateau. The Karakoram Fault is highly oblique to both geological boundaries and the active GPS motions, appears to be seismically dormant and has very limited long-term geological offset. The Altyn Tagh Fault, however, may have a geological offset up to *c*. 400 km but the piercing points are by no means certain.

Conclusions

Southern Tibet was an Andean-type margin dominated by calc-alkaline volcanic rocks (andesites, dacites, rhyolites) and subduction-related I-type (biotite–hornblende-granite–granodiorite) batholiths during the period *c*. 120–48 Ma. Granites (rare garnet and biotite leucogranite dykes) younger than *c*. 48 Ma have a distinct crustal chemistry related to post-collision thickening. Southern Tibet could have had a crustal thickness and topographic elevation similar to that of present-day Peru or Chile, prior to the Indian plate collision at 50 Ma, but precise amounts are unquantifiable.

Crustal thickness beneath SW, western and southern Tibet (*c*. 75–90 km; Wittlinger *et al.* 2004; Schulte-Pelkum *et al.* 2005; Rai *et al.* 2006) suggest that the lower Indian crust must at present be in eclogite (wet) or high-pressure granulite (dry) facies. Thermobarometry and U–Pb dating of monazites in exposures of exhumed lower crust metamorphic rocks and S-type granites in the Karakoram show that *P–T* conditions (650–800 °C; 10–12 kbar) have been high almost continuously since *c*. 65 Ma (Searle *et al.* 2010*a*). These rocks are lateral exhumed equivalents of the central Tibet Qiangtang terrane, suggesting that Tibet could have been undergoing crustal thickening and regional metamorphism also at least since the Indian collision.

Surface-wave tomography implies that high-velocity lithospheric mantle underlies all of Tibet except for the farthest north beneath the Kun Lun (Priestley *et al.* 2008), supporting the model of underthusting cold Indian lithosphere north beneath at

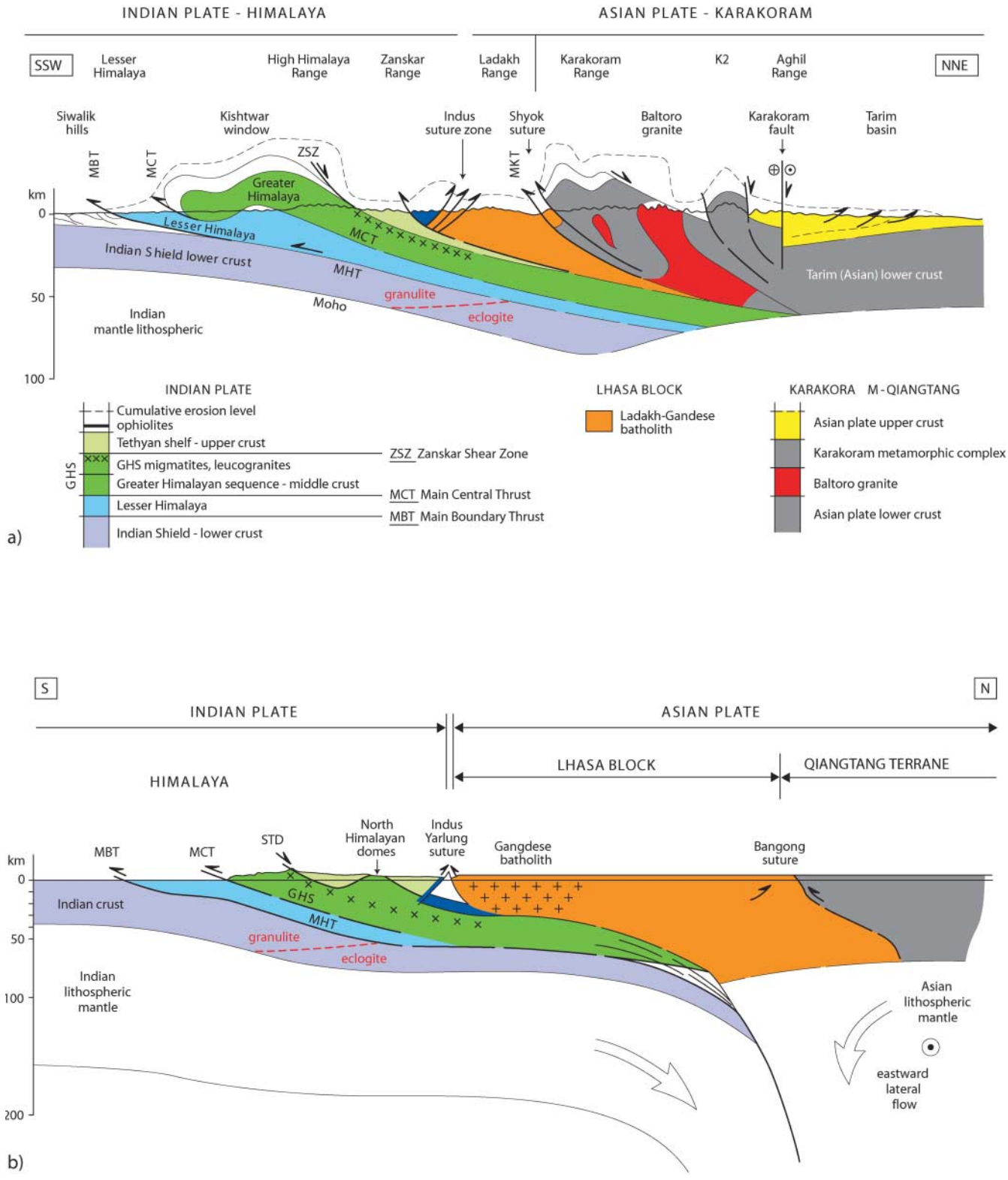

Fig. 15. (**a**) Cross-section of the Western Himalaya and Karakoram Ranges to the Tarim basin, far west Tibet, showing interpretation of the crustal structure, after Searle *et al.* (2010*a*). Depth of Moho is from Wittlinger *et al.* (2004) and Rai *et al.* (2006). MBT, Main Boundary Thrust; MCT, Main Central Thrust; MHT, Main Himalayan Thrust; MKT, Main Karakoram Thrust. (**b**) Cross-section of the Nepal–Tibet region showing our interpretation of the lithospheric structure. Depth of Moho is from Schulte-Pelkum *et al.* (2005) and Nábelek *et al.* (2009).

least the Lhasa block, and suggesting there has been no delamination of lithospheric mantle beneath Tibet. A subvertical low-velocity zone from *c*. 100 to 400 km depth beneath the Bangong suture suggests downwelling of Indian lithosphere (Tilmann *et al.* 2003).

The distribution of mantle-derived shoshonitic potassic and ultrapotassic volcanic rocks across the plateau indicates that hot mantle was progressively shunted northward by the underthrusting of cold Indian lithospheric mantle from the south from 50 Ma to *c*. 13 Ma (Chung *et al.* 2005). Adakitic melts in Tibet indicate partial melting of a garnet-bearing amphibolitic or eclogitic source rock, possibly eclogitized lower crust, from at least *c*. 47 Ma in the Qiangtang block and at least *c*. 30 Ma in the Lhasa block, implying that Tibet was high since the Early–Middle Eocene. The youngest volcanic rocks in northern Tibet, *c*. 15–0 Ma shoshonites that require a deep and hot mantle source, are distributed only along the far north of Tibet in the Kun Lun.

About seven north–south-aligned rift valleys and graben systems cut across the whole plateau north of the Himalaya. Earthquakes in the high plateau region of Tibet all occur within the upper *c*. 18 km of the crust and all show east–west extension. Adakitic, shoshonitic and alkaline rocks intruded along north–south-aligned dykes from 47 to 38 Ma (Wang *et al.* 2010) indicate east–west extension of the high plateau since then. This extension does not necessarily imply 'orogenic collapse' because new material has been constantly underthrust mainly from the south (Himalaya) but also to a lesser extent from the north (Kun Lun–Songpan Ganzi terrane). On the contrary, these normal faults were active during periods of crustal compression and active uplift. There is no evidence that Tibet has 'collapsed' or is decreasing in elevation or crustal thickness.

Deep earthquakes (*c*. 70–90 km) beneath southern Tibet could occur within the lower part of the old, cold Indian craton underthrusting Tibet, or even by slip along the crust–mantle boundary. The Hindu Kush seismic zone along the NW part of India is related to fast and deep subduction of thinned Indian continental crust since *c*. 11 Ma (Pegler & Das 1998; Searle *et al.* 2001).

Metamorphic rocks and granites exhumed along the Karakoram Fault were formed prior to strike-slip shearing along the fault (Searle 1996; Searle *et al.* 1998; Phillips *et al.* 2004; Streule *et al.* 2009) and not during strike-slip shear (Lacassin *et al.* 2004*a*; Valli *et al.* 2007, 2008; Weinberg & Mark 2008; Weinberg *et al.* 2009). U–Pb ages of amphibolite-facies metamorphic rocks cut by the Karakoram Fault at K2 (Searle & Phillips 2007) and Pangong (Streule *et al.* 2009) are Cretaceous in age. Geological markers (notably the intrusive margins of the Baltoro and Nubra–Siachen granites) have been offset dextrally between 25 km (minimum) and 120 km (maximum) since 13 Ma (Phillips & Searle 2007; Searle & Phillips 2007; Searle *et al.* 2010*a*).

The Karakoram Fault does not appear to be particularly active today and has almost no historical earthquake activity, even though it is a major geomorphological feature. The fault also shows very little if any Quaternary offset. Present-day slip rates measured from InSAR along the Karakoram Fault (<7 mm a^{-1}; Wright *et al.* 2004) and Altyn Tagh Fault (*c*. 11 mm a^{-1}; Elliott *et al.* 2008), GPS-determined rates and long-term geological rates can account for only limited eastward extrusion of Tibet since Mid-Miocene time. The relatively minor geological offsets and low slip rates do not support large-scale continental extrusion of Tibetan crust along the Karakoram Fault.

Slip rates for each of the faults appear to be relatively consistent across the three time scales (geological, Quaternary, active). There is therefore little evidence for secular variation in fault slip rates. Slip rates for all the major faults in Tibet are <15 mm a^{-1}, suggesting that distributed deformation is a more suitable model, rather than localized block faulting, for the large-scale deformation of Tibet.

The Altyn Tagh Fault may have geological offsets of as much as *c*. 400 km (Ritts & Biffi 2000; Yue *et al.* 2001, 2003; Cowgill *et al.* 2003) and Cenozoic average slip rates of 12–16 mm a^{-1}. Quaternary and active slip rates measured from InSAR and GPS are between 5 and 15 mm a^{-1}, but with a decrease towards the east (Wright *et al.* 2004; Elliott *et al.* 2008; Jolivet *et al.* 2008) and are not high enough to support large-scale continental extrusion.

The Kun Lun and Xianshui-he faults rotate clockwise about a vertical axis, showing that as India indented into Tibet the eastern margin of the plateau was a large-scale zone of distributed right-lateral shear (England & Molnar 1990). The eastern margin of the Tibetan Plateau (Long Men Shan) shows no evidence of outward easterly crustal flow like the Himalaya; on the contrary, the margin appears to have been passively uplifted along steep west-dipping thrust faults such as those that ruptured during the Wenchuan earthquake.

Neither the 'rigid block' model nor the continuum model adequately explains the geological and geophysical characteristics of the Tibetan Plateau. Tibet instead shows widespread distributed strain both horizontally and vertically, and rheological layering of the crust with prominent layers of weak partially molten crust separated by major flat-lying detachments. Despite major differences between relatively cold mantle in southern Tibet and hot mantle in northern Tibet, there is little difference in topographic elevation across the plateau and only a small difference in crustal thickness.

The Himalayan mid-crustal channel flow model fits all the known geological and geophysical constraints along southernmost Tibet (Indian plate Himalaya). A 10–20 km thick mid-crustal zone of sillimanite-grade gneisses, migmatites and Miocene garnet, two-mica–tourmaline-bearing leucogranites was extruded southward during the Miocene between two thick ductile shear zones, the Main Central Thrust with a compressed inverted metamorphic isograd sequence along the base and the South Tibetan Detachment with a compressed and right-way-up metamorphic isograd sequence along the top. Approximately 100 km or more of relative southward motion occurred beneath the South Tibetan Detachment passive roof fault, and above the Main Central Thrust.

The lower crust flow model for eastern Tibet (Royden *et al.* 1997; Clark & Royden 2000) has no geological evidence from the upper crust to support it, although undoubtedly the temperature and rheology of the lower crust should allow it to flow. Unlike the Himalaya, the Long Men Shan range along the eastern margin of Tibet shows no horizontal extrusion of middle or deep crustal metamorphic rocks, there are no equivalents of the Main Central Thrust or South Tibetan Detachment detachments, and there is no flexural foreland basin to the east in Sichuan. The pattern of GPS 'flow-lines' around the Eastern Himalayan syntaxis does not correspond to the geological structure at all. The GPS lines cut diagonally across all earlier structures including the Red River Fault and Sagaing Fault. GPS motions tell us only about present-day surface motions and tell us nothing about relative motions in the middle or lower crust, or back in time. Only interpreting the geological record correctly can do this.

Broadband seismic experiments support the model of underthrusting of old, cold Indian lithosphere beneath southern Tibet as far as the Bangong suture (Tilmann *et al.* 2003; Hetényi *et al.*

2007; Nábelek *et al.* 2009). Northern Tibet is underlain by 10–20 km thinner crust than the south, with hot mantle and anisotropy interpreted as representing eastward lateral flow. This could support up to *c*. 400 km of finite geological offset along the Altyn Tagh Fault, whereas the Karakoram Fault has much more limited offset (<120 km) and limited extrusion in southern Tibet. Western Tibet and the Karakoram has undergone far greater amounts of crustal thickening, and regional high-grade metamorphism, with correspondingly high exhumation and erosion rates.

We would like to thank P. Molnar, P. Tapponnier, J. Yang, M. St-Onge, R. Parrish, D. Waters, R. Bilham, J.-P. Avouac, A. Watts, E. Burov, M. Yeh and L. Hua Qi for numerous discussions, although they may not agree with some of our conclusions. Thanks go to A. Robinson and P. Kapp for detailed and insightful reviews of the paper. Our work in and around Tibet was funded mainly by NERC (UK) grants and the National Science Council, Taiwan.

References

Akciz, S., Burchfiel, B.C., Crowley, J.L., Jiyun, Y. & Liangzhong, C. 2008. Geometry, kinematics and regional significance of the Chong Shan shear zone, Eastern Himalayan Syntaxis, Yunnan, China. *Geosphere*, **4**, 292–314, doi:10.1130/GES00111.1.

Allen, C.R., Zhuoli, L., Hong, Q., Xueze, W., Huawei, Z. & Weishi, H. 1991. Field study of a highly active fault zone: The Xianshuihe fault of southwestern China. *Geological Society of America Bulletin*, **103**, 1178–1199, doi:10.1130/0016-7606(1991)103<1178:FSOAHA>2.3.CO;2.

Argand, E. 1924. Le tectonique de l'Asie. *Proceedings of the 13th International Geological Congress*, **7**, 171–372.

Armijo, R., Tapponnier, P., Mercier, J.L. & Tonglin, H. 1988. Quaternary extension in Southern Tibet. *Journal of Geophysical Research*, **91**, 13803–13872.

Armijo, R., Tapponnier, P. & Han, T. 1989. Late Cenozoic right-lateral strike-slip faulting in Southern Tibet. *Journal of Geophysical Research*, **94**, 2787–2838.

Avouac, J.-P. & Tapponnier, P. 1993. Kinematic model of active deformation in Central Asia. *Geophysical Research Letters*, **20**, 895–898.

Banerjee, P. & Bürgmann, R. 2002. Convergence across the northwest Himalaya from GPS measurements. *Geophysical Research Letters*, **29**, 1652–1656, doi:10.1029/2002GL015184.

Beaumont, C., Jamieson, R.A., Nguyen, M.H. & Lee, B. 2001. Himalayan tectonics explained by extrusion of a low-velocity channel coupled with focused surface denudation. *Nature*, **414**, 738–742.

Beaumont, C., Jamieson, R.A., Nguyen, M.H. & Medvedev, S. 2004. Crustal channel flows: 1. Numerical models with applications to the tectonics of the Himalayan–Tibetan orogen. *Journal of Geophysical Research*, **109**, B06406, doi:10.1029/2003JB002809.

Bendick, R., Bilham, R., Freymueller, J., Larson, K. & Yin, G.H. 2000. Geodetic evidence for a slow slip rate in the Altyn Tagh fault system. *Nature*, **404**, 69–72.

Bird, P. 1991. Lateral extrusion of lower crust from under high topography, in the isostatic limit. *Journal of Geophysical Research*, **96**, 10275–10286.

Blisniuk, P.M., Hacker, B.R., *et al.* 2001. Normal faulting in central Tibet since at least 13.5 Myr ago. *Nature*, **412**, 628–632.

Brown, E.T., Bendick, R., Bourles, D.L., Gaur, V., Molnar, P., Raisbeck, G.M. & Yiou, F. 2002. Slip rates of the Karakoram Fault, Ladakh, India, determined using cosmic ray exposure dating of debris flows and moraines. *Journal of Geophysical Research*, **107**, 2192, doi:10.1029/2000JB000100.

Brown, E., Molnar, P. & Bourles, D.L. 2005. Comment on Chevalier *et al.* 2005 'Slip rate measurements on the Karakoram fault may imply secular variations in fault motion'. *Science*, **309**, 1326.

Burchfiel, B.C., Deng, Q., Molnar, P., Royden, L., Wang, Y., Zhang, P. & Zhang, W. 1989. Intracrustal detachment within zones of continental deformation. *Geology*, **17**, 748–751.

Burchfiel, B.C., Zhang, P., *et al.* 1991. Geology of the Haiyuan Fault zone, Ningxia–Hui autonomous region, China, and its relation to the evolution of the northeast margin of the Tibetan Plateau. *Tectonics*, **10**, 1091–1110.

Burchfiel, B.C., Zhiliang, C., Hodges, K.V., Yuping, L., Toyden, L., Changron, D. & Jiene, X. 1992. The South Tibetan Detachment System, Himalayan Orogen: Extension contemporaneous with and parallel to shortening in a collisional mountain belt. *In:* Geological Society of America, Special Papers, **269**, 1–41.

Burg, J.P., Brunel, M., Gapais, D. & Chen, G.M. 1984. Deformation of leucogranites in the crystalline Main Central Thrust sheet in southern Tibet (China). *Journal of Structural Geology*, **6**, 535–542.

Burov, E.B. & Watts, A.B. 2006. The long-term strength of the continental lithosphere: 'jelly sandwich' or 'crème-brûlée'? *GSA Today*, **16**, doi:10.1130/1052-5173(2006)016<4 :TLTSO>2.0.cC.);2.

Burtman, V. & Molnar, P. 1993. *Geological and geophysical evidence of deep subduction of continental crust beneath the Pamir*. Geological Society of America, Special Papers, **281**, 76pp.

Caldwell, B., Klemperer, S.L., Rai, S.S. & Lawrence, J.F. 2009. Partial melt in the upper–middle crust of the northwest Himalaya revealed by Rayleigh wave dispersion. *Tectonophysics*, **477**, 58–65.

Cavalie, O., Laserre, C., Doin, M.-P., Peltzer, G., Sun, J., Xu, X. & Shan, Z.-K. 2008. Measurement of interseismic strain across the Haiyuan fault (Gansu, China), by InSAR. *Earth and Planetary Science Letters*, **275**, 246–257, doi:10.1016/j.epsl.2008.07.057.

Chan, G.H.-N., Waters, D.J., *et al.* 2009. Probing the basement of southern Tibet: evidence from crustal xenoliths entrained in a Miocene ultrapotassic dyke. *Journal of the Geological Society, London*, **166**, 45–52.

Chatelain, J.L., Roeker, S.W., Hatzfeld, D. & Molnar, P. 1980. Microearthquake seismicity and fault plane solutions in the Hinku Kush region and their tectonic implications. *Journal of Geophysical Research*, **85**, 1365–1387.

Chen, W-P. & Molnar, P. 1977. Seismic moments of major earthquakes and the average rate of slip in central Asia. *Journal of Geophysical Research*, **82**, 2945–2970, doi:10.1029/JB082i020p02945.

Chen, W.-P. & Molnar, P. 1983. Focal depths of intra-continental and intra-plate earthquakes and their implications for the thermal and mechanical properties of the lithosphere. *Journal of Geophysical Research*, **88**, 4183–4214.

Chen, W.-P. & Tseng, T.-L. 2007. Small 660-km seismic discontinuity beneath Tibet implies resting ground for detached lithosphere. *Journal of Geophysical Research*, **112**, B05309, doi:10.1029/2006JB004607.

Chen, W-P. & Yang, Z. 2004. Earthquakes beneath the Himalayas and Tibet: Evidence for strong lithospheric mantle. *Science*, **304**, 1949–1952.

Chen, Y., Gilder, S., Halim, N., Cogne, J.P. & Courtillot, V. 2002. New paleomagnetic constraints on central Asian kinematics: Displacement along the Altyn Tagh fault and rotation of the Qaidam Basin. *Tectonics*, **21**, 1042, doi:10.1029/2001TC901030.

Chen, Z., Burchfiel, B.C., *et al.* 2000. Global Positioning System measurements from eastern Tibet and their implications for India/Eurasia intercontinental deformation. *Journal of Geophysical Research*, **105**, 16215–16228, doi:10.1029/2000JB900092.

Chevalier, M.-L., Ryerson, F.J., Tapponnier, P., Finkel, R.C., Van der Woerd, J., Haibing, L. & Qing, L. 2005. Slip rate measurements on the Karakoram fault may imply secular variations in fault motion. *Science*, **307**, 411–414.

Chiu, H.-Y., Chung, S.-L., *et al.* 2009. Zircon U–Pb and Hf isotopic constraints from eastern Transhimalayan batholiths on the precollisional magmatic and tectonic evolution in southern Tibet. *Tectonophysics*, doi:10.1016/j.tecto.2009.02.034.

Chu, M.-F., Chung, S.-L., *et al.* 2006. Zircon U–Pb and Hf isotope constraints on the Mesozoic tectonics and crustal evolution of southern Tibet. *Geology*, **34**, 745–748.

Chung, S.-L., Lo, C.-H., *et al.* 1998. Diachronous uplift of the Tibetan Plateau starting 40 Myr ago. *Nature*, **394**, 769–773.

Chung, S.-L., Liu, D., *et al.* 2003. Adakites from continental collision zones: Melting of thickened lower crust beneath southern Tibet. *Geology*, **31**, 1021–1024.

Chung, S.-L., Chu, M.-F., *et al.* 2005. Tibetan tectonic evolution inferred from spatial and temporal variations in post-collisional magmatism. *Earth-Science Reviews*, **68**, 173–196.

Chung, S.-L., Chu, M.-F., *et al.* 2009. The nature and timing of crustal thickening in Southern Tibet: Geochemical and zircon Hf isotopic constraints from postcollisional adakites. *Tectonophysics*, **477**, 36–48.

Clark, M.K. & Royden, L.H. 2000. Topographic ooze: Building the eastern margin of Tibet by lower crustal flow. *Geology*, **28**, 703–706.

Corfield, R.I. & Searle, M.P. 2000. Crustal shortening estimates across the north Indian continental margin, Ladakh, NW India. *In:* Khan, M.A., Treloar, P.J., Searle, M.P. & Jan, M.Q. (eds) *Tectonics of the Nanga Parbat Syntaxis and the Western Himalaya*. Geological Society, London, Special Publications, **170**, 395–410.

Cottle, J.M., Jessup, M.J., Newell, D.L., Searle, M.P., Law, R.D. & Horstwood, M.S.A. 2007. Structural insights into the early stages of exhumation along an orogen-scale detachment: The South Tibetan Detachment System, Dzachaa Chu, Eastern Himalaya. *Journal of Structural Geology*, **29**, 1781–1797.

Cottle, J.M., Searle, M.P., Hortswood, M.S.A. & Waters, D.J. 2009. Timing of midcrustal metamorphism, melting and deformation in the Mount Everest region of Southern Tibet revealed by U(–Th)–Pb geochronology. *Journal of Geology*, **117**, 643–664.

Coward, M.P., Kidd, W.S.F., Pan, Y., Shackleton, R.M. & Zhang, H. 1988. The structure of the 1985 Tibet Geotraverse, Lhasa to Golmud. *Philosophical Transactions of the Royal Society of London, Series A*, **327**, 307–336.

Cowgill, E. 2007. Impact of riser reconstructions on estimation of secular variation in rates of strike slip faulting: Revisiting the Cherchen River site along the Altyn Tagh Fault, NW China, *Earth and Planetary Science Letters*, **254**, 239–255, doi:10.1016/j.epsl.2006.09.015.

Cowgill, E., Yin, A., Harrison, T.M. & Feng, W.X. 2003. Reconstruction of the Altyn Tagh fault based on U–Pb geochronology: Role of backthrusts, mantle sutures and heterogeneous crustal strength in the forming the Tibetan plateau. *Journal of Geophysical Research*, **108**, doi:10.1029/2002JB002080.

Cowgill, E., Gold, R.D., Xuanhua, C., Xiao-Feng, W., Arrowsmith, J.R. & Southon, J. 2009. Low Quaternary slip rate reconciles geodetic and geologic rates along the Altyn Tagh fault, northwestern Tibet. *Geology*, **37**, 647–650, doi:10.1130/G25623A.1.

Darby, B.J., Ritts, B.D., Yue, Y. & Meng, Q. 2005. Did the Altyn Tagh fault extend beyond the Tibetan Plateau? *Earth and Planetary science Letters*, **240**, 425–435.

DeCelles, P.G., Robinson, D.M. & Zandt, G. 2002. Implications of shortening in the Himalayan fold–thrust belt for uplift of the Tibetan Plateau. *Tectonics*, **21**, 1062, doi:10.1029/2001TC001322.

DeCelles, P.G., Quade, J., Kapp, P., Fan, M., Dettman, D.L. & Ding, L. 2007. High and dry in central Tibet during the Late Oligocene. *Earth and Planetary Science Letters*, **253**, 389–401.

Deng, Q., Sung, F., *et al.* 1984. Active faulting and tectonics of the Ningxia–Hui Autonomous Region, China. *Journal of Geophysical Research*, **89**, 4427–4445.

Dewey, J.F. 1988. Extensional collapse of orogens. *Tectonics*, **7**, 1123–1139.

Dewey, J. & Burke, K. 1973. Tibetan, Variscan and Precambrian basement reactivation: Products of a continental collision. *Journal of Geology*, **81**, 683–692.

Dewey, J.F., Shackleton, R.M., Chenfa, C. & Yiyin, S. 1988. The tectonic evolution of the Tibetan Plateau. *Philosophical Transactions of the Royal Society, London, Series A*, **327**, 379–413.

Ding, G., Chan, J., Tian, Q., Shan, X., Xing, C. & Wei, K. 2004. Active faults and magnitudes of left-lateral displacement along the northern margin of the Tibetan Plateau. *Tectonophysics*, **380**, 243–260, doi:10.1016/j.tecto.2003.09.022.

Ding, L., Kapp, P., Yue, Y. & Lai, Q. 2007. Postcollisional calc-alkaline lavas and xenoliths from the southern Qiangtang terrane, central Tibet. *Earth and Planetary Science Letters*, **254**, 28–38.

Ducea, M.N., Lutkov, V., *et al.* 2003. Building the Pamirs: the view from the underside. *Geology*, **31**, 849–852.

Dunlap, W.J., Weinberg, R.F. & Searle, M.P. 1998. Karakoram fault zone rocks cool in two phases. *Journal of the Geological Society, London*, **155**, 519–538.

Elliott, J.R., Biggs, J., Parsons, B. & Wright, T.J. 2008. InSAR slip rate determination on the Altyn Tagh fault, northern Tibet, in the presence of tomographically correlated atmospheric delays. *Geophysical Research Letters*, **35**, L12309, doi:10.1029/2008GL033659.

Elliott, J.R., Walters, R.J., England, P.C., Jackson, J.A., Li, Z. & Parsons, B. 2010. Extension on the Tibetan plateau: recent normal faulting measured by InSAR and body wave seismology. *Geophysical Journal International*, **183**, 503–555, doi:10.1111/j.1365-246X.2010.04754.x.

England, P. & Houseman, G. 1989. Extension during continental convergence with application to the Tibetan Plateau. *Journal of Geophysical Research*, **94**, 17561–17579.

England, P. & Houseman, G. 1985. Role of lithospheric strength heterogeneities in the tectonics of Tibet and neighbouring regions. *Nature*, **315**, 297–301, doi:10.1038/315297a0.

England, P. & Houseman, G. 1986. Finite strain calculations of continental deformation. Comparison with the India-Asia collision zone. *Journal of Geophysical Research*, **91**, 3664–3676, doi:10.1029/JB091iB03p03664.

England, P. & McKenzie, D. 1982. A thin viscous sheet model for continental deformation. *Geophysical Journal of the Royal Astronomical Society*, **70**, 295–321.

England, P. & McKenzie, D. 1983. Correction to: a thin viscous sheet model for continental deformation. *Geophysics Journal International*, **73**, 523–532, doi:10.1111/j.1365-246X.1983.tb03328.x.

England, P. & Molnar, P. 1990. Right-lateral shear and rotation as the explanation for strike-slip faulting in east Tibet. *Nature*, **344**, 140–142.

England, P. & Molnar, P. 1997*a*. Active deformation of Asia: from kinematics to dynamics. *Science*, **278**, 647–650, doi:10.1126/science.278.5338.647.

England, P. & Molnar, P. 1997*b*. The field of crustal velocity in Asia calculated from Quaternary rates of slip on faults. *Geophysics Journal International*, **130**, 551–582, doi:10.1111/j.1365-246X.1997.tb01853.x.

England, P. & Molnar, P. 2005. Late Quaternary to decadal velocity fields in Asia. *Journal of Geophysical Research*, **110**, B12401, doi:10.1029/2004JB003541.

England, P. & Searle, M. 1986. The Cretaceous–Tertiary deformation of the Lhasa Block and its implications for crustal thickening in Tibet. *Tectonics*, **5**, 1–14.

Fan, G. & Ni, J.F. 1989. Source parameters of the 13 February 1980, Karakoram earthquake. *Bulletin of the Seismological Society of America*, **79**, 945–954.

Fielding, E., Isacks, B., Barazangi, M. & Duncan, C. 1994. How flat is Tibet? *Geology*, **22**, 163–167.

Fu, B. & Awata, Y. 2007. Displacement and timing of left-lateral faulting in the Kunlun Fault zone, northern Tibet, inferred from geological and geomorphic features. *Journal of Asian Earth Sciences*, **29**, 253–265.

Gaillard, F., Scaillet, B. & Pichavant, M. 2004. Evidence of present-day leucogranite pluton growth in Tibet. *Geology*, **32**, 801–804.

Gan, W., Zhang, P., *et al.* 2007. Present-day crustal motion within the Tibetan Plateau inferred from GPS measurements. *Journal of Geophysical Research*, **112**, B08416, doi:10.1029/2005JB004120.

Garzanti, E., Baud, A. & Mascle, G. 1987. Sedimentary record of the northward flight of India and its collision with Eurasia (Ladakh Himalaya, India). *Geodinamica Acta*, **1**, 297–312.

Gasse, F., Arnold, M., *et al.* 1991. A 13,000 yr climatic record in western Tibet. *Nature*, **353**, 742–745.

Gasse, F., Fontes, J.C., Van Campo, E. & Wei, K. 1996. Holocene environmental changes in Lake Bangong basin (western Tibet), part 4, Discussion and conclusions. *Palaeogeography Palaeoclimatology Palaeoecology*, **120**, 79–92.

Gaudemer, Y., Tapponnier, P. & Turcotte, D.L. 1989. River offsets across active strike-slip faults. *Annales Tectonicae*, **3**, 55–76.

Gaudemer, Y., Tapponnier, P., *et al.* 1995. Partitioning of crustal slip between linked, active faults in the Eastern Qilian Shan and evidence for a major seismic gap, the Tianzhu gap, on the western Haiyuan fault, Gansu (China). *Geophysical Journal*, **120**, 599–645.

Gehrels, G.E., Yin, A. & Wang, X.F. 2003. Detrital-zircon geochronology of the northeastern Tibetan plateau. *Geological Society of America Bulletin*, **115**, 881–896, doi:10.1130/0016-7606(2003)115<0881:DGOTNT>2.0.CO;2.

Gillespie, A. & Molnar, P. 1995. Asynchronous maximum advances of mountain and continental glaciers. *Reviews of Geophysics*, **33**, 311–364.

Godin, D., Grujic, D., Law, R.D. & Searle, M.P. 2006. Channel flow, ductile extrusion and exhumation in continental collision zones: an introduction. *In:* Law, R.D., Searle, M.P. & Godin, L. (eds) *Channel Flow, Ductile Extrusion and Exhumation in Continental Collision Zones*. Geological Society, London, Special Publications, **268**, 1–23.

Gold, R.D., Cowgill, E., Arrowsmith, J.R., Gosse, J., Chen, X. & Wang, X. 2009. Riser diachroneity, lateral erosion, and uncertainty in rates of strike-slip faulting: A case study from Tuzidun along the Altyn Tagh Fault, NW China. *Journal of Geophysical Research*, **114**, B04401, doi:10.1029/2008JB005913.

Green, O.R., Searle, M.P., Corfield, R.I. & Corfield, R.M. 2008. Cretaceous–Tertiary carbonate platform evolution and the age of the India–Asia collision along the Ladakh Himalaya (Northwest India). *Journal of Geology*, **116**, 331–353.

Grujic, D., Hollister, L. & Parrish, R. 2002. Himalayan metamorphic sequence as an orogenic channel: insight from Bhutan. *Earth and Planetary Science Letters*, **198**, 177–191.

Guo, Z., Wilson, M. & Liu, J. 2007. Post-collisional adakites in south Tibet: Products of partial melting of subduction-modified lower crust. *Lithos*, **96**, 205–224.

Hacker, B., Gnos, E., *et al.* 2000. Hot and dry deep crustal xenoliths from Tibet. *Science*, **287**, 2463–2466.

Hacker, B., Luffi, R., *et al.* 2005. Near ultrahigh pressure processing of continental crust: Miocene crustal xenoliths from the Pamir. *Journal of Petrology*, **46**, 1661–1687.

Haines, S.S., Klemperer, S.L., *et al.* 2003. INDEPTH III seismic data: From surface observations to deep crustal processes in Tibet. *Tectonics*, **22**, doi:10.1029/2001TC001305.

Harkins, N., Kirby, E., Shi, X., Wang, E., Burbank, D. & Chun, F. 2010. Millennial slip rates along the eastern Kunlun fault: Implications for the dynamics of intracontinental deformation in Asia. *Lithosphere*, **2**, 247–266, doi:10.1130/L85.

Harrison, T.M., Copeland, P., Kidd, W.S.F. & Lovera, O.M. 1995. Activation of the Nyainqentanghla Shear Zone: Implication of uplift of the southern Tibetan Plateau. *Tectonics*, **14**, 658–676, doi:10.1029/95TC00608.

Hatzfeld, D. & Molnar, P. 2010. Comparisons of the kinematics and deep structures of the Zagros and Himalaya and of the Iranian and Tibetan Plateaus and geodynamic implications. *Reviews of Geophysics*, **48**, RG2005.

He, J. & Chery, J. 2008. Slip rates of the Altyn Tagh, Kunlun and Karakorum faults (Tibet) from 3D mechanical modeling, *Earth and Planetary Science Letters*, **274**, 50–58, doi:10.1016/j.epsl.2008.06.049.

Hetényi, G., Cattin, R., Brunet, F., Bollinger, L., Vergne, J., Nabelek, J.L. & Diament, M. 2007. Density distribution of the India plate beneath the Tibetan Plateau: Geophysical and petrological constraints on the kinetics of lower crustal eclogitization. *Earth and Planetary Science Letters*, **264**, 226–244.

Hetzel, R., Niedermann, S., *et al.* 2002. Low slip rates and long-term preservation of geomorphic features in Central Asia. *Nature*, **417**, 428–432.

Hildebrand, P.R., Noble, S.R., Searle, M.P., Waters, D.J. & Parrish, R.R. 2001. Old origin for an active mountain range: Geology and geochronology of the eastern Hindu Kush, Pakistan. *Geological Society of America Bulletin*, **113**, 625–639.

Hilley, G.E., Johnson, K.M., Wang, M., Shen, Z.K. & Burgman, R. 2009. Earthquake cycle deformation and fault slip rates in northern Tibet. *Geology*, **37**, 31–34.

Hodges, K.V. 2000. Tectonics of the Himalaya and southern Tibet from two perspectives. *Geological Society of America Bulletin*, **112**, 324–350.

Hoke, L., Lamb, S., Hilton, D.R. & Pored, R.J. 2000. Southern limit of mantle-derived geothermal helium emissions in Tibet: implication for lithospheric structure. *Earth and Planetary Science Letters*, **180**, 297–308.

Holt, W.E., Chamot-Rooke, N., Le-Pichon, X., Haines, A.J., Shen-Tu, B. & Ren, J. 2000. Velocity field in Asia inferred from Quaternary fault slip rates and Global Positioning System observations. *Journal of Geophysical Research*, **105**, 19185–19210, doi:10.1029/2000JB900045.

Horton, B.K., Yin, A., Spurlin, M.S., Zhou, J. & Wang, J. 2002. Paleocene–Eocene syncontractional sedimentation in narrow, lacustrine-dominated basins of east–central Tibet. *Geological Society of America Bulletin*, **114**, 771–786.

Houseman, G. & England, P. 1986. Finite strain calculations of continental deformation. I -Method and general results for convergent zones II - Comparison with the India-Asia collision zone. *Journal of Geophysical Research*, **91**, 3651–3663, doi:10.1029/JB091iB03p03651.

Houseman, G. & England, P.C. 1996. A lithosphere thickenening model for the Indo-Asian collision. *In:* Yin, A. & Harrison, T.M. (eds) *The Tectonic Evolution of Asia*. Cambridge University Press, Cambridge, 3–17.

Houseman, G., McKenzie, D. & Molnar, P. 1981. Convective instability of a thickened boundary layer and its relevance for thermal evolution of continental convergent belts. *Journal of Geophysical Research*, **86**, 6115–6132.

Jackson, J. 2002. Strength of the continental lithosphere: time to abandon the jelly sandwich? *GSA Today*, Sept. 2002, **12(9)**, 4–9.

Jackson, J.A., Austrheim, H., McKenzie, D. & Priestley, K. 2004. Metastability, mechanical strength, and the support of mountain belts. *Geology*, **32**, 625–628, doi:10.1130/1052-5173(2002)012<0004:SOTCLT>2.0.CO;2.

Jackson, J., McKenzie, D., Priestley, K. & Emmerson, B. 2008. New views on the structure and rheology of the lithosphere. *Journal of the Geological Society, London*, **165**, 453–465.

Jade, S., Bhatt, B.C., *et al.* 2004. GPS measurements from the Ladakh Himalaya, India: preliminary tests of plate-like or continuous deformation in Tibet. *Geological Society of America Bulletin*, **116**, 1385–1391.

Jain, A.K. & Singh, S. 2008. Tectonics of the southern Asian Plate margin along the Karakoram Shear Zone: Constraints from field observations and U–Pb SHRIMP ages. *Tectonophysics*, **451**, 186–205.

Jolivet, L., Beyssac, O., *et al.* 2001. Oligo–Miocene mid-crustal sub-horizontal shear zone in Indochina. *Tectonics*, **20**, 46–57.

Jolivet, M., Brunel, M., *et al.* 2003. Neogene extension and volcanism in the Kunlun Fault zone, northern Tibet: New constraints on the age of the Kunlun Fault. *Tectonics*, **22**, TC1052, doi:10.1029/2002TC001428.

Jolivet, R., Cattin, R., Chamot-Rooke, N., Lasserre, C. & Peltzer, G. 2008. Thin-plate modeling of interseismic deformation and asymmetry across the Altyn Tagh fault zone. *Geophysical Research Letters*, **35**, L02309, doi:10.1029/2007GL031511.

Jordan, T.A. & Watts, A.W. 2005. Gravity anomalies, flexure and the elastic thickness structure of the India–Eurasia collision system. *Earth and Planetary Science Letters*, **236**, 732–750.

Kapp, P. & Guynn, J.H. 2004. India punch rifts Tibet. *Geology*, **32**, 993–996.

Kapp, P., Yin, A., Harrison, T.M. & Ding, L. 2005. Cretaceous–Tertiary shortening, basin development and volcanism in central Tibet. *Geological Society of America Bulletin*, **117**, 865–878.

Kapp, P., DeCelles, P.G., Gehrels, G., Heizler, M. & Ding, L. 2007*a*. Geological records of the Lhasa–Qiangtang and Indo-Asian collisions in the Nima area of central Tibet. *Geological Society of America Bulletin*, **119**, 917–932.

Kapp, P., DeCelles, P.G., *et al.* 2007*b*. The Gangdese retroarc thrust belt revealed. *GSA Today*, **17**, 4–9, doi:10.1130/GSAT01707A.1.

Kapp, P., Taylor, M., Stockli, D. & Ding, L. 2008. Development of active low-angle normal fault systems during orogenic collapse: Insight from Tibet. *Geology*, **36**, 7–10, doi:10.1130/G24054A.

Kirby, E., Reiners, P.W., *et al.* 2002. Late Cenozoic evolution of the eastern margin of the Tibetan Plateau: Inferences from $^{40}Ar/^{39}Ar$ and (U–Th)/He thermochronology. *Tectonics*, **21**, TC1001, doi:10.1029/2000TC001246.

Kirby, E., Harkins, N., Wang, E., Shi, X., Fan, C. & Burbank, D. 2007. Slip rate gradients along the eastern Kunlun Fault. *Tectonics*, **26**, TC2010, doi:10.1029/2006TC002033.

Kosarev, G., Kind, R., Sobolev, S., Yuan, X., Hanka, W. & Oreshin, S. 1999. Seismic evidence for a detached Indian lithospheric mantle beneath Tibet. *Science*, **283**, 1306–1308.

Lacassin, R., Valli, F., *et al.* 2004*a*. Large-scale geometry, offset and kinematic evolution of the Karakoram Fault, Tibet. *Earth and Planetary Science Letters*, **219**, 255–269.

Lacassin, R., Valli, F., Arnaud, N. *et al.* 2004*b*. Reply to Comment on "Large-scale geometry, offset and kinematic evolution of the Karakoram fault, Tibet". *Earth and Planetary Science Letters*, **229**, 159–163.

Lasserre, C., Morel, P.-H., *et al.* 1999. Postglacial left slip rate and past occurrence of M>8 earthquakes on the western Haiyuan fault, Gansu, China. *Journal of Geophysical Research*, **104**, doi:10.1029/1998JB900082.

Lasserre, C., Gaudemer, Y., *et al.* 2002. Fast late Pleistocene slip rate on the Leng Long Ling segment of the Haiyuan fault, Qinghai, China. *Journal of Geophysical Research*, **107**, doi:10.1029/2000JB000060.

Lasserre, C., Peltzer, G., Crampe, F., Klinger, Y., Van der Woerd, J. & Tapponnier, P. 2005. Coseismic deformation of the 2001 $M_w = 7.8$ Kokoxili earthquake in Tibet, measured by synthetic aperture radar interferometry. *Journal of Geophysical Research*, **110**, doi:10.1029/2004JB003500.

Law, R.D., Searle, M.P. & Simpson, R.L. 2004. Strain, deformation temperatures and vorticity of flow at the top of the Greater Himalayan Slab, Everest massif, Tibet. *Journal of the Geological Society, London*, **161**, 305–320.

Law, R.D., Searle, M.P. & Godin, L. (eds) 2006. *Channel Flow, Ductile Extrusion and Exhumation in Continental Collision Zones*. Geological Society, London, Special Publications, **268**.

Lee, H.-Y., Chung, S.-L., *et al.* 2003. Miocene Jiale faulting and its implication for Tibetan tectonic evolution. *Earth and Planetary Science Letters*, 20**5**, 185–194.

Lee, H.-Y., Chung, S.-L., Lo, C.-H., Ji, J., Lee, T.-Y., Qian, Q. & Zhang, Q. 2009. Eocene Neotethyan slab breakoff in southern Tibet inferred from the Linzizong volcanic record. *Tectonophysics*, **477**, 20–35.

Lee, J., Hacker, B.R., *et al.* 2000. Evolution of the Kangmar dome, southern Tibet: Structural, petrologic and thermochronologic constraints. *Tectonics*, **19**, 872–895.

Lehmkuhl, F. & Haselein, F. 2000. Quaternary paleoenvironmental change on the Tibetan Plateau and adjacent areas (Western China and Western Mongolia). *Quaternary International*, **65–66**, 121–145.

Leier, A.L., DeCelles, P.G., Kapp, P. & Ding, L. 2007. The Takena Formation of the Lhasa terrane, southern Tibet: record of a Late Cretaceous retroarc foreland basin. *Geological Society of America Bulletin*, **119**, 31–48.

Leloup, P.H. & Kienast, J.-R. 1993. High-temperature metamorphism in a major strike-slip shear zone: the Ailao Shan–Red River, People's Republic of China. *Earth and Planetary Science Letters*, **118**, 213–234.

Leloup, P.H., Harrison, T.M., Ryerson, F.J., Chen, W., Li, Q., Tapponnier, P. & Lacassin, R. 1993. Structural, petrological and thermal evolution of a Tertiary ductile strike-slip shear zone, Diancang Shan, Yunnan. *Journal of Geophysical Research*, **98**, 6715–6743.

Leloup, P.H., Lacassin, R., *et al.* 1995. The Ailao Shan–Red River shear zone (Yunnan, China), Tertiary transform boundary of Indochina. *Tectonophysics*, **251**, 3–84.

Leloup, P.H., Arnaud, N., *et al.* 2001. New constraints on the structure, thermochronology, and timing of the Ailao Shan–Red River shear zone, SE Asia. *Journal of Geophysical Research*, **106**, 6657–6671.

Li, C., Zhang, P., Yin, J. & Min, W. 2009. Late Quaternary left-lateral slip rate of the Haiyuan fault, northeastern margin of the Tibetan Plateau. *Tectonics*, **28**, doi:10.1029/2008TC002302.

Lin, T.-H., Lo, C.-H., *et al.* 2009. $^{40}Ar/^{39}Ar$ dating of the Jiale and Gaoligong shear zones: Implications for crustal deformation around the Eastern Himalayan Syntaxis. *Journal of Asian Earth Sciences*, **34**, 674–685.

Liu, Q. 1993. *Paléoclimat et contraintes chronologiques sur les mouvements récent dans l'Ouest du Tibet: Failles du Karakorum et de Longmu Co–Gozha Co, lacs en pull-apart de Longmu Co et de Sumxi Co*. PhD thesis, Université Paris VII.

Liu-Zeng, J., Klinger, Y., *et al.* 2007. Millennial recurrence of large earthquakes on the Haiyuan Fault near Songshan, Gansu Province, China. *Bulletin of the Seismological Society of America*, **97**, 14–34, doi:10.1785/0120050118.

Lister, G.S., Kelts, K., Zao, C.K., Yu, J.Q. & Niessen, F. 1991. Lake Qinghai, China: Closed basin lake levels and oxygen isotope record for ostracoda since the last Pleistocene. *Palaeogeography, Palaeoclimatology, Palaeoecology*, **84**, 141–162.

Maggi, A., Jackson, J., McKenzie, D. & Priestley, K. 2000. Earthquake focal depths, effective elastic thickness and the strength of the continental lithosphere. *Geology*, **28**, 495–498.

Makovsky, Y., Klemperer, S.L. & Ratschbacher, L. 1999. Midcrustal reflector on INDEPTH wide-angle profiles: an ophiolitic slab beneath the India–Asia suture in southern Tibet? *Tectonics*, **18**, 793–808.

Martin, H. 1998. Adakite magmas: Modern analogues of Archaean granitoids. *Lithos*, **46**, 411–429.

Matte, Ph., Tapponnier, P., *et al.* 1996. Tectonics of Western Tibet, between the

Tarim and the Indus. *Earth and Planetary Science Letters*, **142**, 311–330.

McCaffrey, R. & Nabelek, J. 1998. Role of oblique convergence in the active deformation of the Himalayas and southern Tibet plateau. *Geology*, **26**, 691–694.

McKenna, L.W. & Walker, J.D. 1990. Geochemistry of crustally derived leucocratic igneous rocks from the Ulugh Muztagh area, Northern Tibet and their implications for the formation of the Tibetan Plateau. *Journal of Geophysical Research*, **95**, 21483–21502.

Meade, B.J. 2007. Present-day kinematics at the India–Asia collision zone. *Geology*, **35**, 81–84.

Meriaux, A.-S., Ryerson, F.J., *et al.* 2004. Rapid slip along the central Altyn Tagh Fault: Morphochronologic evidence from Cherchen He and Sulamu Tagh. *Journal of Geophysical Research*, **109**, B06401, doi:10.1029/2003JB002558.

Meriaux, A.-S., Tapponnier, P., *et al.* 2005. The Aksay segment of the northern Altyn Tagh fault: Tectonic geomorphology, landscape evolution, and Holocene slip rate. *Journal of Geophysical Research*, **110**, B04404, doi:10.1029/2004JB003210.

Meyer, B., Tapponnier, P., Gaudemer, Y., Peltzer, G., Shunmin, G. & Zhitai, C. 1996. Rate of left-lateral movement along the easternmost segment of the Altyn Tagh fault, east of 96°E (China). *Geophysics Journal International*, **124**, 29–44, doi:10.1111/j.1365-246X.1996.tb06350.x.

Mo, X.X., Hou, Z.Q., Niu, Y.L., Dong, G.C., Zhao, Z.D. & Yang, Z.M. 2007. Mantle contributions to crustal thickening during continental collision: evidence from Cenozoic igneous rocks in southern Tibet. *Lithos*, **96**, 225–242.

Mo, X.X., Niu, Y.L., Dong, G.C., Zhao, Z.D., Hu, Z.Q., Zhou, S. & Ke, S. 2008. Contribution of syn-collisional felsic magmatism to continental crust growth: a case study of the Palaeogene Linzizong volcanic succession in southern Tibet. *Chemical Geology*, **250**, 49–67.

Molnar, P. & Chen, W.-P. 1983. Focal depths and fault plane solutions of earthquakes under the Tibetan plateau. *Journal of Geophysical Research*, **88**, 1180–1196, doi:10.1029/JB088iB02p01180.

Molnar, P. & Chen, W.-P. 1984. S–P wave travel time residuals and lateral inhomogeneity in the mantle beneath Tibet and the Himalaya. *Journal of Geophysical Research*, **89**, 6911–6917.

Molnar, P. & Tapponnier, P. 1975. Cenozoic tectonics of Asia: Effects of a continental collision. *Science*, **189**, 419–426.

Molnar, P. & Tapponnier, P. 1978. Active tectonics of Tibet. *Journal of Geophysical Research*, **83**, 5361–5376.

Molnar, P. & Lyon-Caen, H. 1989. Fault plane solutions of earthquakes and active tectonics of the Tibetan Plateau and its margins. *Geophysical Journal International*, **99**, 123–153.

Molnar, P., Burchfiel, B.C., K'uangyi, L. & Ziyun, Z. 1987*a*. Geomorphic evidence for active faulting in the Altyn Tagh and northern Tibet and qualitative estimates of its contribution to the convergence of India and Eurasia. *Geology*, **15**, 249–252, doi:10.1130/0091-7613(1987)15.

Molnar, P., Burchfiel, B.C., Ziyun, Z., K'uangyi, L., Shuji, W. & Minmin, H. 1987*b*. Geologic evolution of Northern Tibet: results from an expedition to Ulugh Muztagh. *Science*, **235**, 299–305.

Molnar, P., England, P.C. & Martinod, J. 1993. Mantle dynamics, uplift of the Tibetan Plateau and the Indian monsoon. *Reviews of Geophysics*, **31**, 357–396.

Monsalve, G., McGovern, P. & Sheehan, A. 2009. Mantle fault zones beneath the Himalayan collision: Flexure of the continental lithosphere. *Tectonophysics*, **477**, 66–76.

Murphy, M.A., Yin, A., *et al.* 1997. Did the Indo-Asian collision alone create the Tibetan plateau? *Geology*, **25**, 719–722, doi:10.1130/00917613(1997)025<0719:DTIACA>2.3.CO;2.

Murphy, M.A., Yin, A., Kapp, P., Harrison, T.M., Ding, L. & Jinghua, C. 2000. Southward propagation of the Karakoram Fault, southwest Tibet: timing and magnitude of slip. *Geology*, **28**, 451–454.

Murphy, M.A. & Yin, A. 2003. Structural evolution and sequence of thrusting in the Tethyan fold-thrust belt and Indus-Yalu suture zone, southwest Tibet. *Geological Society of America Bulletin*, **115**, 21–34.

Nábelek, J., Hetényi, G., *et al.* 2009. Underplating in the Himalaya–Tibet collision zone revealed by the Hi-CLIMB experiment. *Science*, **325**, 1371–1374.

Nelson, K.D., Zhao, W., *et al.* 1996. Partially molten middle crust beneath Southern Tibet: Synthesis of Project INDEPTH results. *Sciences*, **274**, 1684–1688.

Ni, J. & York, J.E. 1978. Cenozoic extensional tectonics of the Tibetan Plateau. *Journal of Geophysical Research*, **83**, 5377–5384.

Nishiizumi, K., Armold, J.R., Lal, D., Klein, J. & Middleton, R. 1986. Production of Be-10 and Al-26 by cosmic rays in terrestrial quartz *in situ* and implications for erosion rates. *Nature*, **319**, 134–136, doi:10.1038/319134a0.2.4.2.

Nishiizumi, K., Kohl, C.P., Winterer, E.L., Klein, J. & Middleton, R. 1989. Cosmic ray production rates of Be-10 and Al-26 in quartz from glacially polished rocks. *Journal of Geophysical Research*, **94**, 17907–17915, doi:10.1029/JB094iB12p17907.

Nomade, S., Renne, P.R., Mo, X., Zhao, Z. & Zhou, S. 2004. Miocene volcanism in the Lhasa block, Tibet: spatial trends and geodynamic implications. *Earth and Planetary Science Letters*, **221**, 227–243.

Owens, T.J. & Zandt, G. 1997. Implications of crustal property variations for models of Tibetan plateau evolution. *Nature*, **387**, 37–42.

Pegler, G. & Das, S. 1998. An enhanced image of the Pamir–Hindu Kush seismic zone from relocated earthquake hypocenters. *Geophysical Journal International*, **134**, 573–595, doi:10.1046/j.1365-246x.1998.00582.x.

Peltzer, G. & Tapponnier, P. 1988. Formation and evolution of strike-slip faults, rifts and basins during the India–Asia collision: an experimental approach. *Journal of Geophysical Research*, **93**, 15085–15117.

Peltzer, G., Tapponnier, P. & Armijo, R. 1989. Magnitude of late Quaternary left-lateral displacements along the north edge of Tibet. *Science*, **246**, 1285–1289, doi:10.1126/science.246.4935.1285.

Phillips, R.J. 2008. Geological map of the Karakoram Fault zone, Eastern Karakoram, Ladakh, NW Himalaya. *Journal of Maps*, **2008**, 38–49, doi:10.4113/jom.2008.93.

Phillips, R.J. & Searle, M.P. 2007. Macrostructural and microstructural architecture of the Karakoram fault: Relationship between magmatism and strike-slip faulting. *Tectonics*, **26**, TC3017, doi:10.1029/2006TC00946.

Phillips, R.J., Parrish, R.R. & Searle, M.P. 2004. Age constraints on ductile deformation and long-term slip rates along the Karakoram fault zone, Ladakh. *Earth and Planetary Science Letters*, **226**, 305–319.

Priestley, K. & McKenzie, D. 2006. The thermal structure of the lithosphere from shear wave velocities. *Earth and Planetary Science Letters*, **244**, 285–301.

Priestley, K., Jackson, J. & McKenzie, D. 2008. Lithospheric structure and deep earthquakes beneath India, the Himalaya and southern Tibet. *Geophysical Journal International*, **172**, 345–362.

Rai, S., Priestley, K., Gaur, V., Mitra, S., Singh, M. & Searle, M.P. 2006. Configuration of the Indian Moho beneath the Northwest Himalaya and Ladakh. *Geophysical Research Letters*, **33**, doi:10.1029/2006GL026076.

Ratschbacher, L., Frisch, W., Liu, G. & Chen, C.C. 1996. Distributed deformation in southern and western Tibet during and after the Indo-Asia collision. *Journal of Geophysical Research*, **99**, 19917–19945.

Replumaz, A. & Tapponnier, P. 2003. Reconstruction of the deformed collision zone between India and Asia by backward motion of lithospheric blocks. *Journal of Geophysical Research*, **198**, doi:10.1029/2001JB000661.

Rhodes, T.E., Gasse, F., *et al.* 1996. Late Pleistocene–Holocene lacustrine record from Lake Manas, Zunggar (northern Xinjiang, western China). *Palaeogeography, Palaeoclimatology, Palaeoecology*, **120**, 105–121.

Ritts, B.D. & Biffi, U. 2000. Magnitude of post-Middle Jurassic (Bajocian) displacement on the central Altyn Tagh fault system, northwest China. *Geological Society of America Bulletin*, **112**, 61–74, doi:10.1130/0016-7606(2000)112<61:MOPJBD>2.0.CO;2.

Ritts, B.D., Yue, Y. & Graham, S. 2004. Oligocene–Miocene tectonics and sedimentation along the Altyn Tagh fault, northern Tibetan plateau: Analysis of the Xorkol, Subei, and Aksay basins. *Journal of Geology*, **112**, 207–229, doi:10.1086/381658.

Ritts, B.D., Yue, Y., Graham, S.A., Sobel, E.R., Abbink, O.A. & Stockli, D. 2008. From sea level to high elevation in 15 million years: Uplift history of the northern Tibetan Plateau margin in the Altun Shan. *American Journal of Science*, **308**, 657–678, doi:10.2475/05.2008.01.

Robinson, D.M. 2008. Forward modelling the kinematic sequence of the central Himalayan thrust belt, western Nepal. *Geosphere*, **4**, 785–801, doi: 10.1130/GES00163.1.

Robinson, A.C. 2009*a*. Geologic offsets across the Karakoram Fault: Implications for its role and terrane correlations in the western Himalayan–Tibetan orogen. *Earth and Planetary Science Letters*, **279**, 123–130.

Robinson, A.C. 2009*b*. Evidence against Quaternary slip on the northern Karakoram Fault suggests kinematic reorganization at the western end of the Himalayan–Tibetan orogen. *Earth and Planetary Science Letters*, **286**, 158–170.

Robinson, A.C., Yin, A., Manning, C.E., Harrison, T.M., Zhang, S.-H. & Wang, X.-F. 2004. Tectonic evolution of the northeastern Pamir: constraints from the northern portion of Cenozoic Kongur extensional system. *Geological Society of America Bulletin*, **116**, 953–974.

Robinson, A.C., Yin, A., Manning, C.E., Harrison, T.M., Zhang, S.-H. & Wang, X.-F. 2007. Cenozoic evolution of the eastern Pamir: implications for strain accommodation mechanisms at the western end of the Himalayan–Tibetan orogen. *Geological Society of America Bulletin*, **119**, 882–896.

Roeker, S.W. 1982. Velocity structure of the Pamir–Hindu Kush region: possible evidence of subducted crust. *Journal of Geophysical Research*, **87**, 945–959.

Roger, F., Calassou, S., *et al.* 1995. Miocene emplacement and deformation of the Konga Shan granite (Xianshui He fault zone, west Sichuan, China):

Geodynamic implications. *Earth and Planetary Science Letters*, **130**, 201–216.

Rolland, Y. & Pêcher, A. 2001. The Pangong granulites of the Karakoram Fault (Western Tibet): vertical extrusion within a lithospheric scale fault? *Comptes Rendus de l'Académie des Sciences*, **332**, 363–370.

Rolland, Y., Maheo, G., Guillot, S. & Pêcher, A. 2001. Tectono-metamorphic evolution of the Karakoram Metamorphic Complex (Dassu–Askole area, NE Pakistan): exhumation of mid-crustal HT–MP gneisses in a convergent context. *Journal of Metamorphic Geology*, **19**, 717–737.

Rolland, Y., Maheo, G., Pêcher, A. & Villa, I. 2008. Syn-kinematic emplacement of the Pangong metamorphic and magmatic complex along the Karakoram Fault (north Ladakh). *Journal of Asian Earth Sciences*, doi:10.1016/j.aeaes.2008.03.009.

Rowley, D.B. 1998. Minimum age of initiation of collision between India and Asia north of Mount Everest. *Journal of Geology*, **106**, 229–235.

Rowley, D.B. & Currie, B.S. 2006. Palaeo-altimetry of the Late Miocene Lunpola basin, central Tibet. *Nature*, **439**, 677–681.

Royden, L.H., Burchfiel, B.C., King, R.W., Wang, E., Chen, Z., Shen, F. & Liu, Y. 1997. Surface deformation and lower crust flow in Eastern Tibet. *Science*, **276**, 788–790.

Royden, L.H., Burchfiel, B.C. & Van Der Hilst, R.D. 2008. The geological evolution of the Tibetan Plateau. *Science*, **321**, 1054–1058.

Ryerson, F.J., Peltzer, G., Tapponnier, P., Finkel, R.C., Meriaux, A. & Van der Woerd, J. 1999. Slip-Rates on the Altyn Tagh Fault–Karakax Valley Segment: Constraints from Surface Exposure Dating. *EOS*, **80**, 1008.

Ryerson, F.J., Tapponnier, P., *et al.* 2006. Applications of morphochronology to the active tectonics of Tibet. *In:* Siame, L.L., Bourles, D. & Brown, E.T. (eds) In Situ-*Produced Cosmogenic Nuclides and Quantification of Geological Processes*. Geological Society of America, Special Papers, **415**, 61–86, doi:10.1130%2F2006.2415%2805%29.

Schulte-Pelkum, V., Monsalve, G., Sheehan, A., Pandey, M.R., Sapkota, S., Bilham, R. & Wu, F. 2005. Imaging the Indian subcontinent beneath the Himalaya. *Nature*, **435**, 1222–1225.

Searle, M.P. 1991. *Geology and Tectonics of the Karakoram Mountains*. Wiley, Chichester.

Searle, M.P. 1995. The rise and fall of Tibet. *Nature*, **374**, 17–18.

Searle, M.P. 1996. Geological evidence against large-scale pre-Holocene offsets along the Karakoram Fault: Implications for the limited extrusion of the Tibetan Plateau. *Tectonics*, **15**, 171–186.

Searle, M.P. 2006. Role of the Red River Shear zone, Yunnan and Vietnam, in the continental extrusion of SE Asia. *Journal of the Geological Society, London*, **163**, 1025–1036.

Searle, M.P. 2007. Reply to Discussion on the 'Role of the Red River Shear zone, Yunnan and Vietnam, in the continental extrusion of SE Asia'. *Journal of the Geological Society, London*, **164**, 1253–1260.

Searle, M.P. 2010. Low-angle normal faults in the compressional Himalayan orogen: Evidence from the Annapurna–Dhaulagiri Himalaya, Nepal. *Geosphere*, **6**, 296–315.

Searle, M.P. & Phillips, R.J. 2004. A comment on 'Large-scale geometry, offset and kinematic evolution of the Karakoram Fault, Tibet'. *Earth and Planetary Science Letters*, **229**, 155–158.

Searle, M.P. & Phillips, R.J. 2007. Relationships between right-lateral shear along the Karakoram Fault and metamorphism, magmatism, exhumation and uplift: evidence from the K2–Gasherbrum–Pangong Ranges, north Pakistan and Ladakh. *Journal of the Geological Society, London*, **164**, 439–450.

Searle, M.P. & Rex, A.J. 1989. Thermal model for the Zanskar Himalaya. *Journal of Metamorphic Geology*, **7**, 127–134.

Searle, M.P. & Szulc, A.G. 2005. Channel flow and ductile extrusion of the high Himalayan slab—the Kangchenjunga–Darjeeling profile, Sikkim Himalaya. *Journal Asian Earth Sciences*, **25**, 173–185.

Searle, M.P., Cooper, D.J.W. & Rex, A.J. 1988. Collision tectonics in the Ladakh–Zanskar Himalaya. *Philosophical Transactions of the Royal Society of London, Series A*, **326**, 117–150.

Searle, M.P., Parrish, R.R., Tirrul, R. & Rex, D.C. 1990. Age of crystallisation and cooling of the K2 gneiss in the Baltoro Karakoram. *Journal of the Geological Society, London*, **147**, 603–606.

Searle, M.P., Crawford, M.B. & Rex, A.J. 1992. Field relations, geochemistry, origin and emplacement of the Baltoro granite, central Karakoram. *Transactions of the Royal Society of Edinburgh*, **83**, 519–538.

Searle, M.P., Parrish, R.R., Hodges, K.V., Hurford, A., Ayres, M.W. & Whitehouse, M.J. 1997*a*. Shisha Pangma leucogranite, South Tibetan Himalaya: Field relations, geochemistry, age, origin and emplacement. *Journal of Geology*, **105**, 295–317.

Searle, M.P., Corfield, R.I., Stephenson, B.J. & McCarron, J. 1997*b*. Structure of the North Indian continental margin in the Ladakh–Zanskar Himalayas: implications for the timing of obduction of the Spontang ophiolite, India–Asia collision and deformation events in the Himalaya. *Geological Magazine*, **134**, 297–316.

Searle, M.P., Weinberg, R.F. & Dunlap, W.J. 1998. Transpressional tectonics along the Karakoram fault zone, northern Ladakh: constraints on Tibetan extrusion. *In:* Holdsworth, R.E., Strachan, R.A. & Dewey, J.F. (eds) *Continental Transpressional and Transtensional Tectonics*. Geological Society, London, Special Publications, **135**, 307–326.

Searle, M.P., Hacker, B.R. & Bilham, R. 2001. The Hindu Kush seismic zone as a paradigm for the creation of ultrahigh pressure diamond- and coesite-bearing continental rocks. *Journal of Geology*, **109**, 143–153, doi:10.1086/319244.

Searle, M.P., Simpson, R.L., Law, R.D., Parrish, R.R. & Waters, D.J. 2003. The structural geometry, metamorphic and magmatic evolution of the Everest massif, High Himalaya of Nepal–South Tibet. *Journal of the Geological Society, London*, **160**, 345–366.

Searle, M.P., Law, R.D. & Jessup, M.J. 2006. Crustal structure, restoration and evolution of the Greater Himalaya in Nepal–South Tibet: implications for channel flow and ductile extrusion of the middle crust. *In:* Law, R.D., Searle, M.P. & Godin, L. (eds) *Channel Flow, Ductile Extrusion and Exhumation in Continental Collision Zones*. Geological Society, London, Special Publications, **268**, 355–378.

Searle, M.P., Noble, S.R., Cottle, J.M., Waters, D.J., Mitchell, A.H.G., Hlaing, T. & Horstwood, M.S.A. 2007. Tectonic evolution of the Mogok metamorphic belt, Burma (Myanmar) constrained by U–Th–Pb dating of metamorphic and magmatic rocks. *Tectonics*, **26**, TC3014, doi:10.1029/2006TC002083.

Searle, M.P., Law, R.D., Godin, L., Larson, K.P., Streule, M.J., Cottle, J.M. & Jessup, M.J. 2008. Defining the Himalayan Main Central Thrust in Nepal. *Journal of the Geological Society, London*, **165**, 523–534, doi:10.1144/0016-76492007-081.

Searle, M.P., Parrish, R.R., Thow, A.V., Noble, S.R., Phillips, R.J. & Waters, D.J. 2010*a*. Anatomy, age and evolution of a collisional mountain belt: the Baltoro granite batholith and Karakoram Metamorphic complex, Pakistani Karakoram. *Journal of the Geological Society, London*, **167**, 183–202, doi:10.1144/0016-76492009-043.

Searle, M.P., Cottle, J.M., Streule, M.J. & Waters, D.J. 2010*b*. Crustal melt granites and migmatites along the Himalaya: melt source, segregation, transport and granite emplacement mechanisms. *Transactions of the Royal Society of Edinburgh*, **100**, 219–233, doi:10.1017/S175569100901617X.

Searle, M.P., Yeh, M.-H., Lin, T.-H. & Chung, S.-L. 2010*c*. Structural constraints on the timing of left-lateral shear along the Red River shear zone in the Ailao Shan and Diancang Shan Ranges, Yunnan, Southwest China. *Geosphere*, **6**, 1–23, doi:10.1130/GES00580.1.

Shapiro, N.M., Ritzwoller, M.H., Molnar, P. & Levin, V. 2004. Thinning and flow of Tibetan crust constrained by seismic anisotropy. *Science*, **305**, 233–236.

Shen, Z.K., Wang, M., Li, X.Y., Jackson, D.D., Yin, A., Dong, D.N. & Fang, P. 2001. Crustal deformation along the Altyn Tagh fault system, western China from GPS. *Journal of Geophysical Research*, **106**, 30607–30621.

Shen, Z.-K., Lu, J., Wang, M. & Burgmann, R. 2005. Contemporary crustal deformation around the southeast borderland of the Tibetan Plateau. *Journal of Geophysical Research*, **110**, doi:10.1029/2004JB003421.

Shroder, J.F., Owen, L. & Derbyshire, E. 1993. Quaternary glaciation of the Karakoram and Nanga Parbat Himalaya. *In:* Shroder, J.F. (ed.) *Himalaya to the Sea: Geology, Geomorphology and the Quaternary*. Routledge, London, 132–158.

Sobel, E.R., Arnaud, N., Jolivet, M., Ritts, B.D. & Brunel, M. 2001. Jurassic exhumation history of the Altyn Tagh range, NW China. *In*: Hendrix, M. S. and Davis, G. A. (eds) *Paleozoic and Mesozoic tectonic evolution of central and eastern Asia: From continental assembly to intracontinental deformation*. Geological Society of America Memoir, **194**, 247–251.

Sol, S., Meltzer, A., *et al.* 2010. Geodynamics of the southeastern Tibetan Plateau from seismic anisotropy. *Geology*, **35**, 563–566.

Spurlin, M.S., Yin, A., Horton, B.K., Zhou, J. & Wang, J. 2005. Structural evolution of the Yushu–Nangqian region and its relationship to syncollisional igneous activity, east–central Tibet. *Geological Society of America Bulletin*, **117**, 1293–1317.

Streule, M.J., Phillips, R.J., Searle, M.P., Waters, D.J. & Horstwood, M.S.A. 2009. Evolution and chronology of the Pangong Metamorphic Complex adjacent to the Karakoram fault, Ladakh: Constraints from thermobarometry, metamorphic modeling and U–Pb geochronology. *Journal of the Geological Society, London*, **166**, 919–932.

Tapponnier, P. & Molnar, p. 1976. Slip line field theory and large-scale continental tectonics. *Nature*, **264**, 319–324.

Tapponnier, P. & Molnar, p. 1977. Active faulting and tectonics in China. *Journal of Geophysical Research*, **82**, 2905–2930.

Tapponnier, P., Mercier, J.L., Armijo, R., Tonglin, H. & Ji, Z. 1981. Field evidence for active normal faulting in Tibet. *Nature*, **294**, 410–414, doi:10.1038/294410a0.

Tapponnier, P., Peltzer, G., Ledain, A.Y., Armijo, R. & Cobbold, P.R. 1982.

Propagating extrusion tectonics in Asia: New insights from simple experiments with plasticine. *Geology*, **10**, 611–616.

Tapponnier, P., Ryerson, F. J., Van der Woerd, J., Meriaux, A.-S. & Lasserre, C. 2001*a*. Long-term slip rates and characteristic slip: keys to active fault behaviour and earthquake hazard. *Comptes Rendus de l'Académie des Sciences, Série IIA*, **333**, 483–494, doi:10.1016/S1251-8050(01)01668-8.

Tapponnier, P., Zhiqin, X., Roger, F., Meyer, B., Arnaud, N., Wittlinger, G. & Yang, J. 2001*b*. Oblique stepwise rise and growth of the Tibet Plateau. *Science*, **294**, 1671–1677.

Taylor, M. & Peltzer, G. 2006. Current slip rates on conjugate strike-slip faults in central Tibet using synthetic aperture radar interferometry. *Journal of Geophysical Research*, **111**, B12402, doi:10.1029/2005JB004014.

Taylor, M. & Yin, A. 2009. Active structures of the Himalayan–Tibetan orogen and their relationships to earthquake distribution, contemporary strain field and Cenozoic volcanism. *Geosphere*, **5**, 199–214.

Taylor, M., Yin, A., Ryerson, F.J., Kapp, P. & Ding, L. 2003. Conjugate strike-slip faulting along the Bangong–Nujiang suture zone accommodates coeval east–west extension and north–south shortening in the interior of the Tibetan Plateau. *Tectonics*, **22**, 18, doi:10.1029/2002TC001361.

Taylor, P.J. & Mitchell, W. 2000. The Quaternary glacial history of the Zanskar Range, north-west Indian Himalaya, *Quaternary International*, **65–66**, 81–99.

Thatcher, W. 2007. Microplate model for the present-day deformation of Tibet. *Journal of Geophysical Research*, **112**, B01401, doi:10.1029/2005JB004244.

Thatcher, W. 2009. How the continents deform: The evidence from tectonic geodesy. *Annual Review of Earth and Planetary Sciences*, **37**, 237–262, doi:10.1146/annurev.earth.031208.100035.

Tilmann, F., Ni, J., *et al.* 2003. Seismic imaging of the downwelling Indian lithosphere beneath Central Tibet. *Science*, **300**, 1424–1427.

Turner, S., Hawkesworth, C., Liu, J., Rogers, N., Kelley, S. & Van Calsteren, P. 1993. Timing of Tibetan uplift constrained by analysis of volcanic rocks. *Nature*, **364**, 50–54.

Valli, F., Arnaud, N., *et al.* 2007. Twenty million years of continuous deformation along the Karakorum fault, western Tibet: A thermochronological analysis. *Tectonics*, **26**, TC4004, doi:10.1029/2005TC001913.

Valli, F., Leloup, P.H., *et al.* 2008. New U–Th/Pb constraints on timing of shearing and long-term slip-rate on the Karakorum fault. *Tectonics*, **27**, TC5007, doi:10.1029/2007TC002184.

Van der Woerd, J., Ryerson, F.J., *et al.* 1998. Holocene left-slip rate determined by cosmogenic surface dating on the Xidatan segment of the Kunlun fault (Qinghai, China). *Geology*, **26**, 695–698, doi:10.1130/0091-7613(1998)026.

Van der Woerd, J., Ryerson, F.J., *et al.* 2000. Uniform slip rate along the Kunlun Fault: Implications for seismic behaviour and large-scale tectonics. *Geophysical Research Letters*, **27**, 2353–2356.

Vergne, J., Wittlinger, G., *et al.* 2002. Seismic evidence for stepwise thickening of the crust across NE Tibetan Plateau. *Earth and Planetary Science Letters*, **221**, doi:10.1016/j.epsl.2003.12.012.

Wallace, K., Yin, G. & Bilham, R. 2004. Inescapable slow slip on the Altyn Tagh fault. *Geophysical Research Letters*, **31**, L09613, doi:10.1029/2004GL019724.

Wallis, S., Tsujimori, T., Aoya, M., Kawakami, T., Terada, K., Suzuki, K. & Hyodo, H. 2003. Cenozoic and Mesozoic metamorphism in the Longmenshan orogen: Implications for geodynamic models of eastern Tibet. *Geology*, **31**, 745–748, doi:10.1130/G19562.1.

Wang, E. 1997. Displacement and timing along the northern strand of the Altyn Tagh fault zone, Northern Tibet. *Earth and Planetary Science Letters*, **150**, 55–64, doi:10.1016/S0012-821X(97)00085-X.

Wang, E. & Burchfiel, B.C. 2000. Late Cenozoic to Holocene deformation in southwestern Sichuan and adjacent Yunnan, China, and its role in formation of the southeastern part of the Tibetan Plateau. *Geological Society of America Bulletin*, **112**, 413–423, doi:10.1130/0016-7606(2000)112<413:LCTHDI>2.0.CO;2.

Wang, E., Burchfiel, B.C., Royden, L.H., Liangzhong, C., Jishen, C., Wenxin, L. & Zhiliang, C. 1998. *Late Cenozoic Xianshuihe–Xiaojiang, Red River, and Dali Fault systems of southwestern Sichuan and Central Yunnan, China*. Geological Society of America, Special Papers, **327**, 108pp.

Wang, H., Wright, T. J. & Biggs, J. 2009*a*. Interseismic slip rate of the northwestern Xianshuihe fault from InSAR data. *Geophysical Research Letters*, **36**, doi:10.1029/2008GL036560.

Wang, Q., Zhang, P.Z., *et al.* 2001. Present-day crustal deformation in China constrained by global positioning system measurements. *Science*, **294**, 574–577.

Wang, Q., Wyman, D.A., *et al.* 2010. Eocene north–south trending dikes in central Tibet: New constraints on the timing of east–west extension with implication for early plateau uplift. *Earth and Planetary Science Letters*, 10.1016/j.epsl.2010.07.046.

Wang, S., Fang, X., Zheng, D. & Wang, E. 2009*b*. Initiation of slip along the Xianshuihe fault zone, eastern Tibet, constrained by K/Ar and fission-track ages. *International Geology Review*, **51**, 1121–1131, doi:10.1080/00206810902945132.

Washburn, Z., Arrowsmith, J.R., Forman, S.L., Cowgill, E., Xiaofeng, W., Yueqiao, Z. & Zhengle, C. 2001. Late Holocene earthquake history of the central Altyn Tagh fault, China. *Geology*, **29**, 1051–1054, doi: 10.1130/0091-7613(2001)029<1051:LHEHOT>2.0.CO;2.

Washburn, Z., Arrowsmith, J.R., Dupont-Nivet, G., Feng, W.X., Qiao, Z.Y. & Zhengle, C. 2003. Paleoseismology of the Xorxol Segment of the Central Altyn Tagh Fault, Xinjiang, China. *Annali di Geofisica*, **46**, 1015–1034.

Wei, W., Unsworth, M., *et al.* 2001. Detection of widespread fluids in the Tibetan crust by magnetotelluric studies. *Science*, **292**, 716–718.

Weinberg, R.F. & Mark, G. 2008. Magma migration, folding, and disaggregation of migmatites in the Karakoram Shear Zone, Ladakh, NW India. *Geological Society of America Bulletin*, doi:10.1130/B26227.

Weinberg, R.F. & Searle, M.P. 1998. The Pangong Injection Complex, Indian Karakoram: a case of pervasive granite flow through hot viscous crust. *Journal of the Geological Society, London*, **155**, 883–891.

Weinberg, R.F., Mark, G. & Reichardt, H. 2009. Magma ponding in the Karakoram shear zone, Ladakh, NW India. *Geological Society of America Bulletin*, doi:10.1130/B26358.

Wen, D.-R., Liu, D., *et al.* 2008*a*. Zircon SHRIMP U–Pb ages of the Gangdese Batholith and implications for Neotehtyan subduction in southern Tibet. *Chemical Geology*, **252**, 191–201.

Wen, D.-R., Chung, S.-L., *et al.* 2008*b*. Late Cretaceous Gangdese intrusions of adakitic geochemical characteristics, SE Tibet: Petrogenesis and tectonic implications. *Lithos*, doi:10.1016/j.lithos.2008.02.005.

Wittlinger, G., Vergne, J., *et al.* 2004. Teleseismic imaging of subducting lithosphere and Moho offsets beneath western Tibet. *Earth and Planetary Science Letters*, **221**, 117–130.

Wright, T.J., Parsons, B., England, P.C. & Fielding, E.J. 2004. InSAR observations of low slip rates on the major faults of western Tibet. *Science*, **305**, 236–240.

Xiong, X., Park, P.-H., Zheng, Y., Hsu, H. & Han, U. 2003. Present-day slip-rate of Altyn Tagh Fault: Numerical result constrained by GPS data. *Earth, Planets, and Space*, **55**, 509–514.

Xu, X., Wen, X., Zheng, R., Ma, W., Song, F. & Yu, G. 2003. Pattern of latest tectonic motion and its dynamics for active blocks in Sichuan–Yunnan region, China. *Science in China*, **46**, 210–226, doi:10.1360/03dz0017.

Xu, X., Tapponnier, P., *et al.* 2005. Late Quaternary sinistral slip rate along the Altyn Tagh fault and its structural transformation model. *Science in China Series D: Earth Sciences*, **48**, 384–397, doi:10.1360/02yd0436.

Yang, J., Xu, Z., *et al.* 2009. Discovery of an eclogite belt in the Lhasa block, Tibet: A new border for Palaeo-Tethys? *Journal of Asian Earth Sciences*, **34**, 76–89.

Yao, H.J., Beghein, C. & Van Der Hilst, R.D. 2008. Surface wave array tomography in SE Tibet from ambient seismic noise and two-station analysis—II. Crustal and upper-mantle structure. *Geophysical Journal International*, **173**, 205–219.

Yeh, M.-W., Le, T.-Y., Lo, C.-H., Chung, S.-L., Lan, C.-Y. & Anh, T.T. 2008. Structural evolution of the DayNuiConVoi metamorphic complex: Implications of the development of the Red River shear zone, North Vietnam. *Journal of Structural Geology*, **30**, 1540–1553.

Yin, A. 2000. Mode of Cenozoic east–west extension in Tibet suggesting a common origin of rifts in Asia during the Indo-Asia collision. *Journal of Geophysical Research*, **105**, 21745–21759.

Yin, A. & Harrison, T.M. 2000. Geological evolution of the Himalayan–Tibetan orogen. *Annual Review of Earth and Planetary Sciences*, **28**, 211–280.

Yin, A., Kapp, P.A., *et al.* 1999. Significant late Neogene east–west extension in northern Tibet. *Geology*, **27**, 787–790.

Yin, A., Rumelhart, P.E., *et al.* 2002. Tectonic history of the Altyn Tagh fault system in northern Tibet inferred from Cenozoic sedimentation. *Geological Society of America Bulletin*, **114**, 1257–1295.

Yue, Y. & Liou, J. 1999. Two-stage evolution model for the Altyn Tagh fault, China. *Geology*, **27**, 227–230.

Yue, Y., Ritts, B.D. & Graham, S.A. 2001. Initiation and long-term slip history of the Altyn Tagh fault. *International Geological Review*, **43**, 1087–1093, doi: 10.1080/00206810109465062.

Yue, Y., Ritts, B.D., Graham, S.A., Wooden, J.L., Gehrels, G.E. & Zhang, Z. 2003. Slowing extrusion tectonics: lowered estimate of post-Early Miocene slip rate for the Altyn Tagh fault. *Earth and Planetary Science Letters*, **217**, 111–122.

Yue, Y., Graham, S.A., Ritts, B.D. & Wooden, J.L. 2005. Detrital zircon provenance evidence for large-scale extrusion along the Altyn Tagh fault. *Tectonophysics*, **406**, 165–178, doi:10.1016/j.tecto.2005.05.023.

Zhang, H., Harris, N., Guo, L. & Xu, W. 2009. The significance of Cenozoic magmatism from the western margin of the eastern syntaxis, southeast Tibet. *Contributions to Mineralogy and Petrology*, doi:10.1007/s00410-009-0467-5.

Zhang, P., Molnar, P., *et al.* 1988. Bounds on the Holocene slip rate of the

Haiyuan Fault, North–Central China. *Quaternary Research*, **30**, 151–164.

Zhang, J., Zhang, Z., Xu, Z., Yang, J. & Cui, J. 2001. Petrology and geochronology of eclogites from the western segment of the Altyn Tagh, northwestern China. *Lithos*, **56**, 187–206, doi:10.1016/S0024-4937(00)00052-9.

Zhang, P., Molnar, P. & Xu, X. 2007. Late Quaternary and present-day rates of slip along the Altyn Tagh Fault, northern margin of the Tibetan Plateau. *Tectonics*, **26**, doi:10.1029/2006TC002014.

Zhang, P.Z., Shen, Z., Wang, M., Gan, W.J., Burgman, R. & Molnar, P. 2004. Continuous deformation of the Tibetan Plateau from global positioning system data. *Geology*, **32**, 809–812.

Zhang, Z.M., Zhao, G.C., Santosh, M., Wang, J.L., Dong, X. & Liou, J.G. 2010. Two stages of granulite facies metamorphism in the eastern Himalayan syntaxis, south Tibet: petrology, zircon geochronology and implications for the subduction of Neo-Tethys and the Indian continent beneath Asia. *Journal of Metamorphic Geology*, **28**, 719–733.

Zhao, W., Nelson, W.D., *et al.* 1993. Deep seismic reflection evidence for continental underthrusting beneath Tibet. *Nature*, **366**, 557–559.

Zhu, B., Kidd, W.S.F., Rowley, D.B., Currie, B.S. & Shaifique, N. 2005. Age of initiation of the India–Asia collision in the east–central Himalayas. *Journal of Geology*, **113**, 265–285.

Received 23 August 2010; revised typescript accepted 30 November 2010.
Scientific editing by Rob Strachan.